NATIONAL BUREAU OF STANDARDS REPORT

NBS PROJECT

4214441
4214102

February 1, 1972

NBS REPORT

10 689

A STUDY OF AIR DISTRIBUTION IN SURVIVAL SHELTERS USING A SMALL-SCALE MODELING TECHNIQUE

Final Report

by
E. M. Barber
T. Kusuda
P. J. Reynolds
F. J. Powell

Report to
Office of Civil Defense
Office of the Secretary of the Army
Washington, D. C. 20310

OCD Review Notice: This report has been reviewed in the Office of Civil Defense and approved for publication. Approval does not signify that the contents necessarily reflect the views and policies of the Office of Civil Defense.

NBS

U.S. DEPARTMENT OF COMMERCE

NATIONAL BUREAU OF STANDARDS

DISCLAIMER NOTICE

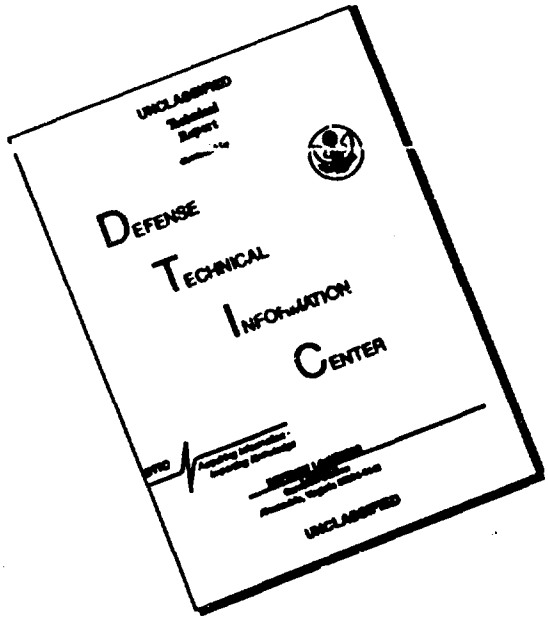

THIS DOCUMENT IS BEST QUALITY AVAILABLE. THE COPY FURNISHED TO DTIC CONTAINED A SIGNIFICANT NUMBER OF PAGES WHICH DO NOT REPRODUCE LEGIBLY.

Table of Contents

Disclaimer

Commercial materials are identified in this report in order to adequately specify the experimental procedure. In no case does such identification imply recommendations or endorsement by the National Bureau of Standards, nor does it imply that the equipment identified is necessarily the best available for the purpose.

Abstract

The development of an experimental small-scale modeling technique for conducting simulations of air distribution patterns in full-sized rooms is described. The technique was applied to simulate the motion of air in a single-room survival shelter. The parameters that describe and must satisfy the principles of dynamic similarity for a comparison of convection between a model and a full-scale room were determined. The main parameters were the Grashof and Prandtl numbers of the fluid and the aspect ratio of the room. High temperature water was used in place of air as the fluid in the model. The model was 6" x 6" (width by height) and 18" deep. A tracer particle was injected into the water in the model. Time exposure photographs were made of the tracer to reveal fluid motion. A description of the experimental apparatus is given including a sample test procedure. Experimental results obtained are presented and discussed.

Acknowledgments

The authors appreciate the technical assistance of Walter M. Ellis in the fabrication, maintenance and operation of the experimental apparatus. Frank Powell's and David Didion's editing and suggestions for the organization of this paper were invaluable. The manuscript was typed by Sharon Crampton. Her efforts and patience are very much appreciated.

1. Introduction

In an emergency, survival shelters may be occupied for several days or perhaps for several weeks. The actual occupancy period must depend on conditions prevailing outside the shelter. The comfort, indeed the survival, of an occupant in such a shelter depends on whether or not the shelter receives an adequate amount of ventilation and if the ventilation air is properly distributed within the shelter. Since electric power cannot be depended upon completely for mechanical ventilation during the time when the shelters are likely to be occupied, the forces that produce natural ventilation should be used to a maximum.

Some research has been reported on natural ventilation of both above and below ground shelters [1, 2]. This work concentrated mainly on the quantity of air moving into and out of a shelter with little emphasis on the distribution of air within the shelter. Studying the air distribution in a full scale shelter would be both time consuming and costly; particularly when a variety of conditions are considered. For this reason, the major emphasis of this program was given to the development of a small scale modeling technique which would be applicable for naturally ventilated survival shelters.

The modeling of any convection system requires close agreement between the similarity parameters of the model and the actual system being simulated. For a natural convection system these parameters are usually limited to Grashof and Prandtl numbers and a geometric dimension. The premise upon which this study is based is that because of the agreement between their Grashof and Prandtl numbers and aspect ratio high temperature, high pressure water in a small "table top" model adequately simulates convection patterns of air in a full sized room.

The objective of this study was ultimately to obtain overall convection flow descriptions for single room shelters for both vented and non-vented conditions, with and without occupants. However, since the experimental method offered a number of advantages for future work as well, the development of the method was an equally important objective. This report is presented in two distinct parts. The main body considers the theoretical justification of the model and the actual experimental results. The Appendix is a translation of these results to a simulated case of air in a full sized room. Although this translation has several limitations it is felt that the results yielded are of significance to the designer of survival shelters.

2. Theoretical Considerations for Scale Modeling

The differential equations governing continuity and the transfer of momentum and energy are well known for the case of natural convection in a space enclosed by a rectangular parallelepiped. A study of these equations was made in order to determine modeling criteria.

The general differential equations and boundary conditions governing the behavior of a fluid within an enclosure may be expressed as follows [5]:

a. Momentum equation

$$\rho \frac{DW}{Dt} = F - \text{grad } p + \mu \nabla^2 W$$

b. Energy equation

$$\rho C \frac{DT}{Dt} = \eta \nabla^2 T - p \frac{\text{div } W}{J} + \mu \Phi - \text{div } q_r$$

c. Continuity equation

$$\frac{D}{Dt} (\rho W) = 0$$

d. Boundary conditions along the inside surfaces of the enclosure may be described as

$$W = 0$$

$$T; \text{ a given function of position}$$

In the above equations the following nomenclature is employed:

W = velocity vector

T = temperature

p = pressure

F = external force (such as gravitational force) vector

μ = dynamic viscosity

ρ = density

C = specific heat

k = thermal conductivity

J = mechanical equivalent of heat

Φ = Rayleigh energy dissipation function

q_r = radiation heat flux vector

t = time

In the energy equation the term involving p div W is the reversible compression work done by the fluid, and the term involving $\mu \Phi$ is the irreversible work done on the fluid element. These terms are usually very small for the natural convection process.

Assuming that the convection system can be characterized by a reference length d (such as the width of the enclosure) and a reference temperature difference ΔT (the difference between the maximum surface temperature, T_1, and minimum surface temperature, T_2), the following dimensionless variables may be introduced:

dimensionless velocity, $U = \frac{Wd}{\nu}$

where kinematic viscosity $\nu = \mu/\rho$

dimensionless temperature, $\theta = \frac{T - T_c}{}$

dimensionless pressure, $P = \frac{pd^2}{\rho\nu^2}$

dimensionless time, $\tau = \frac{\nu t}{d^2}$

dimensionless external force, $f = F/(\rho - \rho_0)\, g$

dimensionless length, $X = x/d$

$Y = y/d$

The differential equation can now be expressed with these dimensionless parameters as follows:

$$\frac{DU}{D\tau} = Gr \cdot \theta \cdot f - \text{grad } P + \nabla^2 U$$

$$\frac{D\theta}{D\tau} = \frac{1}{Pr} \nabla^2 \theta - \frac{1}{\rho C} \text{div } q_r$$

where Gr and Pr are Grashof and Prandtl numbers respectively and defined as follows

$$Gr = \frac{g\beta\Theta d^3}{\nu^2}$$

$$Pr = \frac{\mu C}{k}$$

and β = thermal expansion coefficient of the convecting fluid.

The dimensionless forms of the differential equations suggest that a solution to this set of differential equations can be applicable to a variety of natural convection systems of different thermophysical properties and characteristics. In order for this to be so, each system must have the same values of Gr and Pr, have the same radiation vector characteristics, and have similar geometrical shape and temperature profile along the surface boundaries.

For example, consider two convection systems with characteristic lengths, d_1 and d_2, reference temperature differences ΔT_1 and ΔT_2, and the reference temperature levels T_{1R}, and T_{2R}. The velocity and temperature patterns of both systems are correlated as follows:

$$U = \frac{W_1 d_1}{\nu_1} = \frac{W_2 d_2}{\nu_2}$$

$$\theta = \frac{T_1 - T_{1,R}}{\Delta T_1} = \frac{T_2 - T_{2,R}}{\Delta T_2}$$

for time t_1 and t_2, such that

$$\tau = \frac{\nu_1 t_1}{d_1^2} = \frac{\nu_2 t_2}{d_2^2}$$

The same relationships may be used to translate experimentally observed velocity and temperature patterns of system 1 into those for system 2.

The Grashof number for natural convection in a room 8' wide by 8' high and with a 10 °F temperature difference between opposite walls is on the order of 10^{10} (based on the width, d, as the critical dimension). This is within the region of turbulent convection since the region of transition from laminar to turbulent flow is on the order of (10^{9}). The Prandtl number of air at 80 °F is about 0.72 [6], and the aspect ratio of the above mentioned room is 1.

In order to model the natural convection of air in a room, it is desirable to have a fluid which will produce the same Grashof number and Prandtl number in a scale model as air will have in an average-size room. A number of fluids were found which would give a high Grashof number in a small (6" high x 6" wide) enclosure, but their Prandtl number was much higher than that for air. Of the many fluids considered, only high temperature water gives a high Grashof number and a Prandtl number close to that of air (see figure 1). Water at 500 °F has a Prandtl number of 0.87 [6] which approaches the value of .72 for 80 °F air.

Figures 2, 3, and 4 show the thermophysical properties of air and water that comprise the Prandtl number. The Prandtl number of water decreases rapidly from a value of 6.5 at room temperature to slightly less than unity as it is heated to 500 °F. This reduction is primarily due to a decrease in viscosity. Examination of these figures provide the following important information:

a. High temperature water, at 500 °F, used inside a small-scale model can provide a convection fluid with the Prandtl number close to that for convection conditions found in room air.

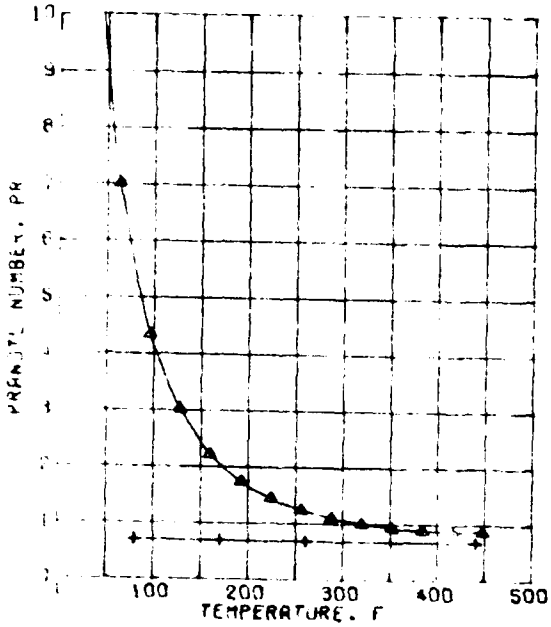

Figure 1

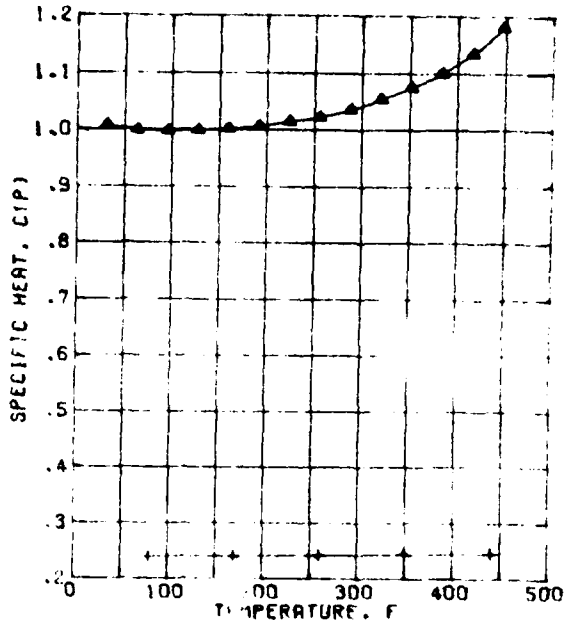

Figure 2

+ AIR
Δ WATER

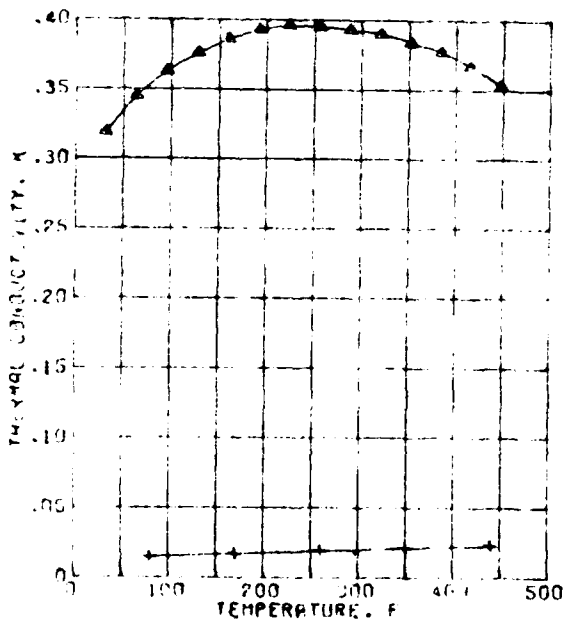

Figure 3

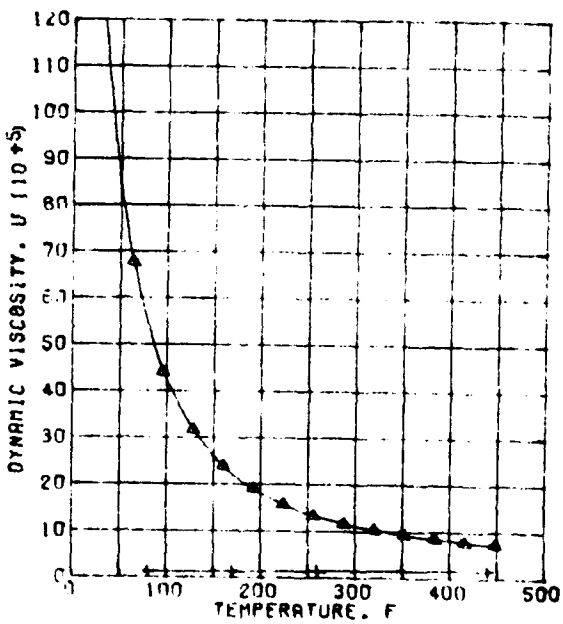

Figure 4

b. Thermophysical properties of hot water are relatively constant with respect to temperature change, thus inaccuracies due to property value variation across the boundary layer along the heat transfer surfaces are minimized. In contrast the viscosity of low temperature water changes considerably with the temperature changes across a boundary layer, severely affecting the convection flow pattern.

Although not shown in these figures, the pressure level for the high temperature water tank increases very rapidly with temperature. Thus high pressure and high temperature must both be considered when designing an apparatus in which high temperature water is used as a modeling fluid.

It was concluded that natural convection in a room can be simulated by a small-scale model using hot water in place of air. This conclusion is valid if the effect of thermal radiation can be ignored in the original differential equations, or if the radiation effect is equal for hot water and air. A detailed analysis of this subject is involved and a comprehensive treatment can be found in reference [5]. The assumption that convecting fluids are gray (radiant heat transfer independent of wavelength) and non-scattering will be discussed here briefly.

In the absence of carbon dioxide and water vapor the air in a room may be considered transparent to thermal radiation. But carbon dioxide (up to 3%) and water vapor (up to 1.5% at 70 °F) are present in the atmosphere and they do absorb some of the incident radiant energy. Also airborne dust particles scatter some of this incident radiation. For example, the absorbing and scattering effects of the air surrounding the earth reduce by 20% the amount of normal incident solar radiation at the earth's surface. This holds true even during cloudless days (the approximate absorption coefficient for air is 0.374 ft^{-1} at standard atmospheric pressure).

However, since the optical thickness involved in a room size enclosure is very much smaller than the atmospheric layer, it has been customary to ignore the radiation term (div q_r) in the energy equation. The rationale for this is the fact that the experimentally observed air velocity and temperature profiles in the laminar boundary layer flowing along a vertical plate show good agreement with the calculated values of velocity and temperature based upon the energy equation without the radiation term [7].

On the other hand, liquid water is practically opaque to thermal radiation (its absorption coefficient is approximately 15,000 ft^{-1}). According to Sparrow [5], this constitutes a case for the optically thick limit, which in effect permits the div q_r term to be omitted.

Neglecting the radiation term in the energy equation, however, is not meant to imply that radiant heat transfer is unimportant in room air convection. On the contrary, room air motion is profoundly affected by the radiant heat exchange among room surfaces by heaters and by incident solar and sky radiation entering through windows. However, the influence of this radiant heat transfer first appears in the form of a surface temperature pattern in the room rather than as a direct influence on some fluid element within the room. It is this surface temperature pattern then which actually influences convective heating and the subsequent change of air motion. This means that the convective heat transfer from room surfaces to room air and the radiation heat exchange among various surfaces must be considered simultaneously.

Such a combined analysis of heat transfer modes is extremely complex and probably iterative but radiant heat transfer among surfaces in a room can be calculated independently. The difficulty caused by radiant heat exchange among room surfaces can, however, be circumvented experimentally by insuring that surface temperatures of a small-scale model be kept very close to those of a room being modeled.

Although high temperature water is an excellent fluid for the scale-model study of room air convection, the high pressure associated with this fluid becomes a major consideration in the design of an experimental apparatus. A low Prandtl number of water (0.87) can be attained only by heating the water to 500 °F requiring a saturation pressure of 680 psia to prevent boiling. The tank must safely restrain high temperatures and pressures, provide an adequate size view window for flow observations, contain a system for both measuring and controlling temperature, and

accommodate a mechanism for injecting the trace particles.

There is yet some question as to whether or not the flow and temperature patterns are truly dependent upon the Prandtl number when turbulent flow conditions actually occur in a room or shelter. Moreover, it is hypothesized that the heat transfer rate at the fluid-surface interface is less affected by the Prandtl number value for turbulent boundary layer flow than it is for laminar flow condition.

To evaluate the magnitude of the effect of Pr upon convection characteristics, the energy equation (without the radiation term) was solved numerically with the use of a finite-difference technique [8]. Figures 5, 6, 7, 8, 9, 10, 11 and 12 illustrate some of the results obtained. As shown, Pr and Gr strongly influence both velocity and temperature profiles for a span Gr from 10^3 to 10^6. The convection flow at both these Grashof numbers are in the laminar region. Numerical calculations for Gr higher than 10^6 are extremely time- and memory-consuming for a computer, but they are not impossible.

Rockett and Torrance [9, 10] reported a numerical and experimental study of convection of air in a room. In their work, however, air movement was caused by a localized source of heating, such as a waste-basket fire. They used a "finite-difference" technique to solve the equations governing natural convection. They also conducted an experimental study using air in a scale model and found close agreement between the numerical and experimental results in the laminar-flow range. This close agreement adds confidence to the theory that the Grashof and Prandtl numbers of the fluid and the aspect ratio of the enclosure are the factors which must be kept consistent between a scale model and a full-scale room

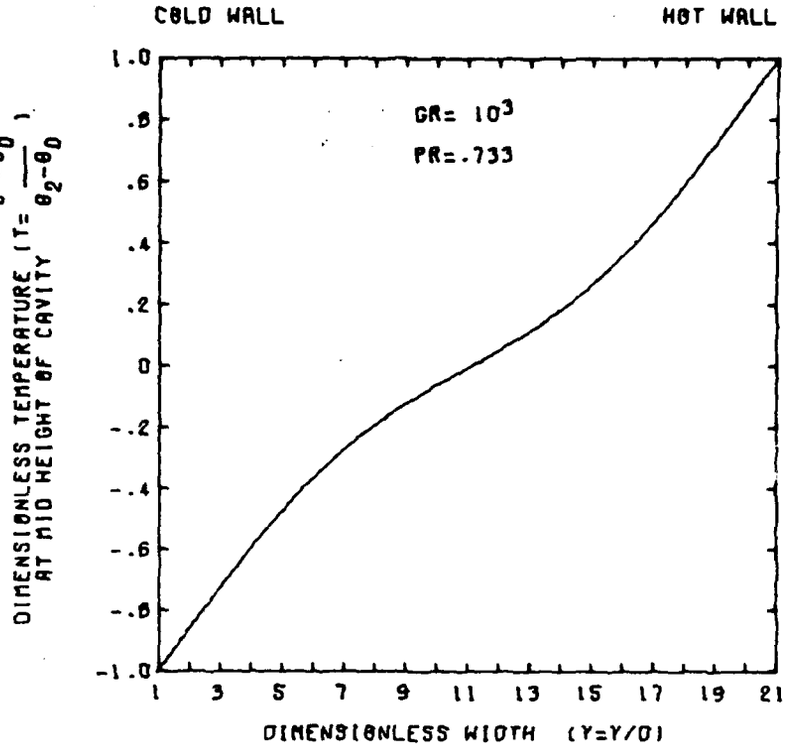
COLD WALL
HOT WALL
GR= 10^3
PR=.733
DIMENSIONLESS TEMPERATURE (T= $\frac{\theta-\theta_0}{\theta_2-\theta_0}$)
AT MID HEIGHT OF CAVITY
1.0
.8
.6
.4
.2
0
-.2
-.4
-.6
-.8
-1.0
1 3 5 7 9 11 13 15 17 19 21
DIMENSIONLESS WIDTH (Y=Y/D)

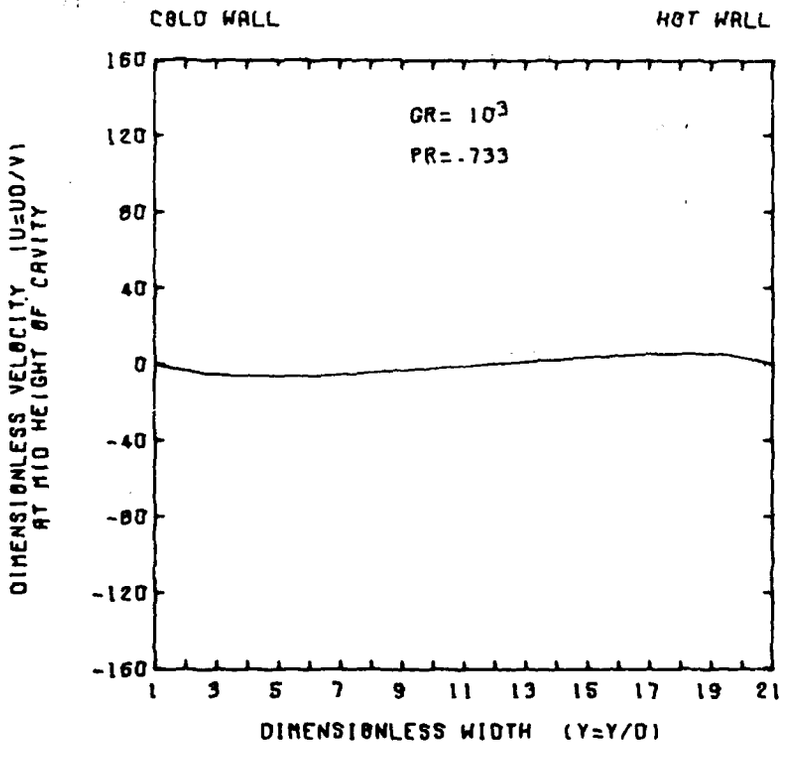
COLD WALL
HOT WALL
GR= 10^3
PR=.733
DIMENSIONLESS VELOCITY (U=UD/V)
AT MID HEIGHT OF CAVITY
160
120
80
40
0
-40
-80
-120
-160
1 3 5 7 9 11 13 15 17 19 21
DIMENSIONLESS WIDTH (Y=Y/D)

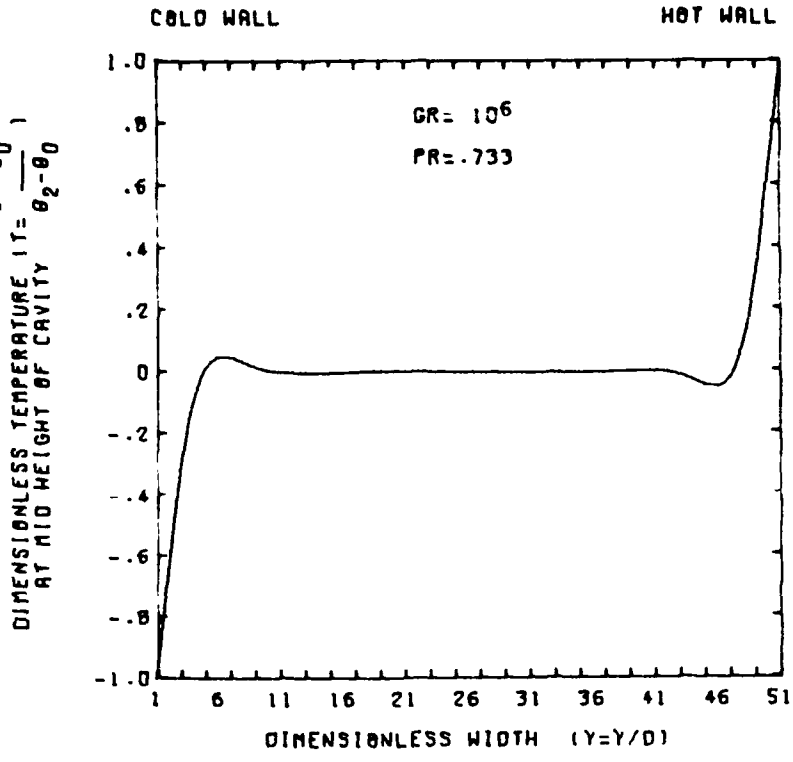
COLD WALL
HOT WALL
GR= 10^6
PR=.733
DIMENSIONLESS TEMPERATURE (T= (θ -θ0)/(θ2-θ0))
AT MID HEIGHT OF CAVITY
1.0
.8
.6
.4
.2
0
-.2
-.4
-.6
-.8
-1.0
1
6
11
16
21
26
31
36
41
46
51
DIMENSIONLESS WIDTH (Y=Y/D)

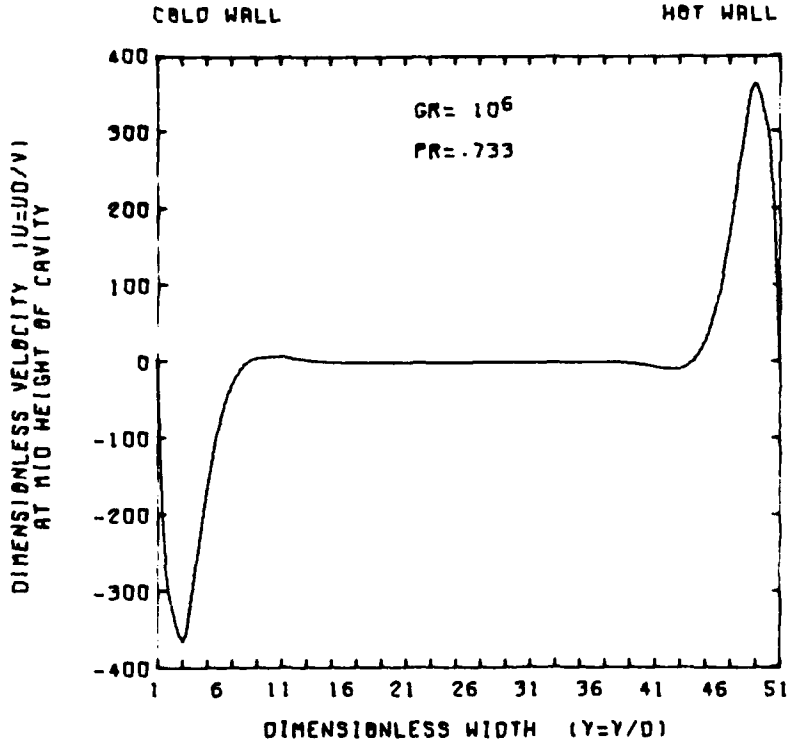
COLD WALL
HOT WALL
GR= 10^6
PR=.733
DIMENSIONLESS VELOCITY (U=UD/V)
AT MID HEIGHT OF CAVITY
400
300
200
100
0
-100
-200
-300
-400
1
6
11
16
21
26
31
36
41
46
51
DIMENSIONLESS WIDTH (Y=Y/D)

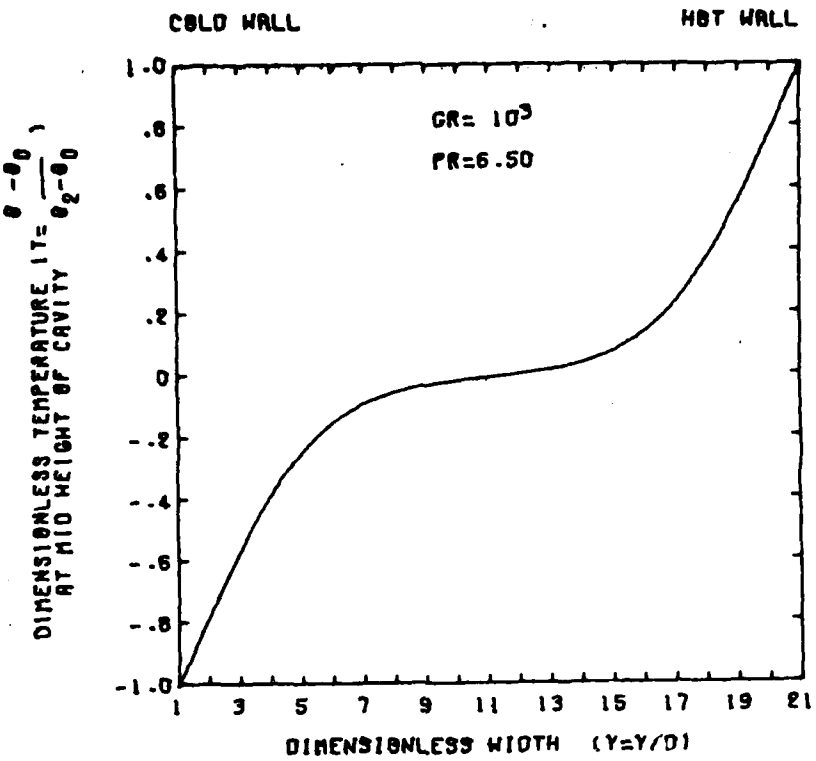
COLD WALL
HOT WALL
GR= 10^3
PR=6.50
DIMENSIONLESS TEMPERATURE ($\theta=\frac{\theta-\theta_0}{\theta_2-\theta_0}$) AT MID HEIGHT OF CAVITY
1.0
.8
.6
.4
.2
0
-.2
-.4
-.6
-.8
-1.0
1 3 5 7 9 11 13 15 17 19 21
DIMENSIONLESS WIDTH (Y=Y/D)

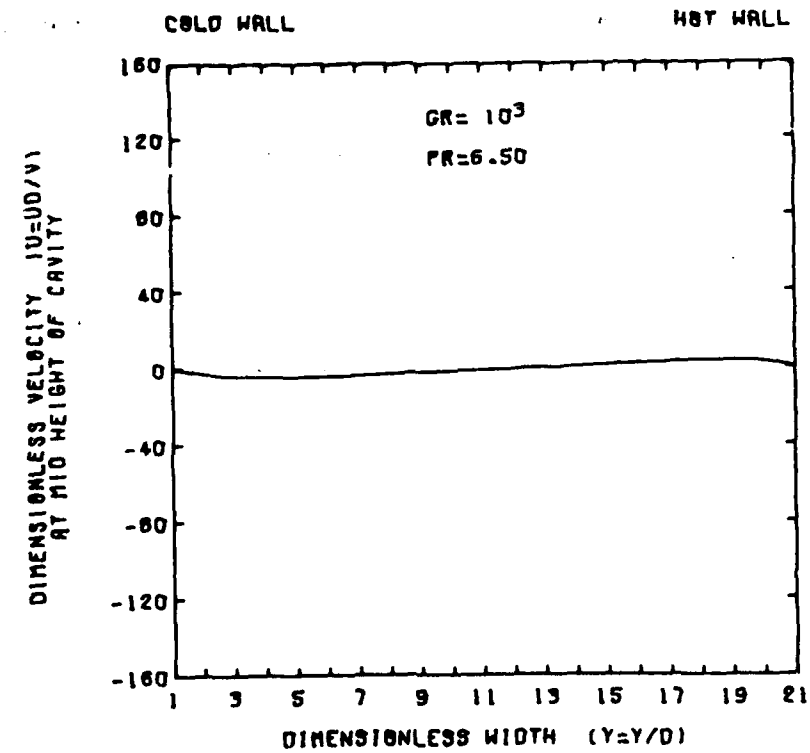
COLD WALL
HOT WALL
GR= 10^3
PR=6.50
DIMENSIONLESS VELOCITY (U=UD/V) AT MID HEIGHT OF CAVITY
160
120
80
40
0
-40
-80
-120
-160
1 3 5 7 9 11 13 15 17 19 21
DIMENSIONLESS WIDTH (Y=Y/D)

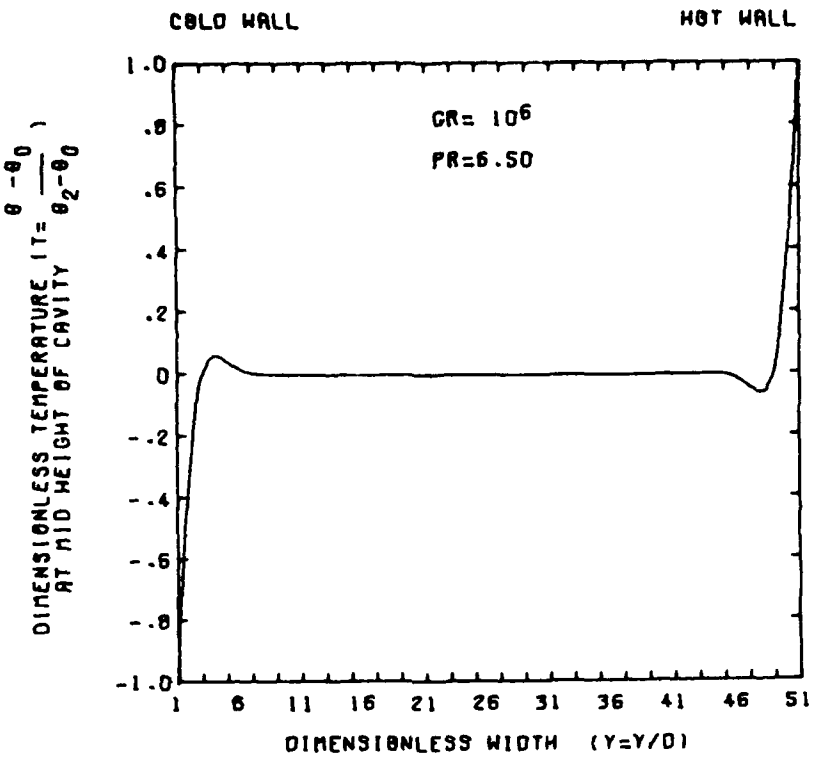
COLD WALL
HOT WALL
DIMENSIONLESS TEMPERATURE (T= θ -θ0 / θ2-θ0)
AT MID HEIGHT OF CAVITY
GR= 10^6
PR=6.50
1.0
.8
.6
.4
.2
0
-.2
-.4
-.6
-.8
-1.0
1
6
11
16
21
26
31
36
41
46
51
DIMENSIONLESS WIDTH (Y=Y/D)

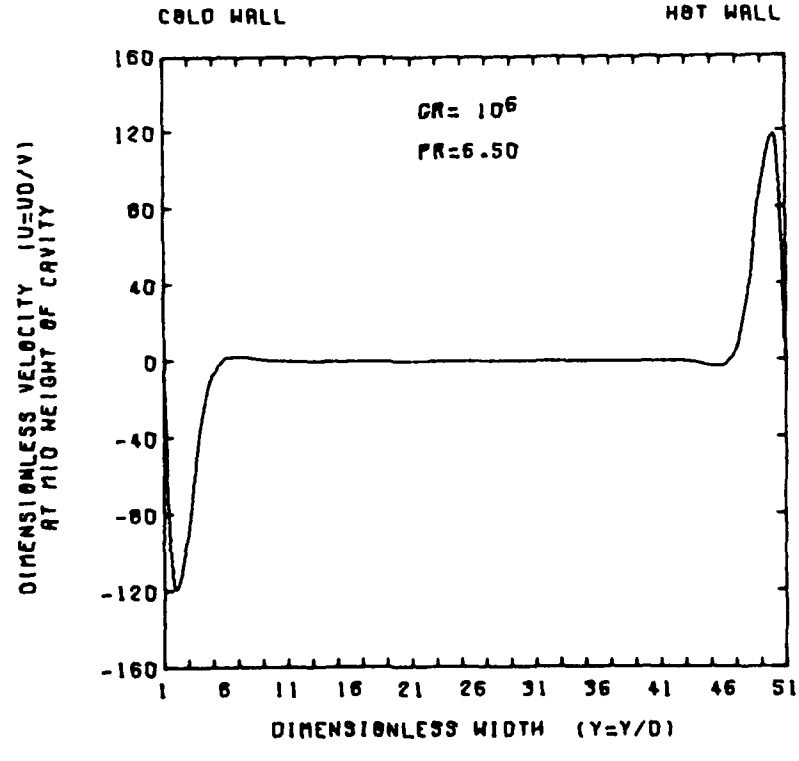
COLD WALL
HOT WALL
DIMENSIONLESS VELOCITY (U=UD/V)
AT MID HEIGHT OF CAVITY
GR= 10^6
PR=6.50
160
120
80
40
0
-40
-80
-120
-160
1
6
11
16
21
26
31
36
41
46
51
DIMENSIONLESS WIDTH (Y=Y/D)

in order to show dynamic similarity of the flows in each.

The Rockett and Torrance studies were carried out mainly in the laminar flow range. Only one of their numerical simulations was made in the turbulent range and it is difficult to judge how close an agreement was obtained between experiment and theory. Thus, the question remains as to the real necessity of having similar Pr and Gr numbers between small scale model and full sized room, in the turbulent range of convection.

An approximate analysis for the turbulent region can be made by a von-Karman-type solution as was done by Eckert and Jackson [11]. They analyzed the experimental data of Griffiths and Davis [12] and found that the velocity and temperature profile of the turbulent natural convection boundary layer along a heated vertical flat plate can be expressed by the following equations:

$$U = U_1 \left(\frac{y}{\delta}\right)^{1/7} \left(1 - \frac{y}{\delta}\right)^4$$

$$\theta = \Theta \left(1 - \frac{y}{\delta}\right)$$

where

$$U_1 = 1.185 \frac{\nu}{x} (Gr)^{1/2} \left(1 + 0.0494 (Pr)^{2/3}\right)^{-1/2}$$

$$\delta = 0.565 \, x \, (Gr)^{-0.1} (Pr)^{-8/15} \left(1 + 0.0494 (Pr)^{2/3}\right)^{-1/2}$$

y is the coordinate perpendicular to the plate

x is the coordinate parallel to the plate

Θ is the temperature difference between the wall and the free stream

δ is the boundary layer thickness at x.

In order to examine the combined effect of U_1 and δ, the net total flow may be calculated as follows:

$$\rho\, U_1 \int_0^{\delta} \left(\frac{Y}{\delta}\right)^{1/7} \left(1 - \frac{Y}{\delta}\right)^{4} dy$$

Making use of the dimensionless notations introduced previously a dimensionless total flow, q, can be defined as

$$q = \int_0^{\infty} UdY = C_1\ (Gr)^{0.4}\ (Pr)^{-8/15}\ (1 + 0.0494\ Pr^{2/3})^{-0.4}$$

where C_1 is a constant and its exact value is not important for this discussion.

A similar relation for the laminar boundary layer flow or for the convection with the low Grashof number is

$$q = \int UdY = C_2\ (1 + 1.05\ Pr)^{-0.25}\ (Pr)^{-0.5}\ (Gr)^{0.25}$$

A calculation was then made to check the influence of the Prandtl number on the flow in a rectangular cavity. When these net flow parameters were evaluated at the laminar Grashof number, the overall flow rate for Pr = 0.7 was found to be 4.44 times as much as that for Pr = 7.0. While at a turbulent flow condition the overall flow rate for Pr = 0.7 was 3.55 times as much as for Pr = 7.0.

This analysis, therefore, indicates that the Prandtl number dependence on the convection flow pattern is still very strong in a condition of turbulent boundary layer flow and high Grashof number.

3. Experimental Apparatus

A steel pressure chamber was constructed, to contain high temperature water, as shown schematically in figure 13. The overall dimensions were 20" long by 12" in diameter. The viewing window was of tempered plate glass 3/4" thick and 8" in diameter. The lighting port at top was 1" wide and 10" long.

Figure 14 is a schematic of the modeling enclosure which was located inside the chamber. It was a rectangular parallelepiped 6" x 6" x 18" with the front end open for observing the flow. It was made of 1/8" thick copper faced with black anodized aluminum plates to provide good contrast in photographs. A slit was cut in the ceiling of the model, in line with the lighting port of the chamber, and fitted with a glass for passing light to the interior. On the floor of the enclosure, also in line with the lighting port in the outer chamber, was located a mirror to increase illumination. On the outside of the enclosure serpentine coils were soldered to the walls and floor for circulating water to allow individual control of surface temperature.

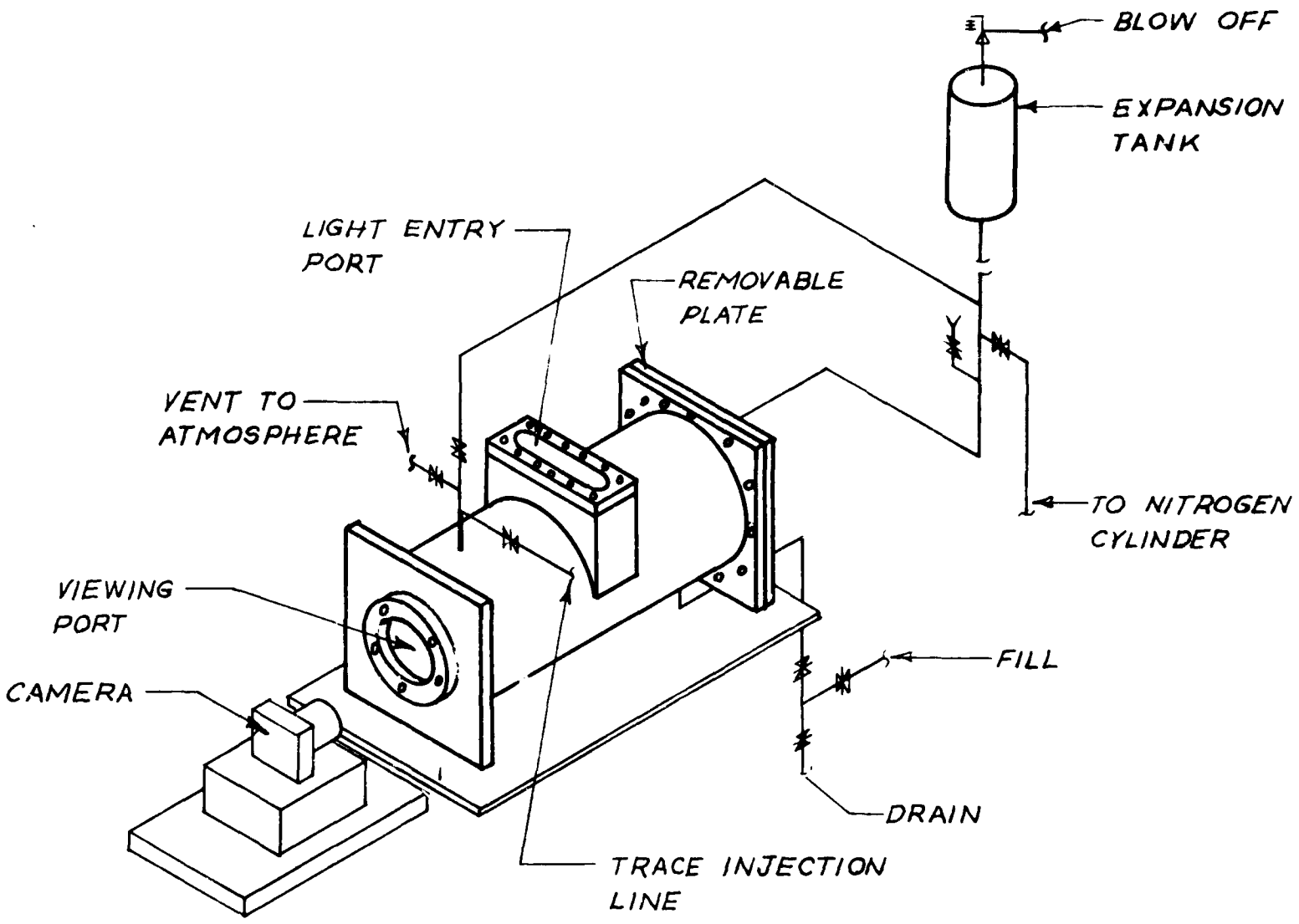

Figure 13 Schematic of Pressure Chamber for Modified Enclosure

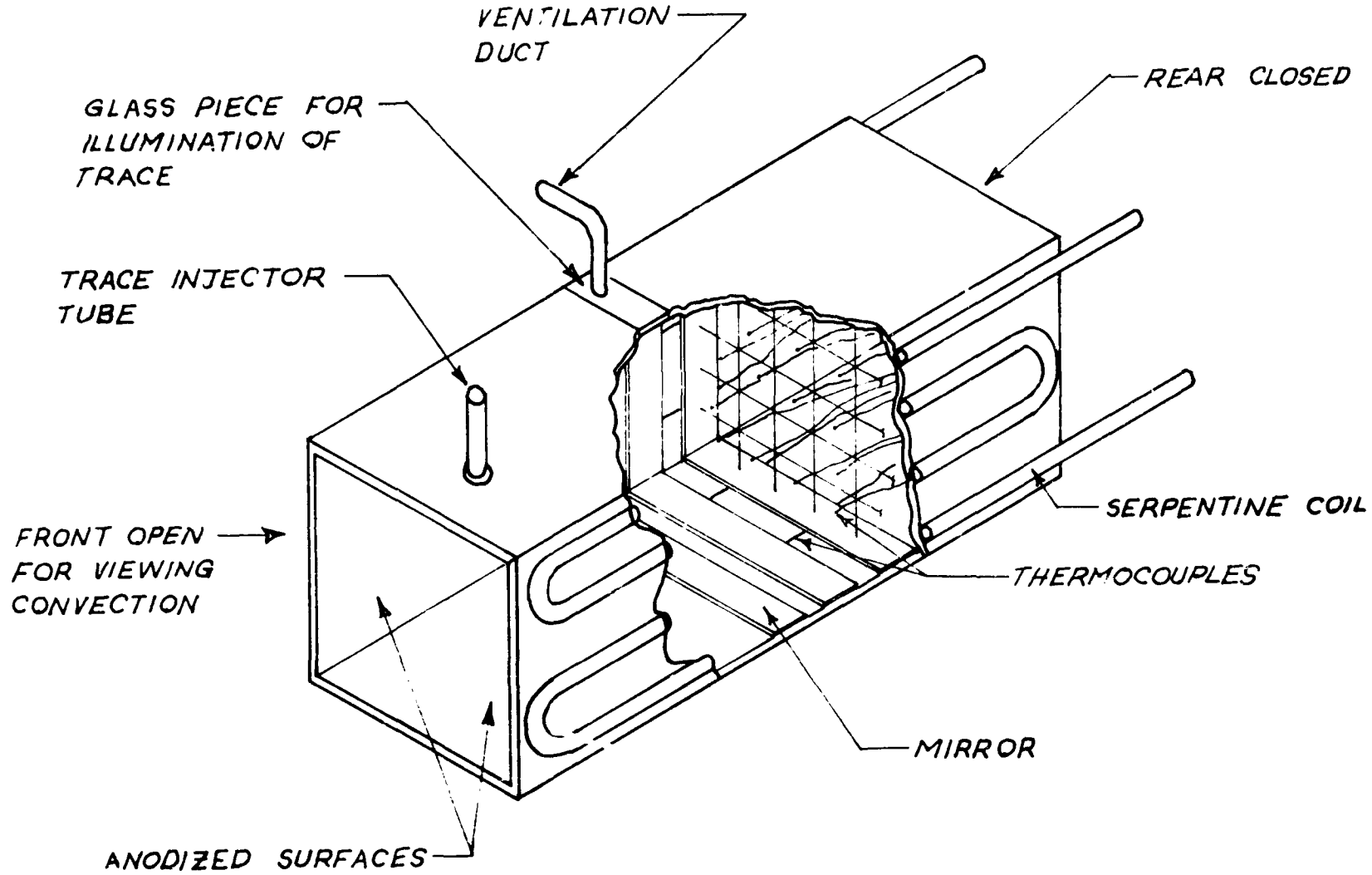

Figure 14 SCHEMATIC OF MODELING ENCLOSURE

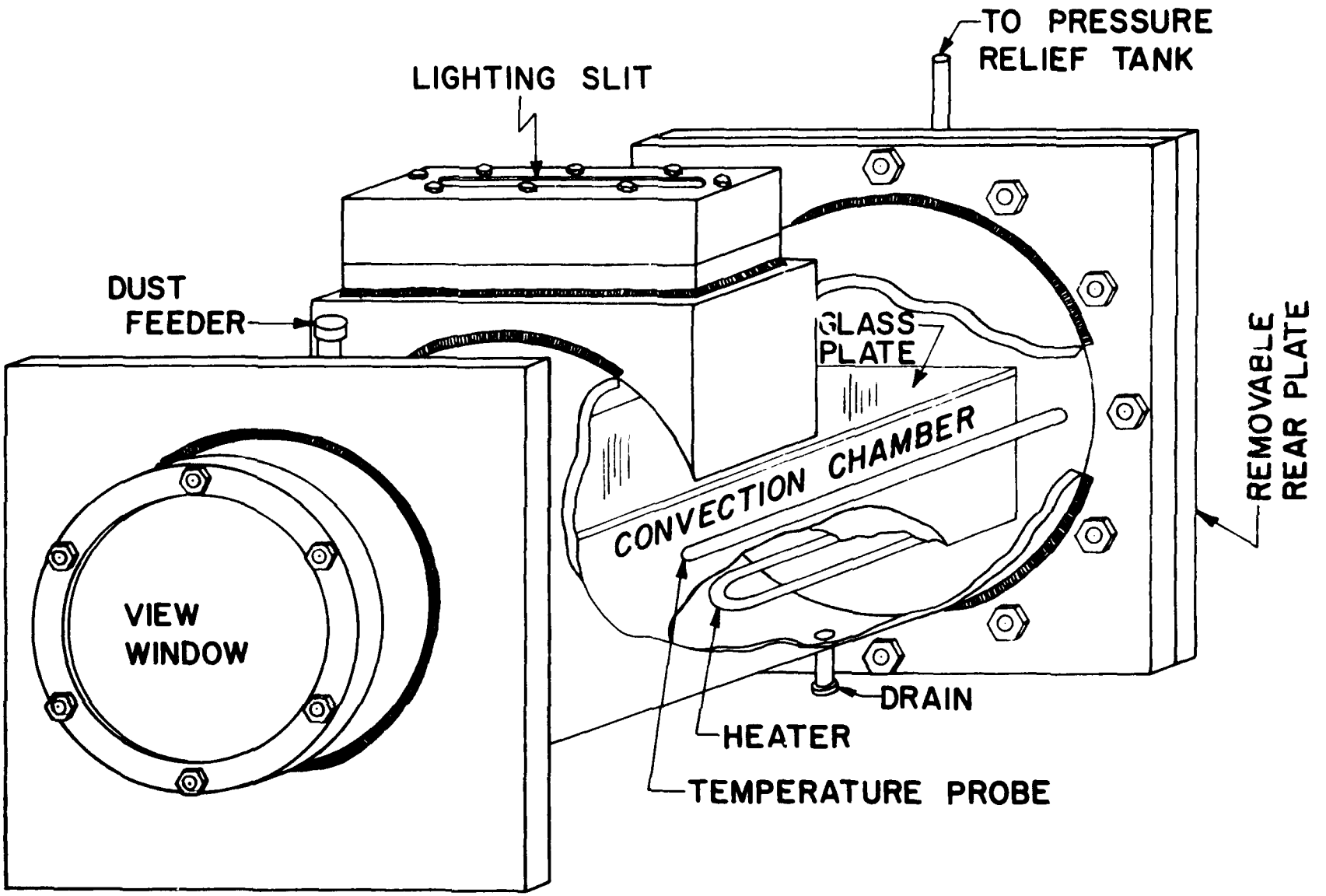

Figure 15 Schematic of Modeling Enclosure Inside the Pressure Chamber

In figure 14 thermocouples are shown behind the light slot, that is, toward the rear of the model farthest from the viewing window. Eight thermocouples were held against the surfaces, two on each of the four surfaces. Sixteen of them were held away from the walls, positioned in a grid to measure the fluid temperature, and two were used to measure the temperature of water in the two ventilation ducts. The temperatures were read by an indicating potentiometer. The thermocouple leads were 40-gage copper-constantan wire jacketed in a stainless steel tube. They entered the chamber through a pressure fitting in the removable rear plate.

Figure 15 shows the enclosure as it fit inside the pressure chamber. Figure 16 is a schematic showing the heat exchange system used to provide hot water to the serpentine coils and to the natural ventilation heat exchanger. The modeling enclosure was ventilated naturally by a supply-and-return duct. These ducts were connected to the natural ventilation heat exchanger and entered the top of the modeling enclosure through the light entry port. They were used to simulate the exchange of fluid with an external environment. The portion of both ducts directly above the light entry port was made of glass tubing to minimize shadows in the modeling area.

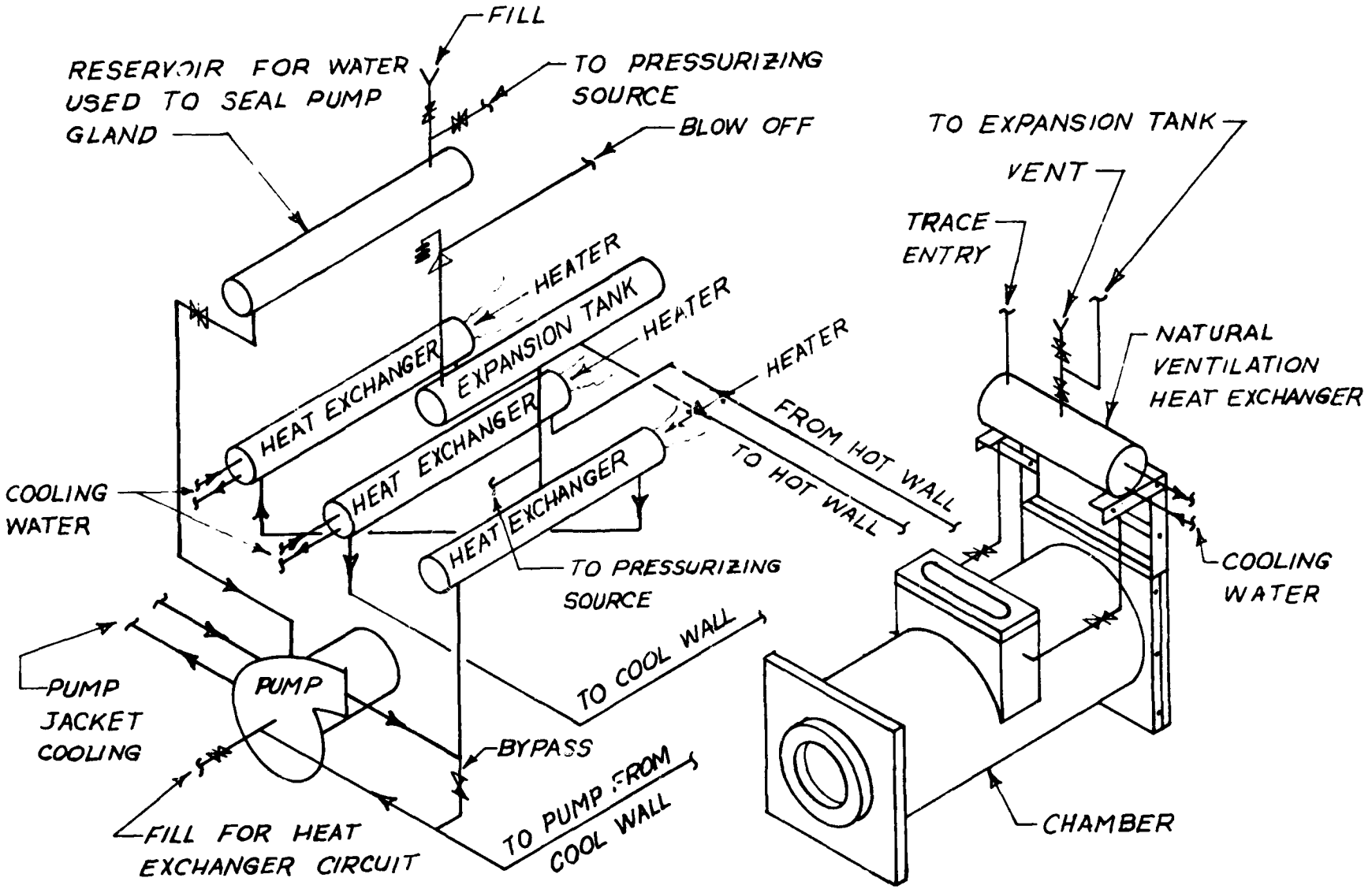

Figure 16 Schematic of Heat Exchange System

A rust inhibitor, sodium chromate, was added to the water in the chamber. About 0.8 oz. was used normally. The chromate added a yellowish cast to the water, but this was not objectionable since it did not seem to impair the quality of the photographs until the temperature rose above 300 °F. Above 300 °F the water became a rather reddish brown color and was too cloudy for good photographs. (Sodium chromate should be handled with caution because it is quite toxic.)

The tracer particles were small aluminum flakes ($\approx 4 \times 3 \times 10\ \mu$) which had been sifted through a 325 mesh during manufacture. A coating of styric acid for lubrication was applied to the flakes. The tracer injector is shown in the schematic in figure 17. This device was needed because the tracer particles had to be injected at a pressure slightly above that of the chamber. The injector was designed so that the pressurizing gas was not carried into the chamber with the tracer since this would cause bubbles which would impair the photographic results.

The simulated occupant, which can be seen in the photographs toward the end of the Results Section, contained a heating element which was used to maintain its surface temperature above that of the surrounding water.

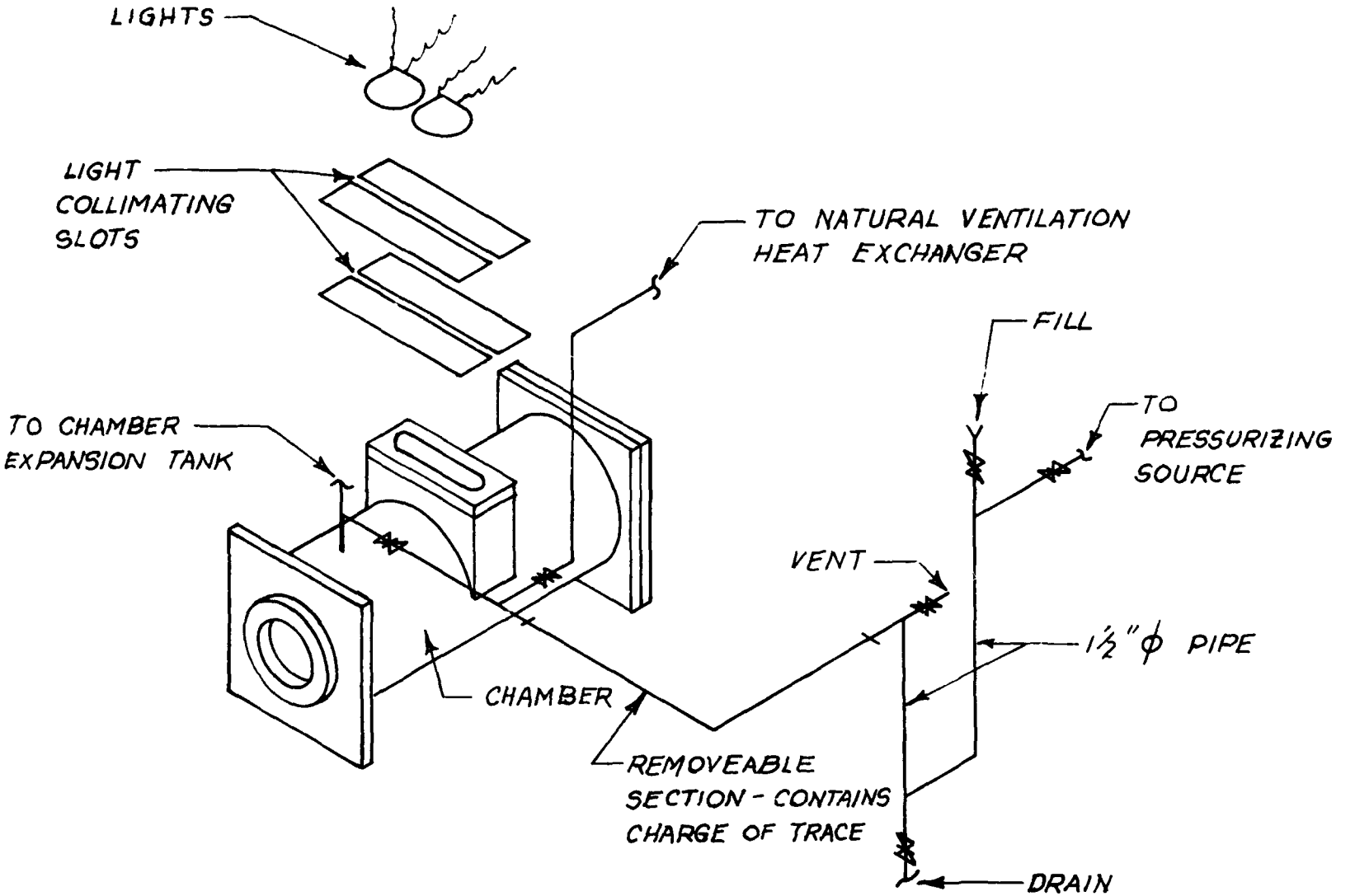

Figure 17 Schematic of Lighting Arrangement and Trace Injector System

The lighting equipment is also shown in the schematic on figure 17. The lights were high-intensity photo flood lights. Variable voltage transformers controlled the power to the lights. Ammeters were placed in the lighting circuits so that identical intensity levels could be repeated during photographic sessions. The collimating slits shown between the lights and the light entry port on the chamber were adjustable in width and in vertical position. A 1/2" slit width usually provided adequate illumination in the model.

The camera shown in figure 13 was mounted on a base having three degrees of freedom for proper position and focusing. The camera had an f2.8, 100 mm lens. The back was detachable so that a ground glass focusing screen, a roll film back, or a Polaroid back could be used. The roll film used was 120 Tri-X-Pan film.

4. Experimental Procedure

As a first step the entire chamber was flushed with water. The modeling area, especially, was cleaned of aluminum particles used during the previous test. The flushing removed not only the trace particles but also the cloudiness due to rusting which was present after each test. Often three or four flushings were required to thoroughly clean the chamber The viewing window, the light entry slot at the top of the modeling area, and the light entry port at the top of the chamber were cleaned with an ordinary glass cleaning compound.

The apparatus was designed so that the majority of the necessary changes within the model could be made through the front viewing port which was easily removed. Most of these changes involved varying the positions of the ventilation ducts and installing simulated occupants.

After the last flushing the chamber was sealed, and hot water added through the fill line. Hot water was used because less time was then needed to reach normal operating conditions, and the hot water usually contained less dissolved air. Sodium chromate was added to this water.

Once the chamber was filled, the pump and the heaters were turned on to bring the water in the chamber to operating temperature. By the time the water in the model reached 205 °F, or slightly below boiling, the air originally dissolved in the water would have escaped from the water and would have to be vented. Above 205 °F the chamber would be pressurized to about 20 psig above the saturation pressure. Insulation was placed over the front viewing window to minimize the three-dimensional convection in the cavity.

As the water in the chamber was heated to operating conditions, the clarity of the water was checked. If the chamber was not flushed adequately or if boiling occurred, there would occur a cloudiness which would become so dense that photographs could not be taken. In such a case the test would be abandoned.

Temperature recordings were taken every half hour prior to and throughout the photographic session. Photographs were taken when it appeared from the temperature recordings that the conditions were relatively stable, that is a drift of less than one degree per hour.

The camera was positioned in front of the viewing port and the trace particles were injected. The injector pressure had to be above the chamber pressure. The trace-injector valve was opened slightly to permit a small steady stream of particles to enter the modeling area. Great care was taken to regulate the rate of entry. If too much trace had been permitted to enter, the glass on top of the illuminated area might very well have been entirely covered with aluminum, blocking the light from above and forcing abandonment of the test. The trace was injected until it was sufficiently distributed throughout the chamber.

The camera was focused on the particles in the illuminated area. To obtain the sharpest image the camera was first focused at widest aperture then stopped down to normal shooting aperture. Sufficient time (no less than 25 minutes) was allowed for the disturbance caused by the trace injection to die out before photographs were taken. Exposure time, light intensity, and aperture settings for photographs were determined by trial and error. Variation of these three parameters usually produced at least three out of ten usable exposures. The lights were raised to maximum intensity as quickly as possible during the last second of the exposure. This caused a bright dot to appear on one end of the trace image, and thus direction of flow could be denoted. The time was recorded at the completion of each exposure.

The film was developed as soon as possible after making the exposures in order to preserve the sharpest image. A high acutance developer (Rodinal) was used because the softer working developers do not produce streaks of sufficient definition. A high-contrast grade of printing paper (Agfa Brovia No. 6) was used for best results, and the paper developer (Dektol) was used in concentrated form to further increase the contrast.

About five hours were usually required to complete a run at one test condition.

5. Experimental Results

The basic convection producing mechanisms which influenced the heated water were (1) a temperature difference between opposite walls of the model, (2) a simulated occupant whose temperature was above that of the chamber, and (3) natural ventilation due to a temperature difference between the water outside and inside the chamber. The tests have been segregated into four basic conditions which are as follows:

Condition I : A chamber without ventilation or simulated occupant

Condition II : A chamber with natural ventilation but without simulated occupant(s)

Condition III: A chamber without natural ventilation but with simulated occupant(s)

Condition IV : A chamber with natural ventilation and with simulated occupant(s)

The results of the tests are presented in the following format: a narrative description of the fluid motion, a photograph of the flow, a schematic of the flow pattern shown in the photograph, and a figure showing the temperatures at specific locations recorded during the test.

In all of the photographs of the flow patterns four vertical and four horizontal lines appear. This was the wire grid used to support the thermocouples. The grid was located about four inches behind the illuminated area; one thermocouple was fastened to each intersection. The thermocouples extended beyond the grid to a location immediately to the rear of the illuminated area. In many photographs two bright lines appear to be going into the ceiling. These were the thermocouples used to measure the ventilation supply and return temperatures.

All temperatures shown on the following figures are in degrees Fahrenheit.

Condition I

Natural convection was induced only by a temperature difference between the walls, the right wall was maintained at a warmer temperature than the left, giving a counter-clockwise rotation in the modeling area. Test results representative of Condition I are shown in figures 18-23.

The flow patterns (figures 19 and 22) due to the ΔT between the walls were dependent on the water temperature and the magnitude of the ΔT between the walls. Two water temperatures were considered for this situation--124 °F and 250 °F. A counter-clockwise vortex appeared in the bottom right corner at both of these temperatures. The flow from bottom to top occurred entirely in the right wall boundary layer. The interior flow pattern of the 250 °F test consisted mostly of horizontal motion while the interior flow pattern for the 124 °F test was primarily vertical from top to bottom. For the 250 °F case this flow appeared to originate in the downward-moving left wall boundary layer and terminated near the right wall. A vortex existed in the upper left corner. A stream originating a half inch below the ceiling in the left wall boundary layer flowed toward the right wall. This stream turned downward just before touching the right wall boundary layer and terminated in the floor boundary layer.

Condition II

Ventilation ducts were introduced into the model to produce added convection effects. The simplest duct configuration consisted of ducts at the top right and top left of the chamber. The water flowed out of the chamber through one duct, was cooled, and then returned via the other duct. Test results representative of Condition II are shown in figures 24-41.

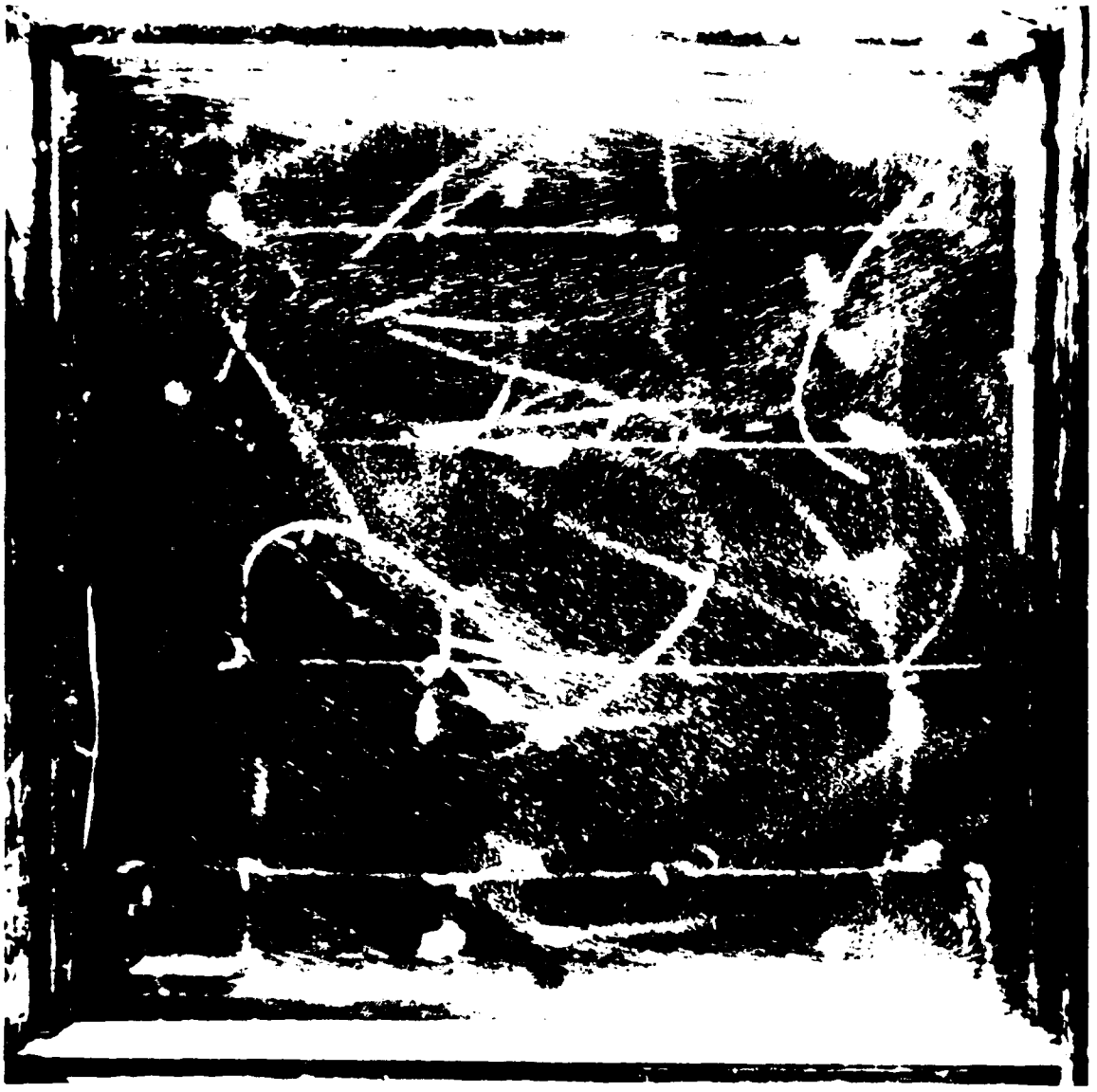

Figure 1° Photo of convection occurring in chamber with 1.. °F water and a 5 °F T between walls (Condition I)

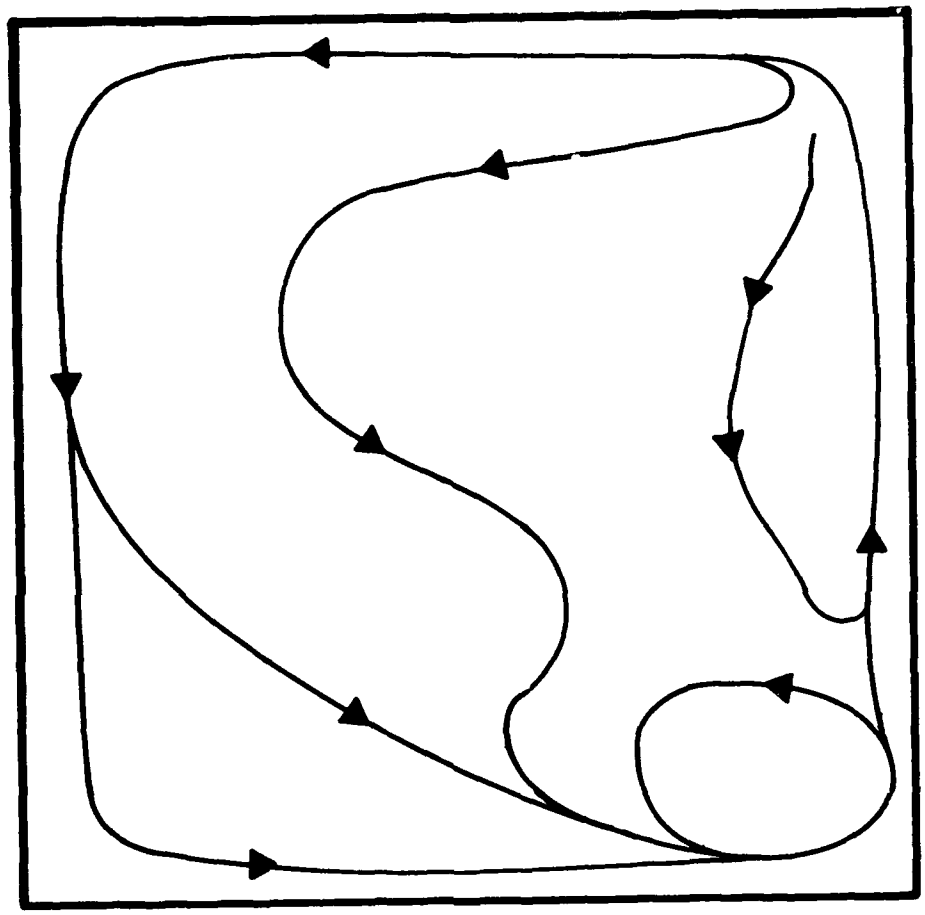

Figure 19 Schematic of flow distribution for Condition I (refer to Figure 18)

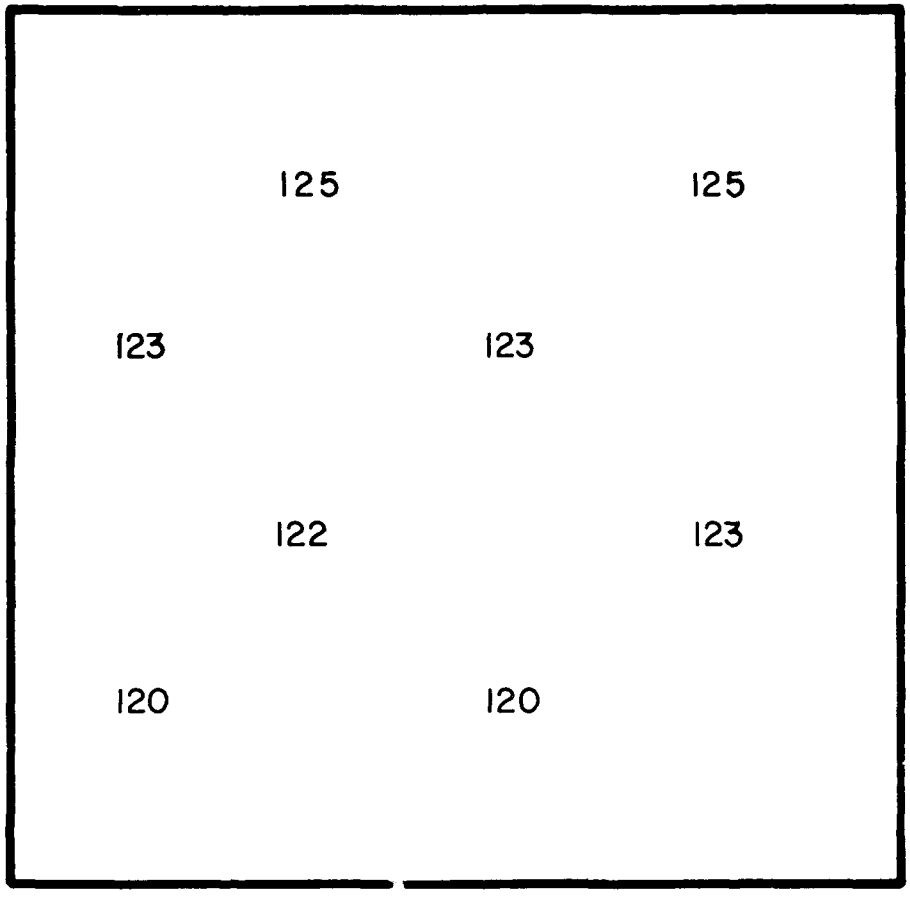

Figure 20 Temperature distribution for Condition I (refer to figure 18)

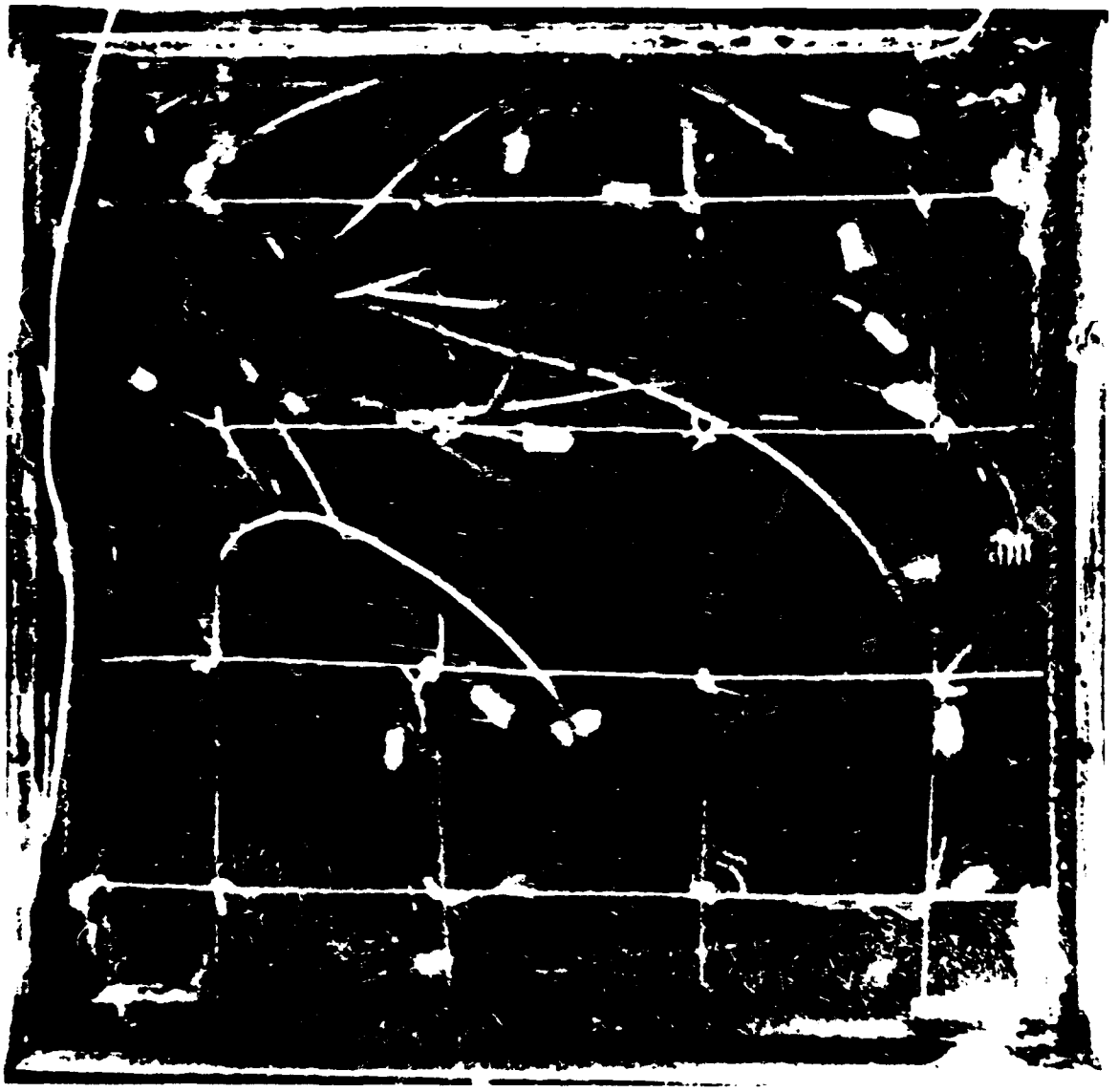

Figure 21 Photo of convection occurring in chamber with 240 °F water and a 3.4 °F T between walls (Condition I)

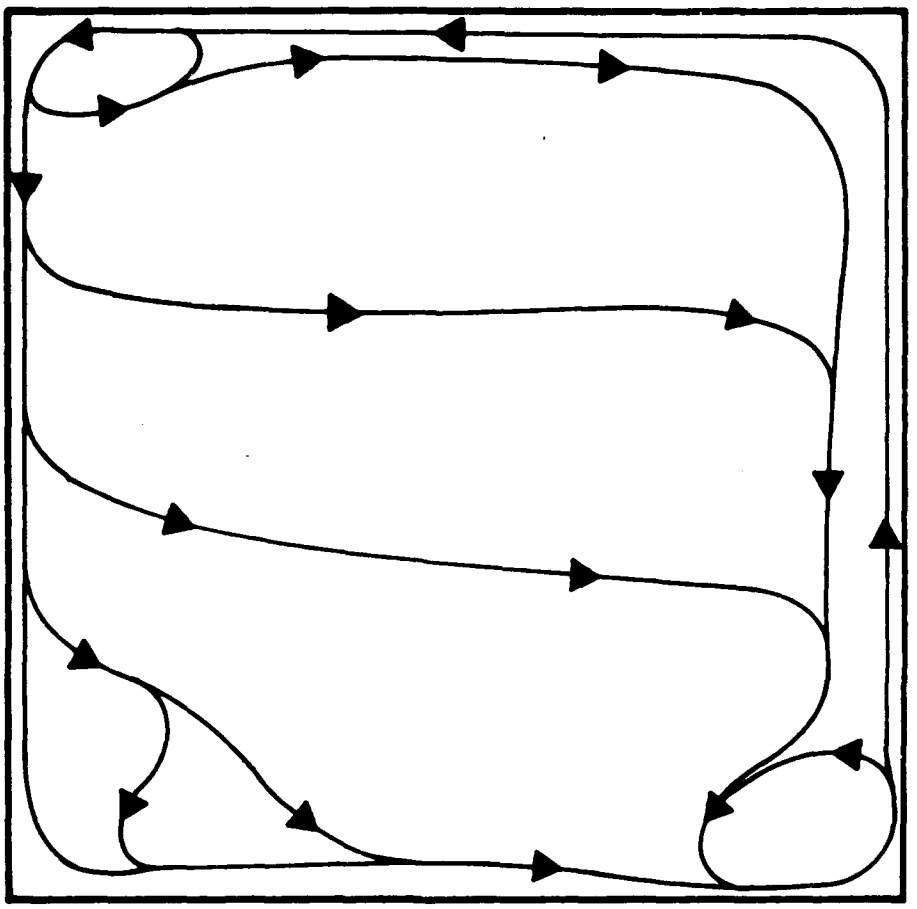

Figure 22 Schematic of flow distribution for Condition I (refer to figure 21)

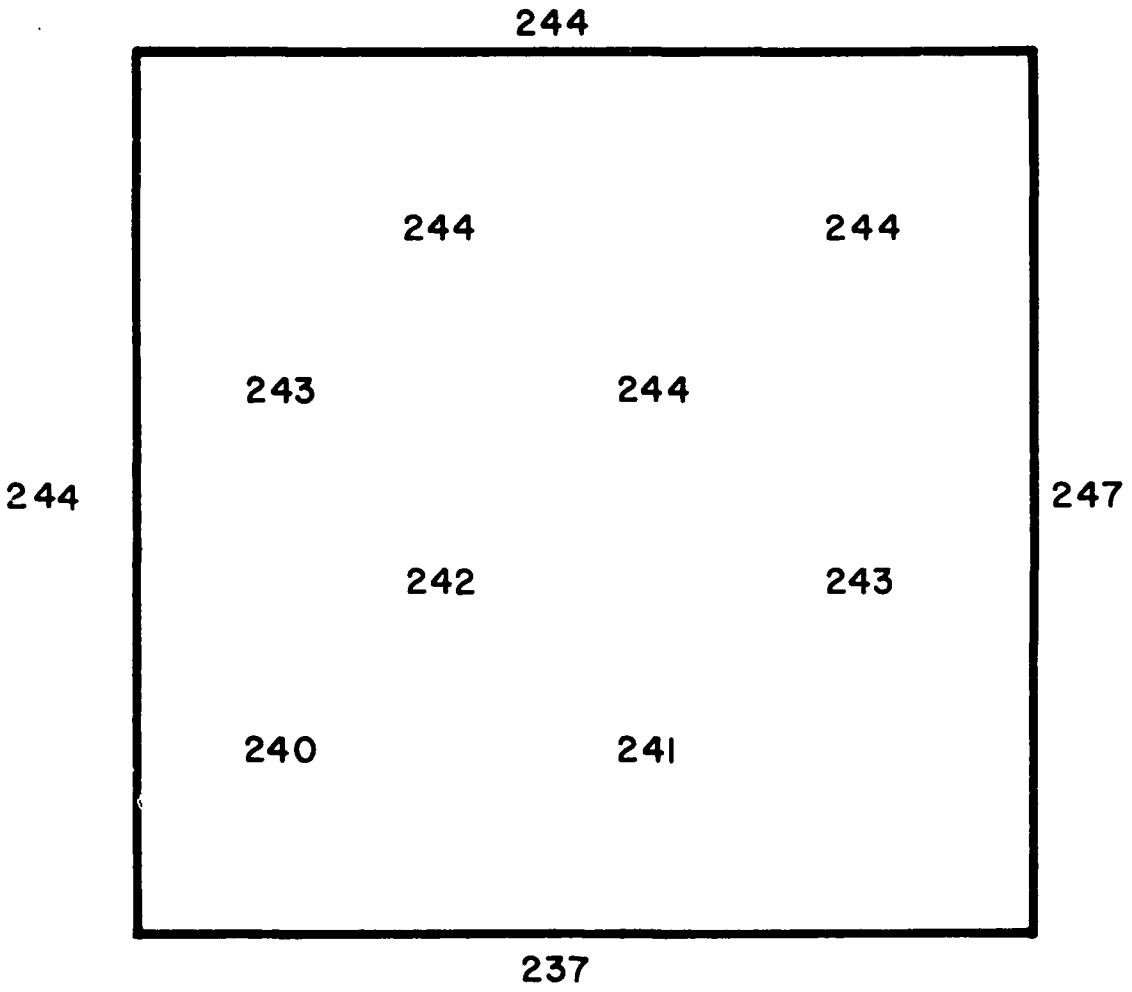

Figure 23 Temperature distribution for Condition 1 (refer to figure 21)

A characteristic flow pattern showing the streamlines for the simple duct case can be seen in figure 25. Three-dimensional effects, i.e., water flowing out of the lighted two-dimensional slice into the surrounding darkened water and vise-versa, were observed in these photographs. These three-dimensional effects appeared as sources and sinks in the photographs. In the flow-pattern drawings the sources are depicted as circles or ovals (without arrow points) and the sinks are indicated by X's. The term source implies flow into the lighted area from the surrounding water; a sink implies water flowing out of the lighted area.

With the addition of ventilation ducts the flow pattern became considerably more complicated than in the non-vented case. In this cas there was a 2 °F ΔT between the walls and a 15 °F ΔT between the water entering the modeling area through one duct and leaving through the other duct. The water entering the model flowed down along the left wall to the floor. The water then flowed out across the floor, much of it passing out of the lighted field. There appeared to be a source near the right wall approximately a third of the distance from the top of the chamber, and a sink appeared in the bottom left corner. Most of the water that left the model through the exhaust duct did not come from the lighted field. The water entering the exhaust duct was supplied by a source located at the top center of the cavity. Some of the water entering the exhaust duct was supplied by the boundary-layer flow coming up the right wall and crossing the ceiling.

Figure 24 Photo of convection in chamber with 250 °F water, a 2 °F ΔT between walls and a 16.2 °F ΔT between supply and exhaust duct (Condition II)

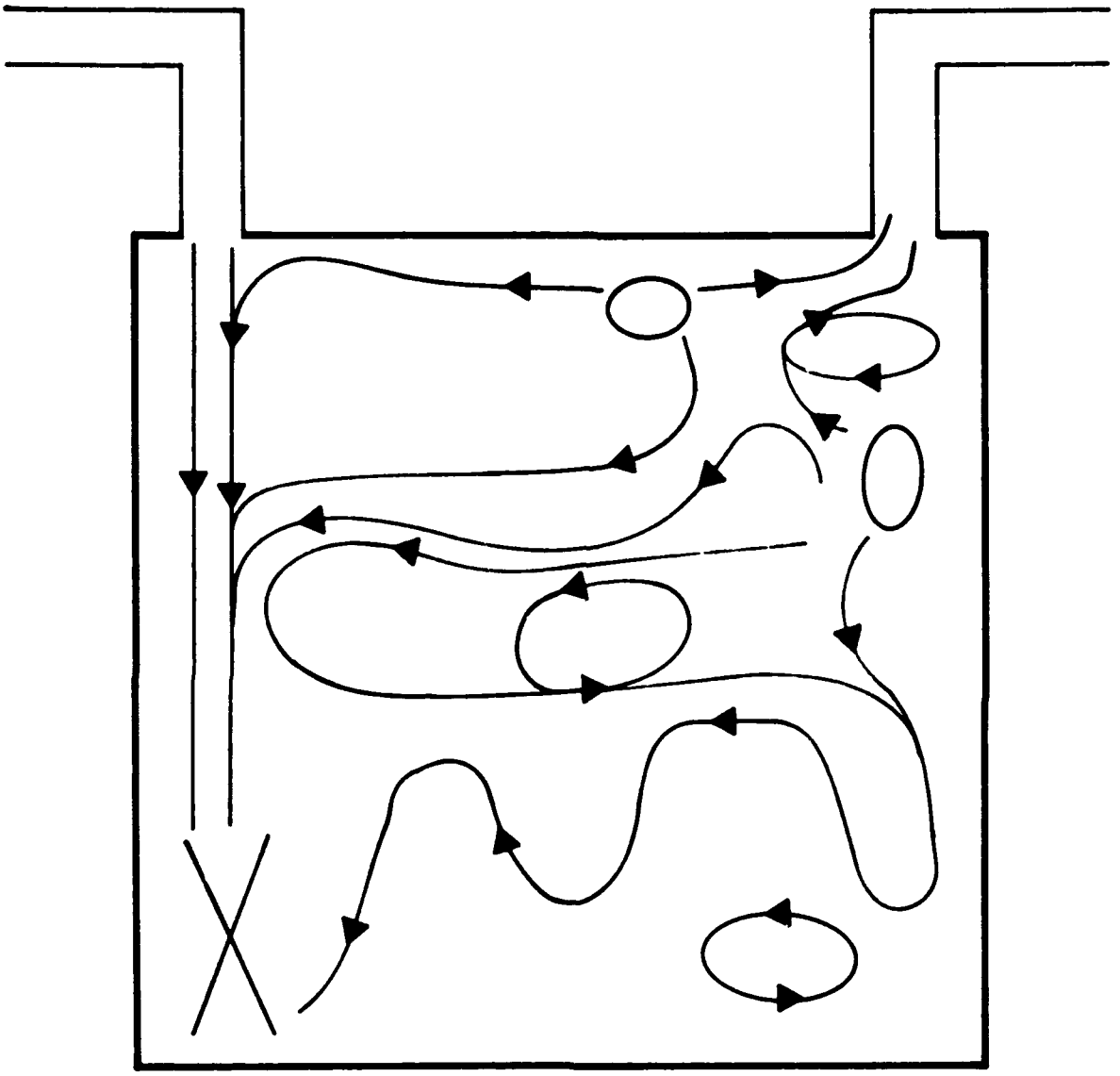

Figure 25 Schematic of flow distribution for Condition II (refer to figure 24)

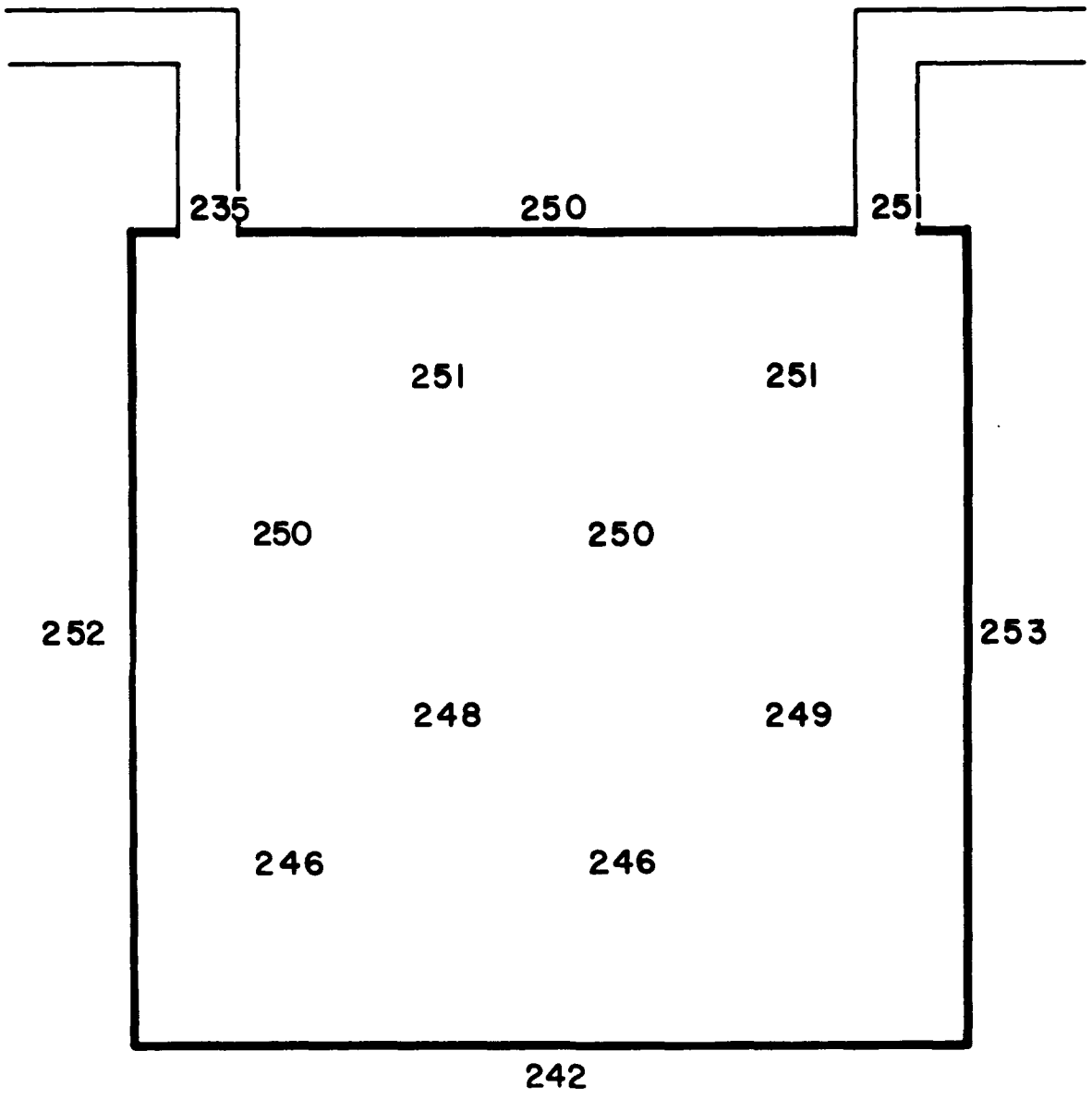

Figure 26 Temperature distribution for Condition II (refer to figure 24)

Longer ventilation ducts were installed, extending approximately one inch into the cavity. A series of three tests were conducted with these new ducts. The temperature conditions for these tests are shown in the following table.

Table No. 1

Test No.	Water Temp. (°F)	ΔT between ventilation ducts (°F)	ΔT between walls (°F)
I	250	24	4
II	250	25	2
III	300	40	2

Figure 28 is the schematic flow diagram for Test I. The flow was generally from right to left. There was a vortex in the bottom right corner and another one approximately two inches below the exhaust duct. Two sources existed: one immediately below and to the left of the exhaust duct; the other, adjacent to the right side of the supply duct. There was a sink beneath the supply duct just above the floor.

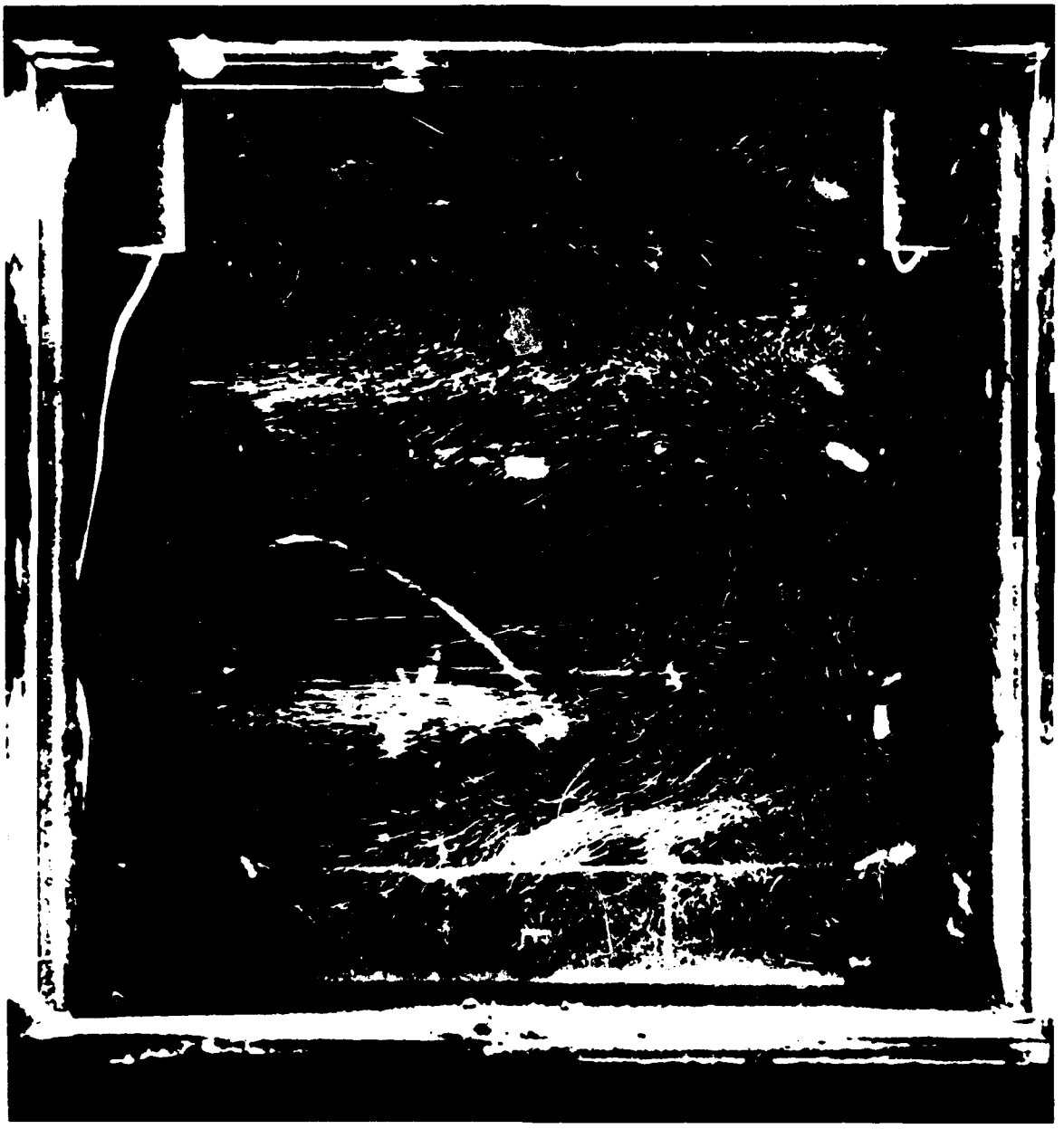

Figure 27 Photo of convection occurring in chamber with 246 °F water, a 4 °F ΔT between walls and a 22.6 °F ΔT between supply and exhaust ducts (Condition II, Test 1)

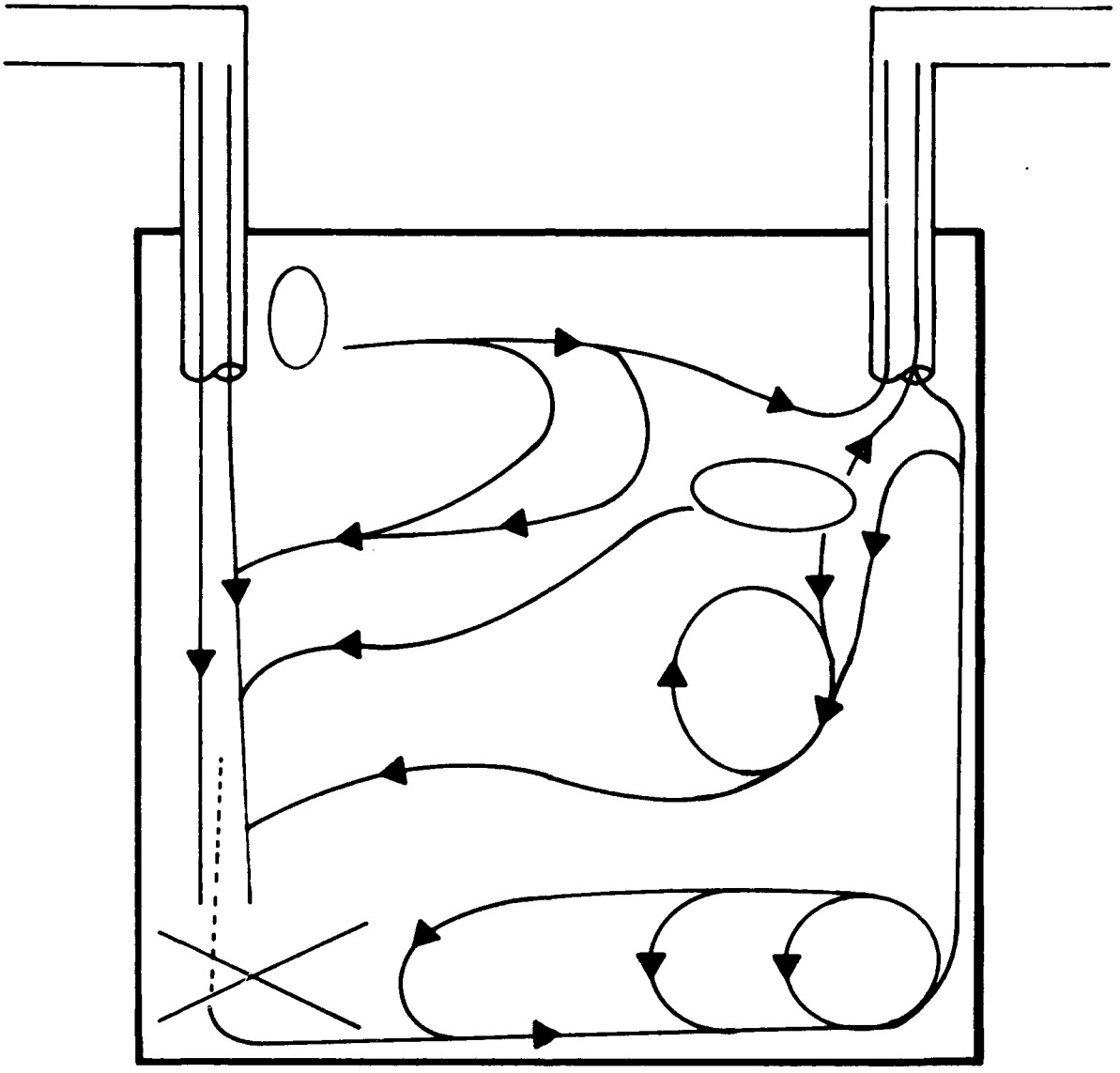

Figure 28 Schematic of flow distribution for Condition II, Test I (refer to figure 27)

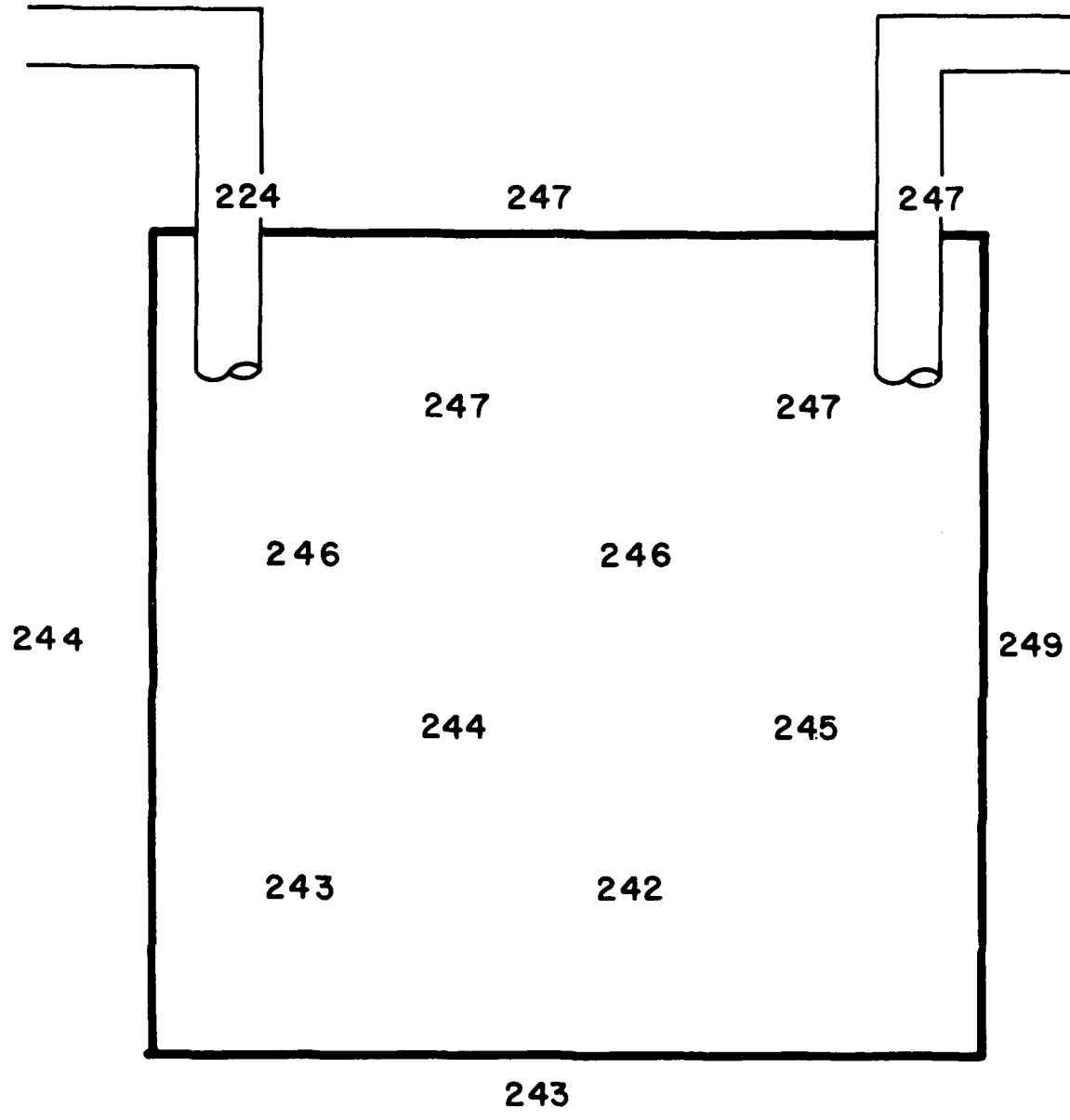

Figure 29 Temperature distribution for Condition II, Test I (refer to figure 27)

The schematic flow diagram for Test II is shown in figure 31. The flow originates from the right wall boundary layer and a source beneath and to the left of the exhaust duct. The flow from the source did not move toward the exhaust duct as one might expect, but moved directly toward the left and joined the downward flowing water leaving the supply duct. Several vortices were present in this test. These were located in the bottom right corner, at the base of the water column leaving the supply duct, and at the ceiling midway between the two ducts. All of these vortices rotated in a counter-clockwise direction.

Figure 34 is the flow diagram for Test III. The flow patterns in this test subdivided into three areas. In the upper third of the model the flow was generally from left to right. The streamlines in this upper third eventually ended at the exhaust duct. In the bottom left third of the model the flow was basically from right to left. These streams terminated in the downward flowing water from the supply duct. The flow in the bottom right third consisted of four vortices. These vortices were vertically stacked. The bottom vortex turned counter-clockwise. Each adjacent vortex had an opposite direction of spin.

Another duct configuration simply extended the length of the return duct. This added length brought the bottom of this duct to within an inch of the floor.

Figure 30 Photo of convection in chamber with 250 °F water, a 2 °F ΔT between walls and a 24 °F ΔT between supply and exhaust ducts (Condition II, Test II)

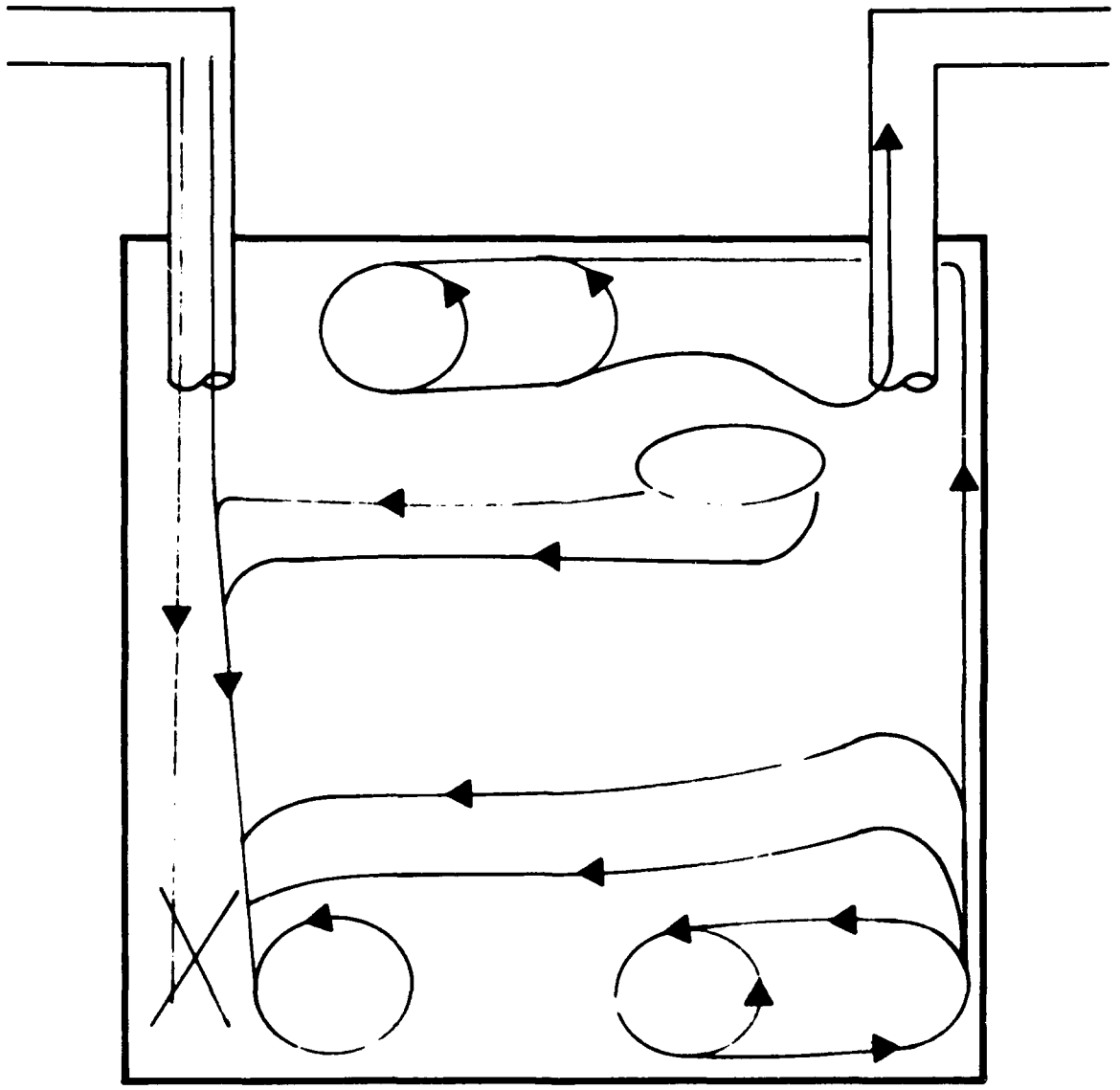

Figure 31 Schematic of flow distribution for Condition I, Test II (refer to figure 30)

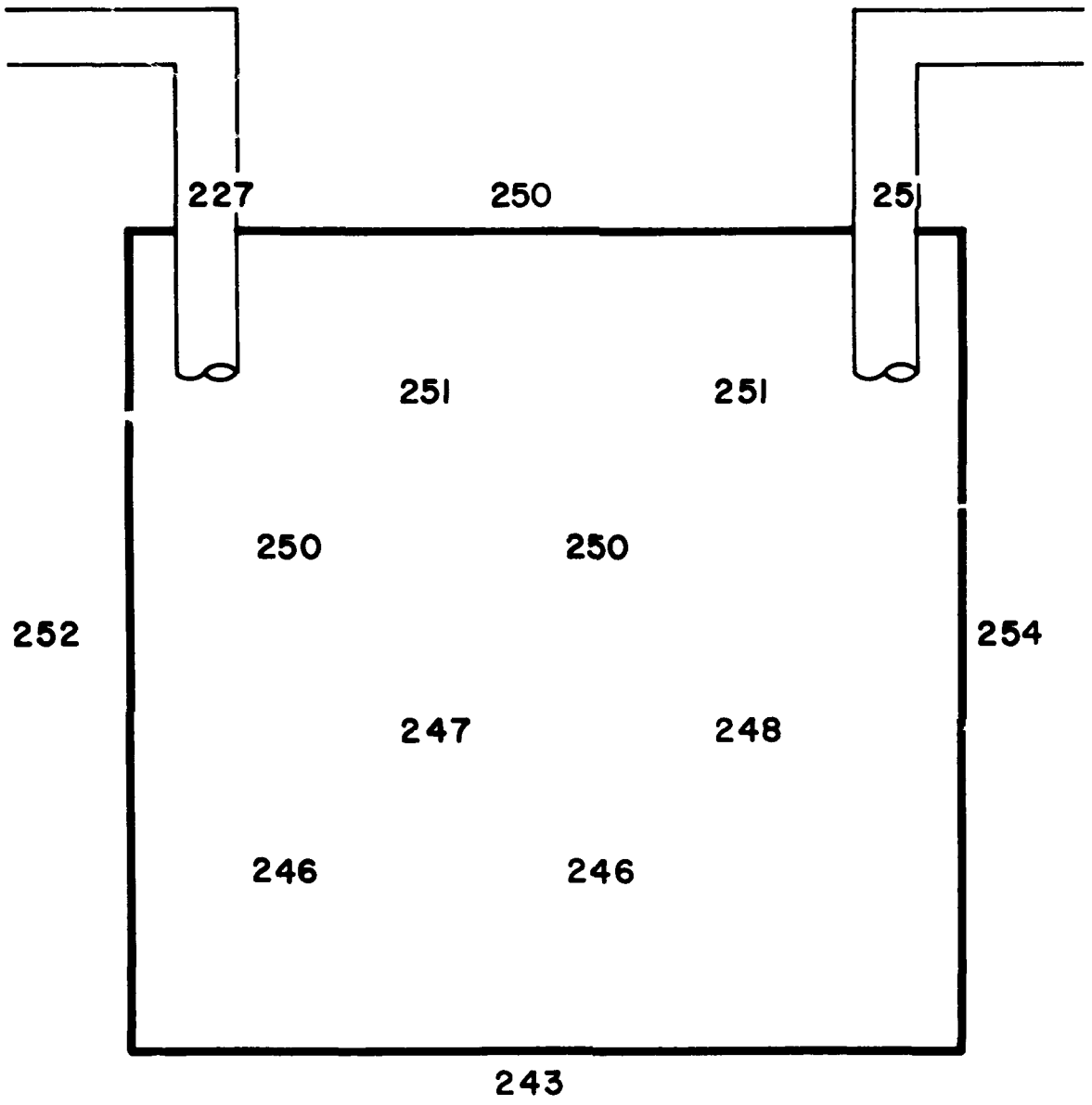

Figure 32 Temperature distribution for Condition II, Test II (refer to figure 30)

Figure 33 Photo of convection in chamber with 293 °F water, a 1.9 °F ΔT between walls and a 39 °F ΔT between supply and exhaust ducts (Condition II, Test III)

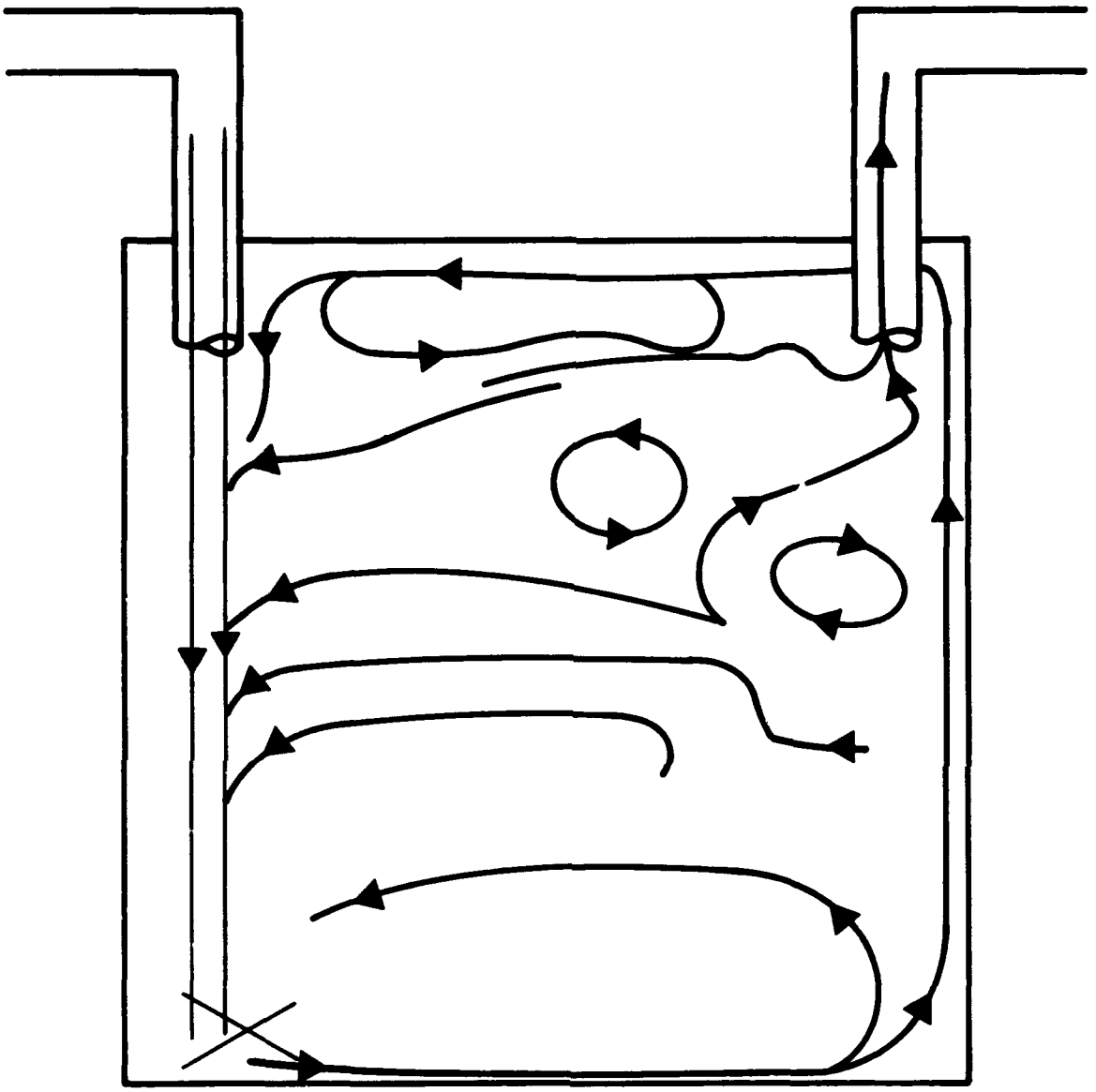

Figure 34 Schematic of flow distribution for Condition II, Test III (refer to figure 33)

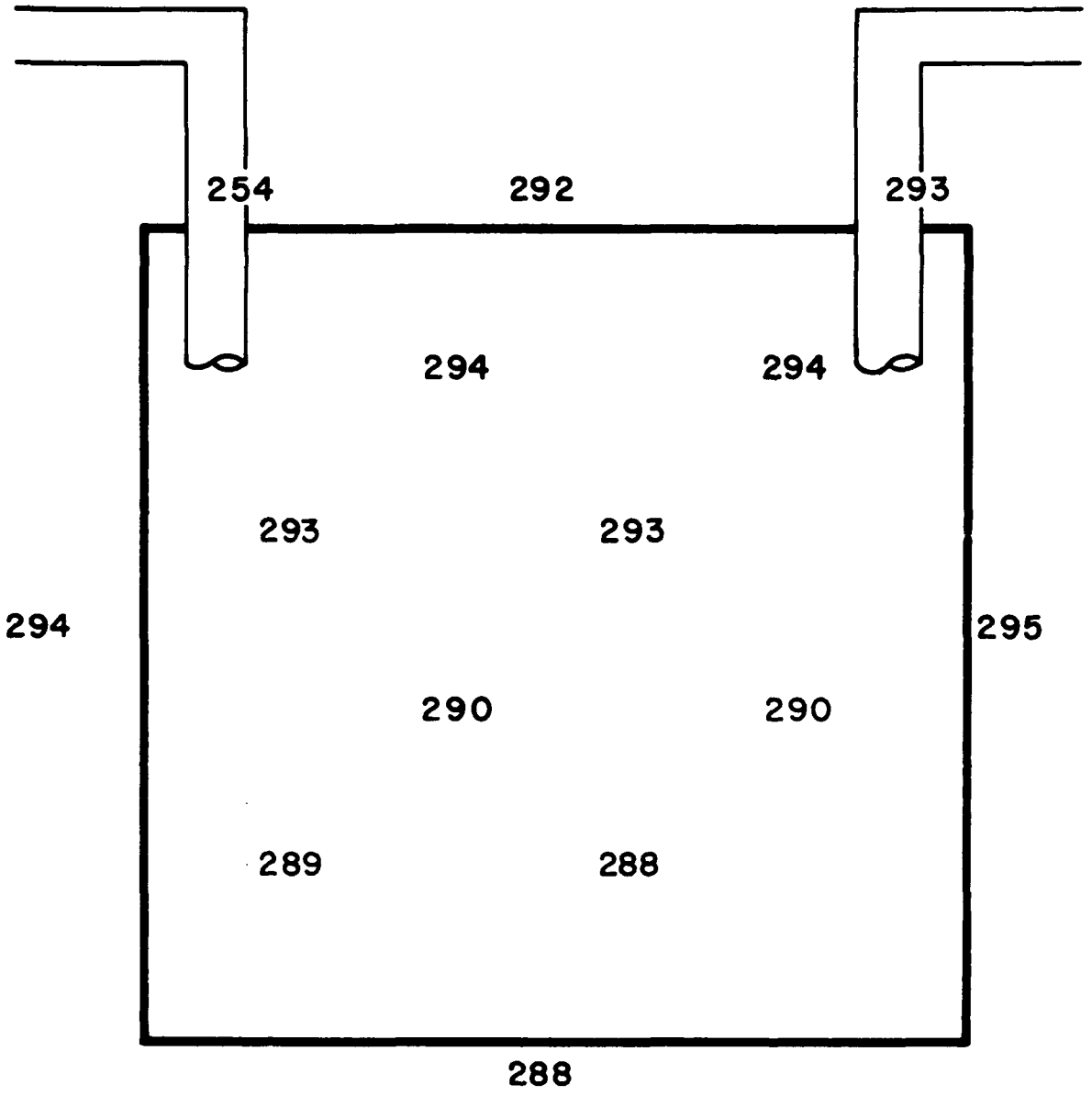

Figure 35 Temperature distribution for Condition II, Test III (refer to figure 33)

The flow shown in figure 37 was primarily from left to right. The stream originated in the left wall boundary layer and terminated in the right wall boundary layer. Deviations from this left to right flow occurred along the floor and ceiling. Approximately three quarters of an inch above the floor there was a stream moving from right to left. This stream was connected to the floor boundary layer by several downward moving streams. The upper third of the cavity mirrored the flow just described at the floor of the cavity. The volume of water moving in the upper third of the cavity was considerably greater than that moving near the floor.

One test was conducted with the ducts in the configuration shown in figure 39. Right angle elbows, aimed toward the center of the cavity, were attached to the ends of the ducts. The average water temperature was 251 °F. The ΔT between the wall surfaces was 2.5 °F, and between the convection ducts it was 15 °F. The flow pattern is shown in figure 40. The streams move primarily from top to bottom. Approximately one inch above the floor a stream which moved horizontally from left to right picked up the vertical stream. This horizontal stream terminated in the left wall boundary layer. In the upper quarter of the cavity most of the streams originated in the ceiling boundary layer and, making a "U" turn, terminated in the exhaust duct.

Figure 36 Photo of convection occurring in chamber with 196 °F water, a 5 °F ΔT between walls and a 24.5 °F ΔT between supply and exhaust ducts (Condition II)

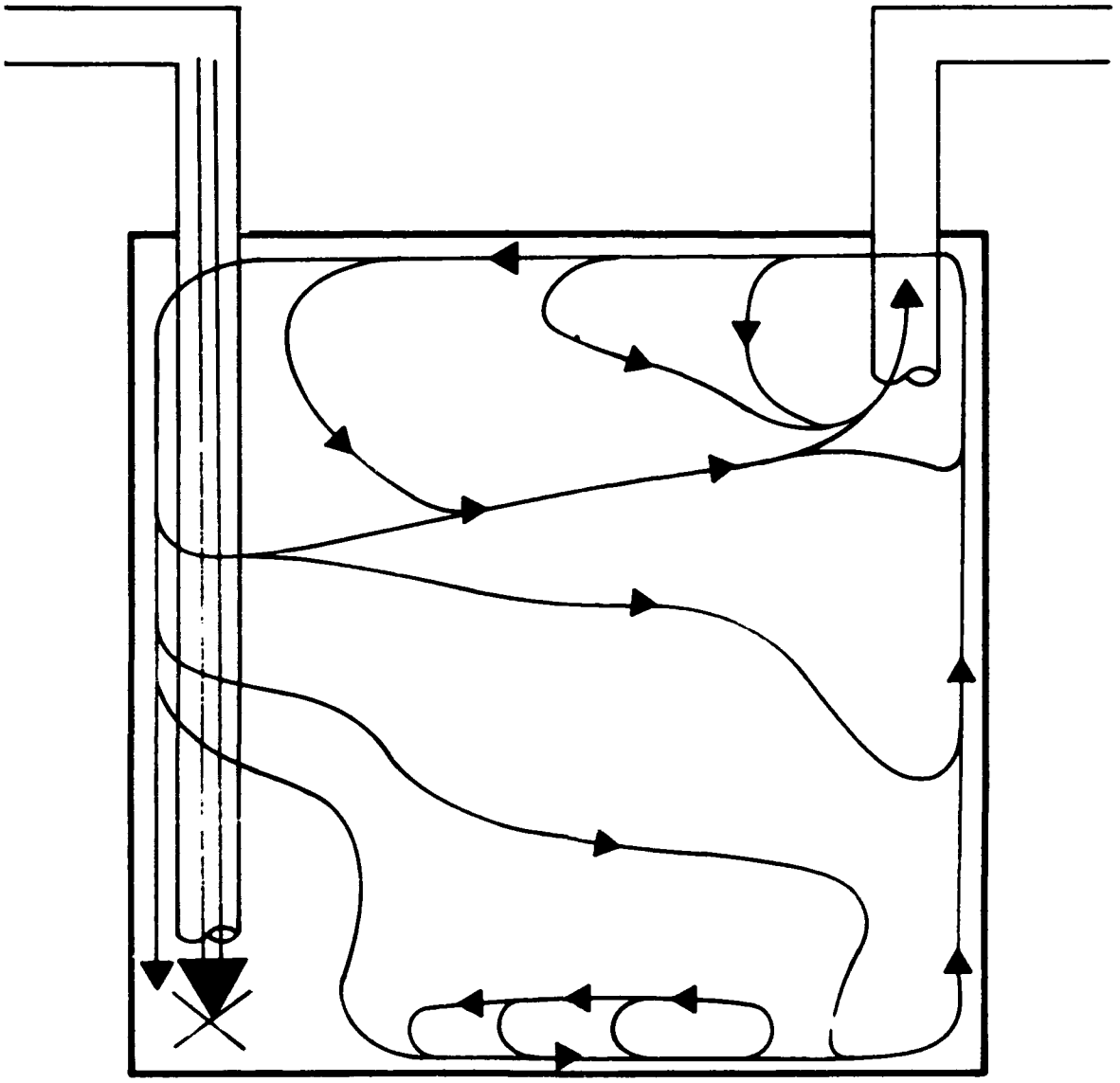

Figure 37 Schematic of flow distribution for Condition II (refer to figure 36)

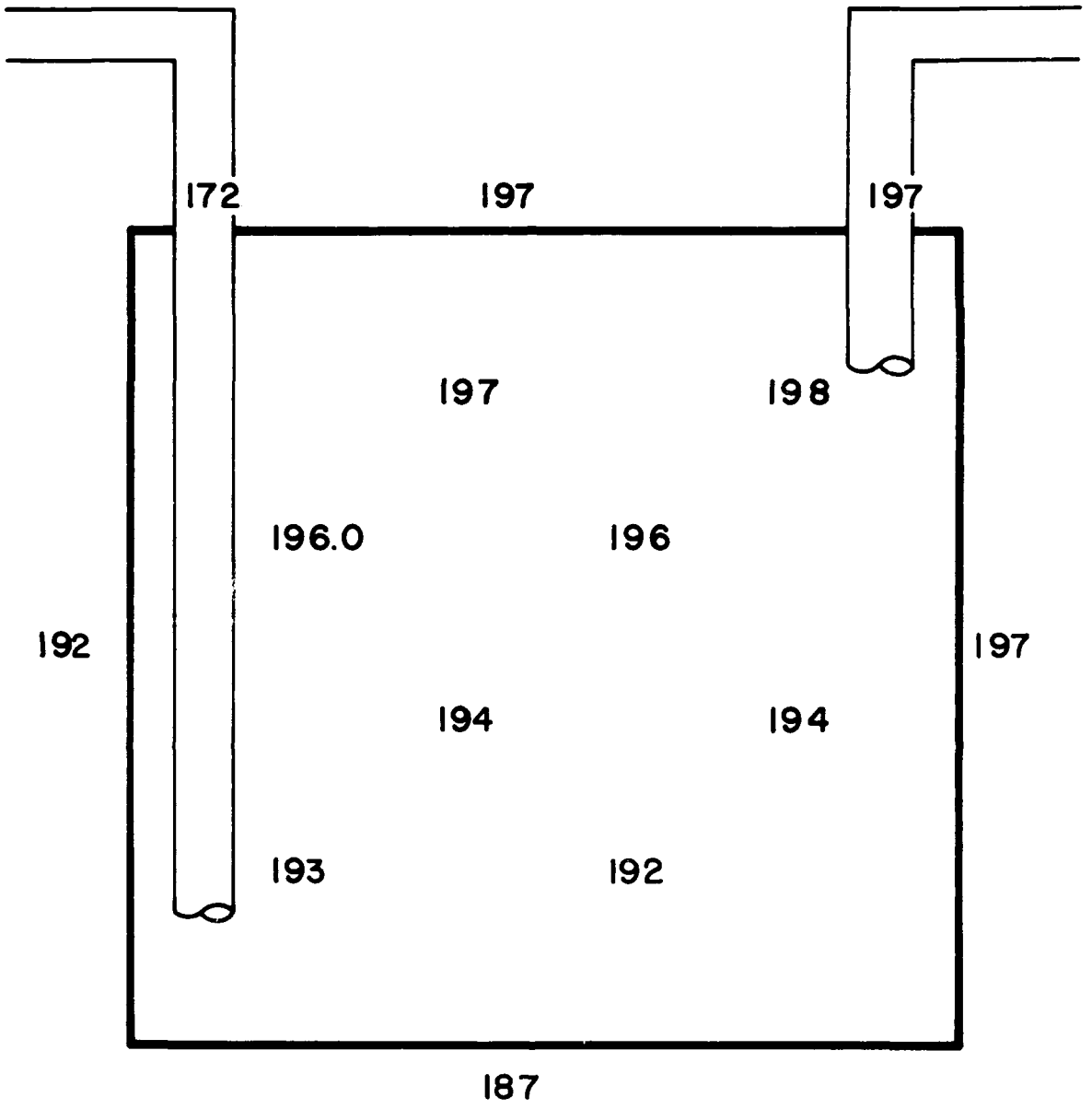

Figure 38 Temperature distribution for Condition II (refer to figure 36)

Figure 39 Photo of convection occurring in chamber with 253 °F water, a 1.9 °F ΔT between walls and a 14 °F ΔT between supply and exhaust ducts (Condition II)

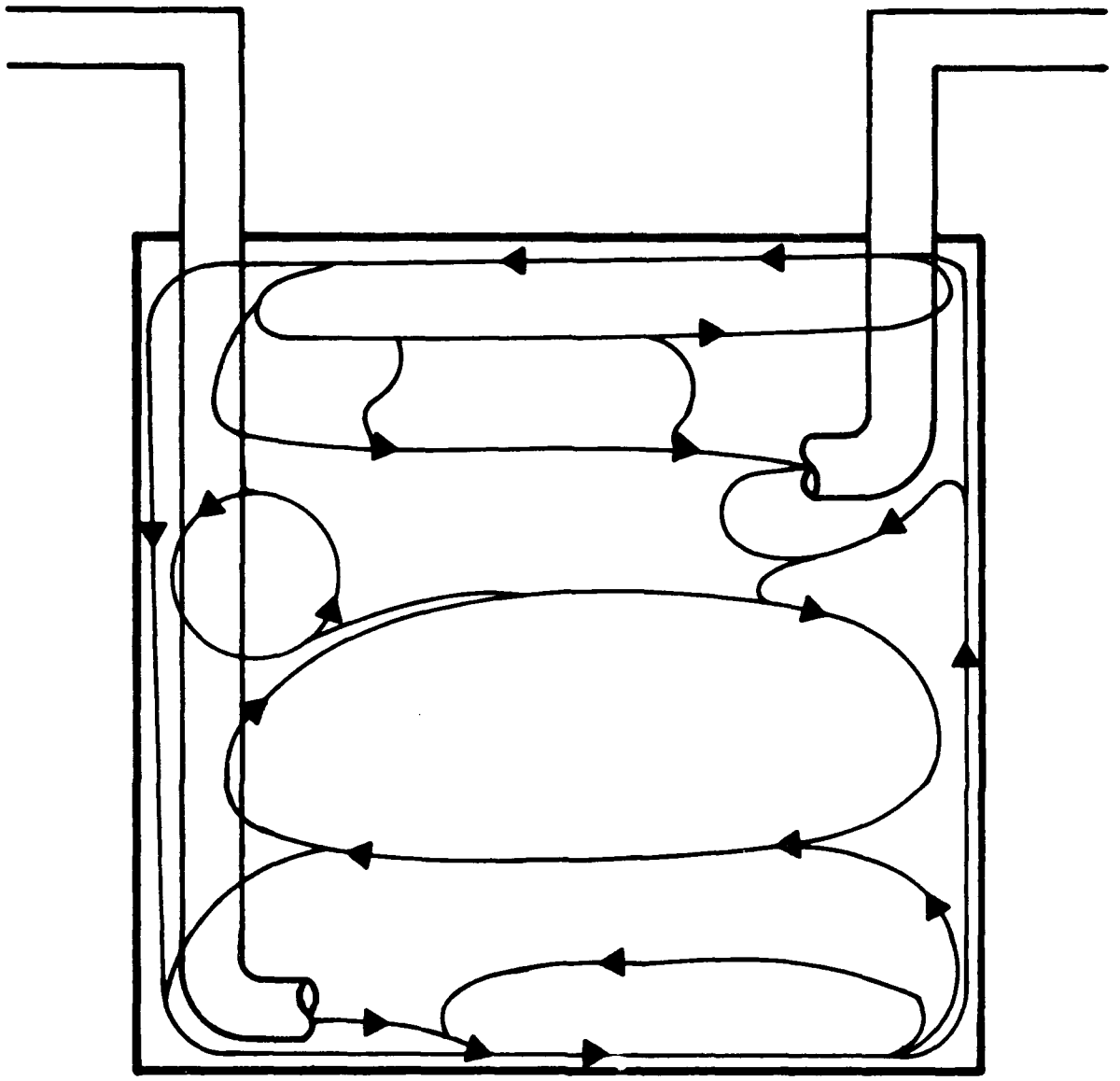

Figure 40 Schematic of flow distribution for Condition II (refer to figure 39)

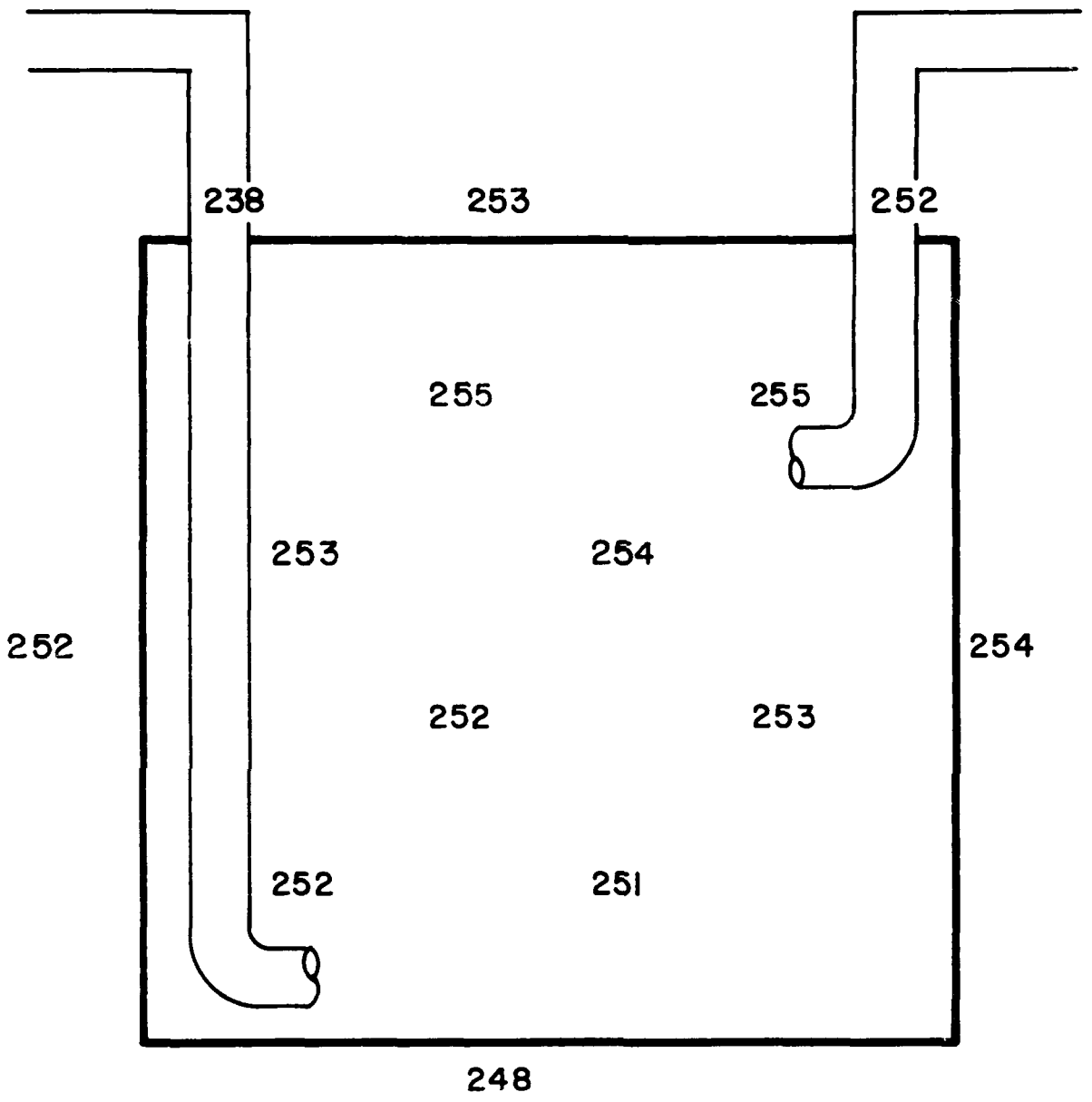

Figure 41 Temperature distribution for Condition II (refer to figure 39)

Condition III

This set of tests incorporated the use of one and then two simulated occupants. These occupants added heat to their surroundings and induced convection. Cylindrical figures were used specifying the size and heat dissipation of the simulated occupants. Test results representative of Condition III are shown in figures 42-47.

The first of these tests was run with one occupant. The ventilation ducts were removed from the cavity. The left wall was kept 1.5 °F cooler than the right wall, and the average water temperature was 255 °F. The flow pattern for this particular case can be seen in figure 43.

The ΔT between the wall surfaces set up a counter-clockwise boundary layer flow. The simulated occupant, located at the center of the floor, caused a vertical upward flow of relatively high velocity. This stream divided to the right and left at the ceiling. The stream to the left of the occupant wandered in an "S"-like fashion toward the left wall boundary layer. A counter-clockwise turning vortex was formed just left of center at the ceiling. The flows off from the right of the occupant followed four different paths before reaching the boundary layer. The uppermost started a left to right boundary layer flow. This flow was in opposition to the existing boundary layer flow and resulted in turbulence along the ceiling. The second highest flow turned downward and to the right. This intersected the right wall boundary layer approximately two inches from the ceiling. The third highest flow followed an "S" course to the floor boundary layer. The lowest flow followed a similar "S" path to within an inch of the floor. At this point the flow turned to the left and united with the floor boundary layer approximately one inch from the

Figure 42 Photo of convection in chamber with 55 °F water, and a 1.5 °F ΔT between walls. (one simulated occupant, Condition III)

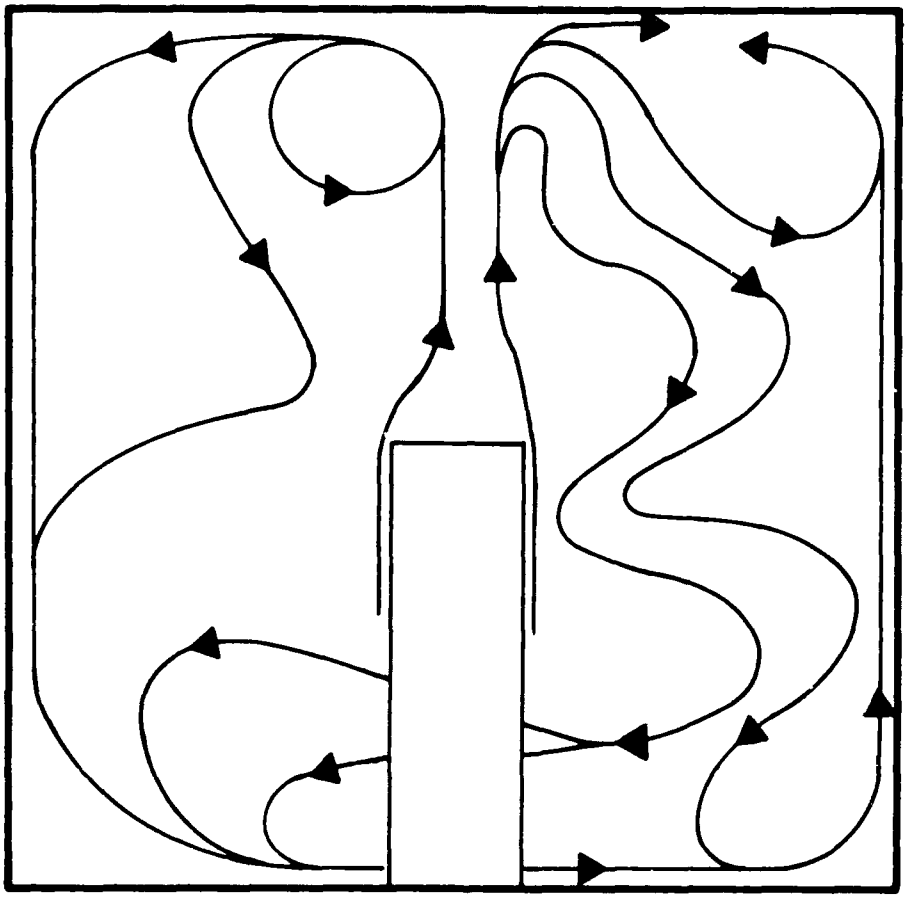

Figure 43 Schematic of flow distribution for Condition III (refer to figure 42)

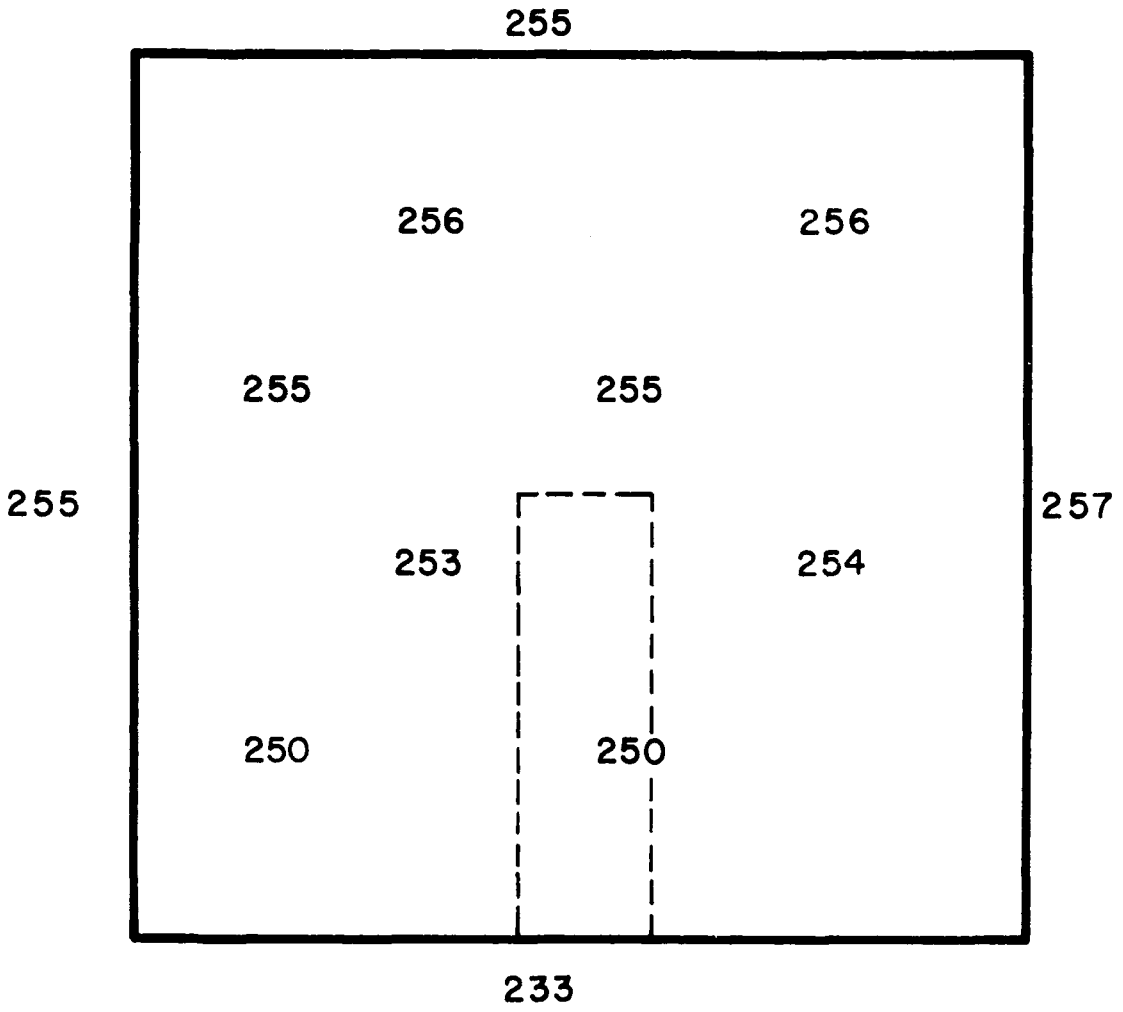

Figure 44 Temperature distribution for Condition III (refer to Figure 42)

left wall.

One observation of this single occupant test is particularly noteworthy. Except boundary layer flows, all flows that move from top to bottom move toward the center of the cavity as they pass by the top of the occupant. After passing the top of the occupant, they move outward again toward the sides of the cavity.

For the next test involving two simulated occupants, 250 °F water was used and there was a 2.5 °F ΔT between the inside wall surfaces. No convection ducts were used for this test. The resulting flow pattern can be seen in figure 46.

Three-dimensional effects were prevalent in this two-occupant test. Streamlines commenced and terminated without appearing to have a logical source or sink. A vortex occurred in the upper left corner. This vortex was fed primarily by the ceiling boundary layer. A flow leaving the left wall boundary layer, just below this vortex, traveled downward and to the right. This flow bifurcated just prior to touching the vertical flow leaving the left occupant. One branch mated with the flow leaving the occupant. The other branch flowed downward and to the left, terminating in the left wall boundary layer. Another flow appeared to originate from behind the left occupant about a half inch from the top of the occupant. This flow moved to the left, turned downward, and then flowed back to the right whereupon it divided into two branches before disappearing behind the left occupant.

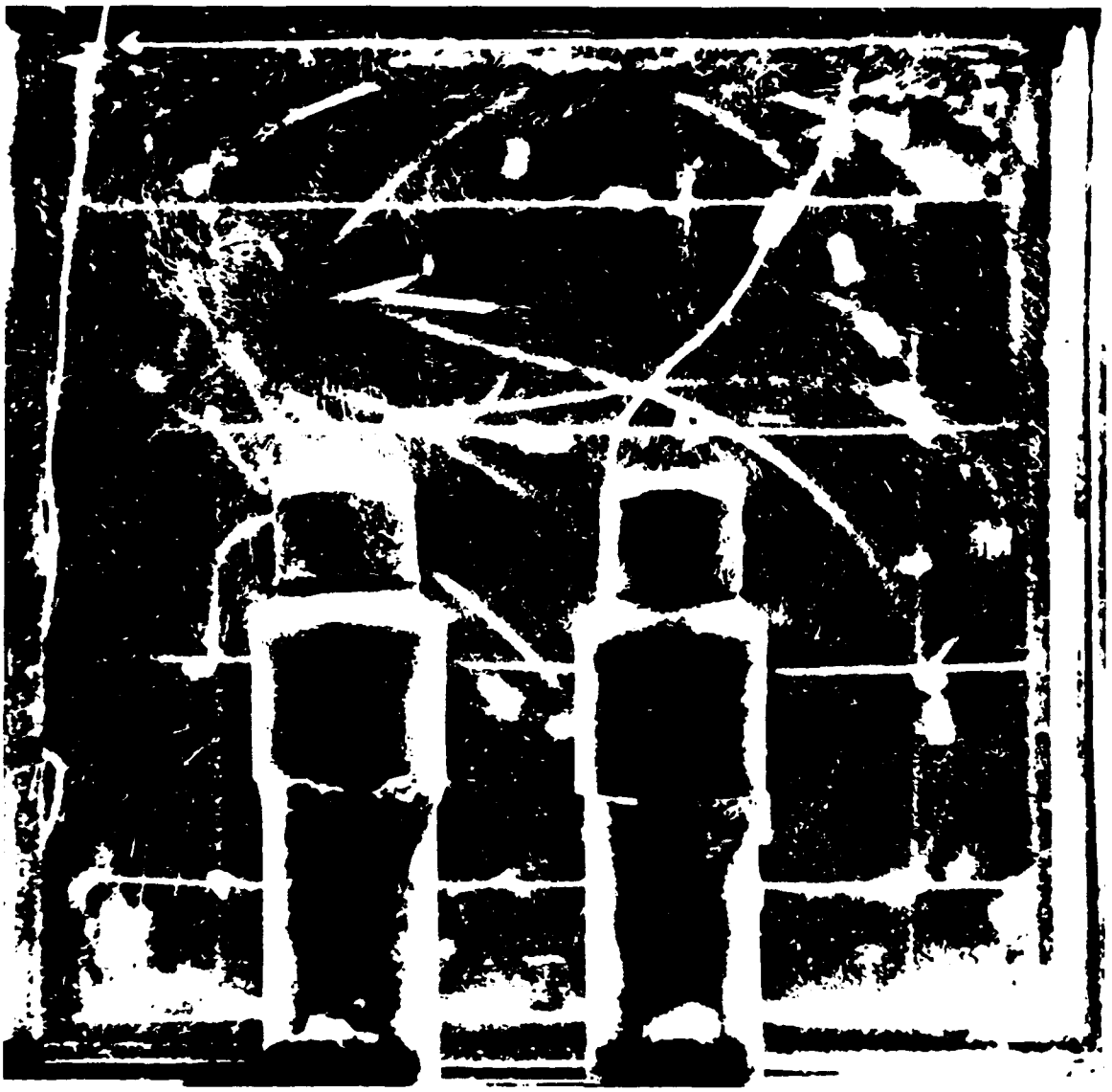

Figure 45 Photo of convection occurring in chamber with 242 °F water and a 3 °F ΔT between walls (two simulated occupants, Condition III)

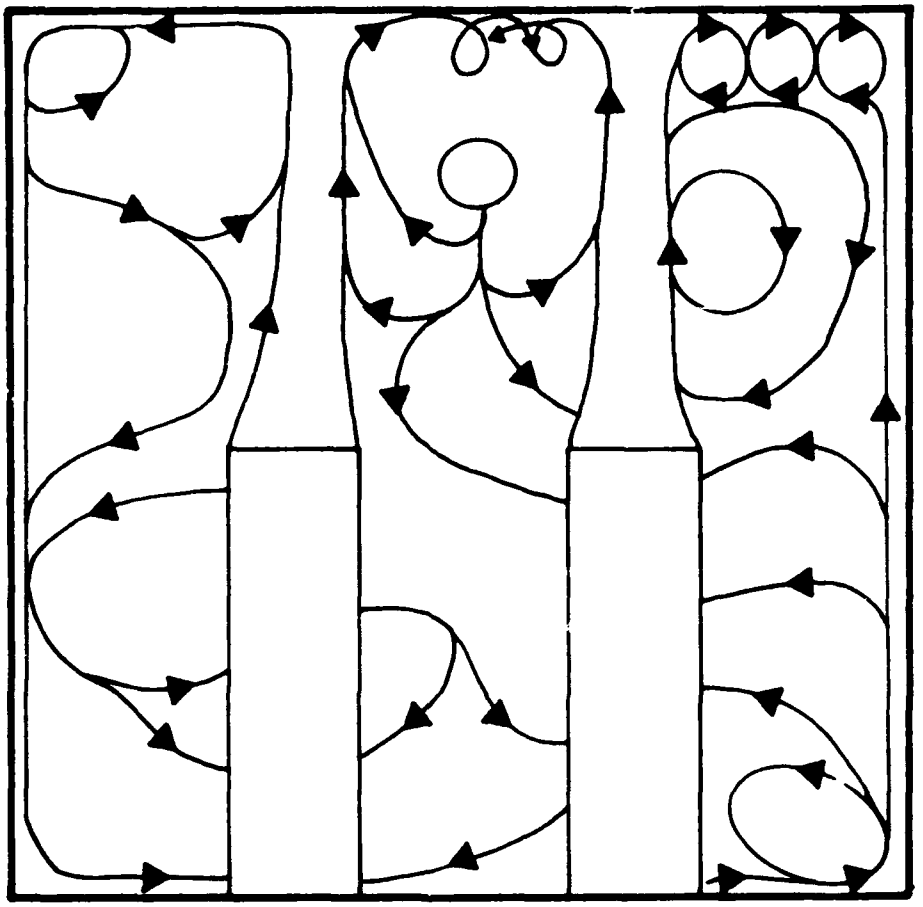

Figure 46 Schematic of flow distribution for Condition III (refer to figure 45)

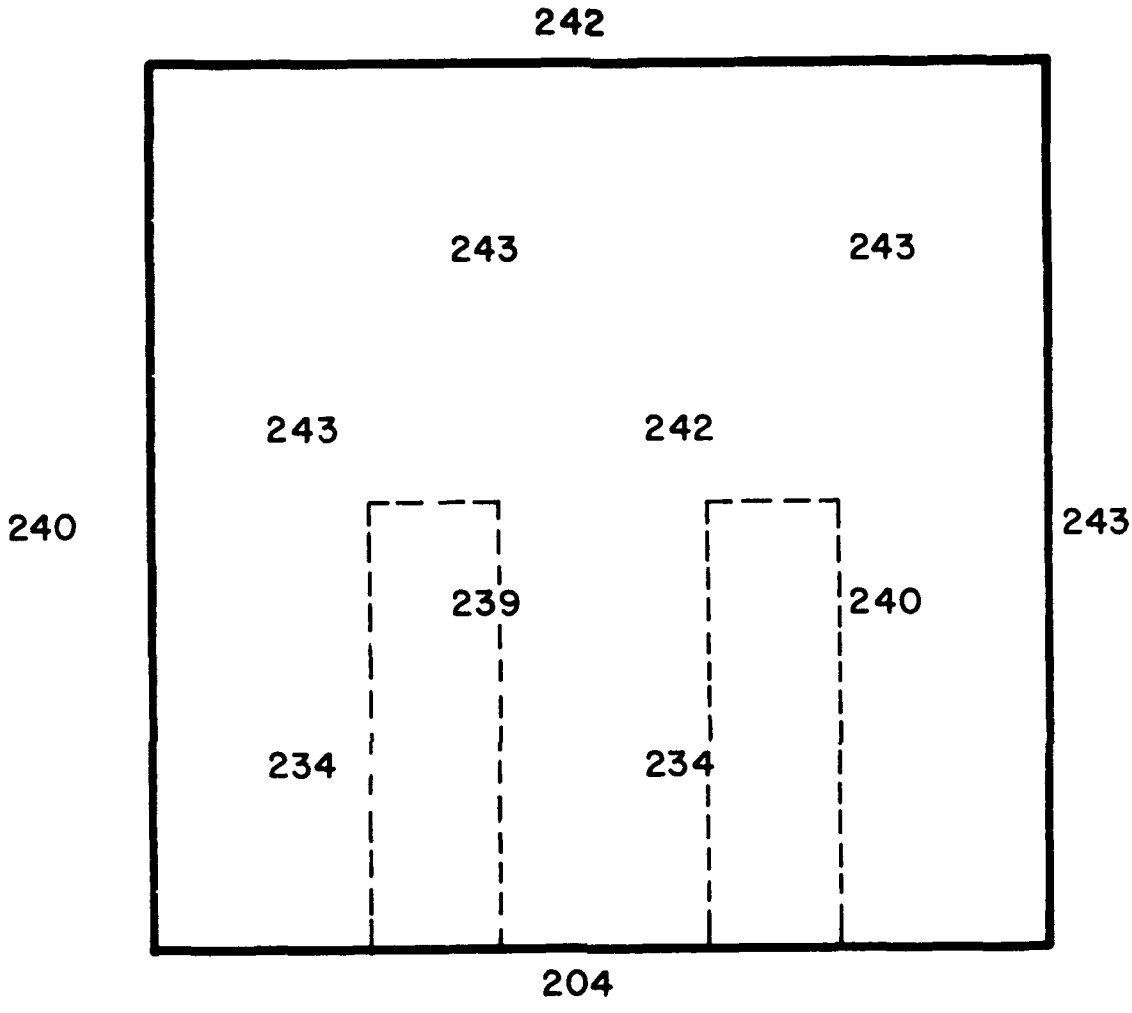

Figure 47 Temperature distribution for Condition III (refer to figure 45)

The flow along the ceiling was turbulent. Half way between the occupants, approximately one inch from the ceiling, a source fed a flow that terminated in the vertically rising currents of both occupants. There was considerable turbulence and vorticity along the ceiling to the right of the right occupant. Two skewed concentric flow loops originated and terminated on the right side of the rising currents leaving the right occupant. In the bottom right corner was a vortex which turned counter-clockwise. A flow originated in the right wall boundary layer and terminated behind the right occupant.

Condition IV

Natural convection was induced by a combination of the temperature difference between the walls, the presence of simulated occupants, and natural ventilation to the modeling area. Test results representative of Condition IV can be seen in figures 48-53.

Ventilation ducts were used in this test which involved one simulated occupant. These ducts did not penetrate the ceiling of the cavity, i.e., the openings were flush with the ceiling. The water temperature was 250 °F, the ΔT between the wall surfaces was 1 °F, and the ΔT between the convection ducts was 30 °F. The flow pattern for this test can be seen in figure 49.

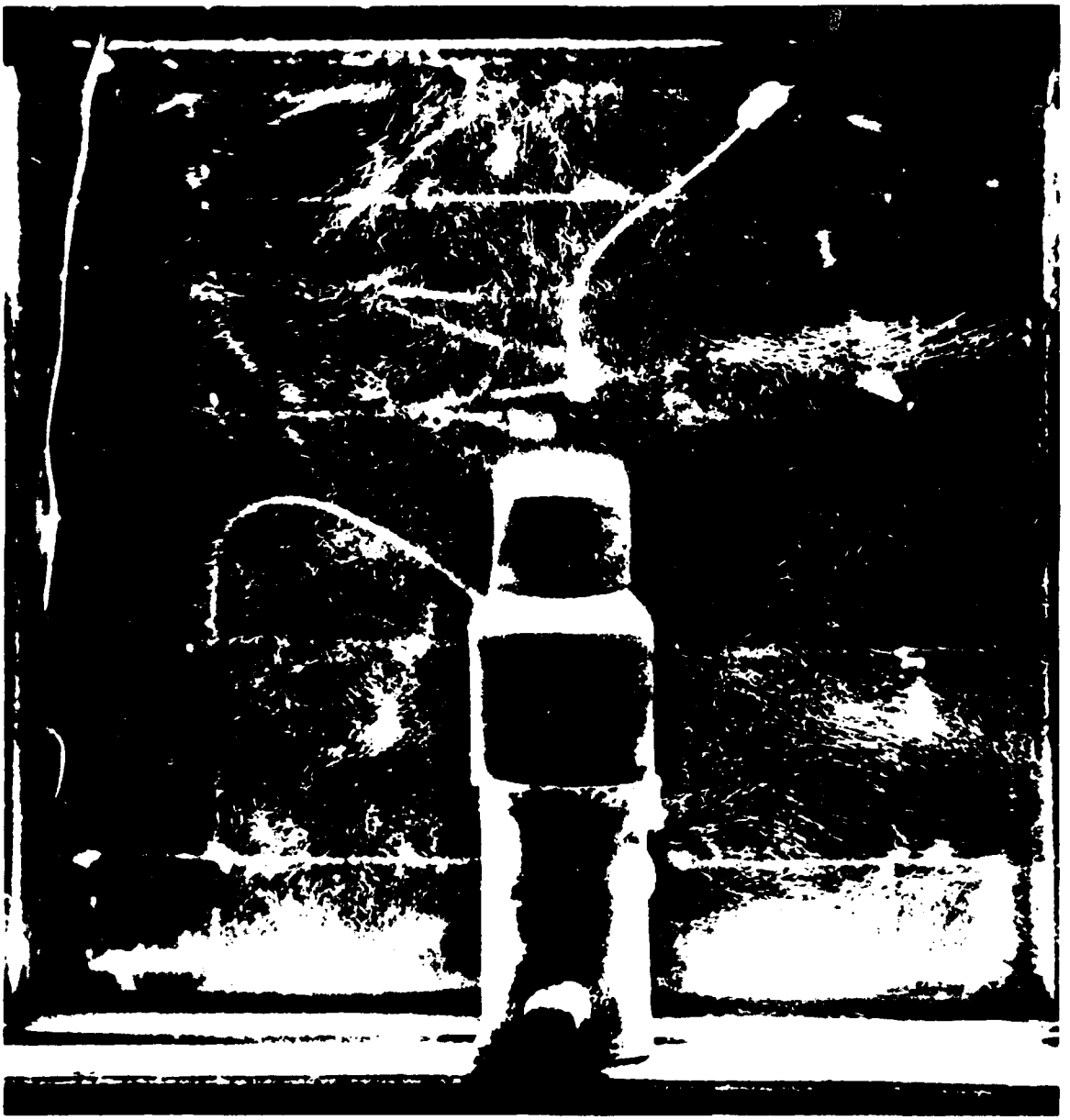

Figure 48 Photo of convection occurring in chamber with 247 °F water, a 2.1 °F ΔT between walls and a 27 °F ΔT between supply and exhaust ducts (one simulated occupant, Condition IV)

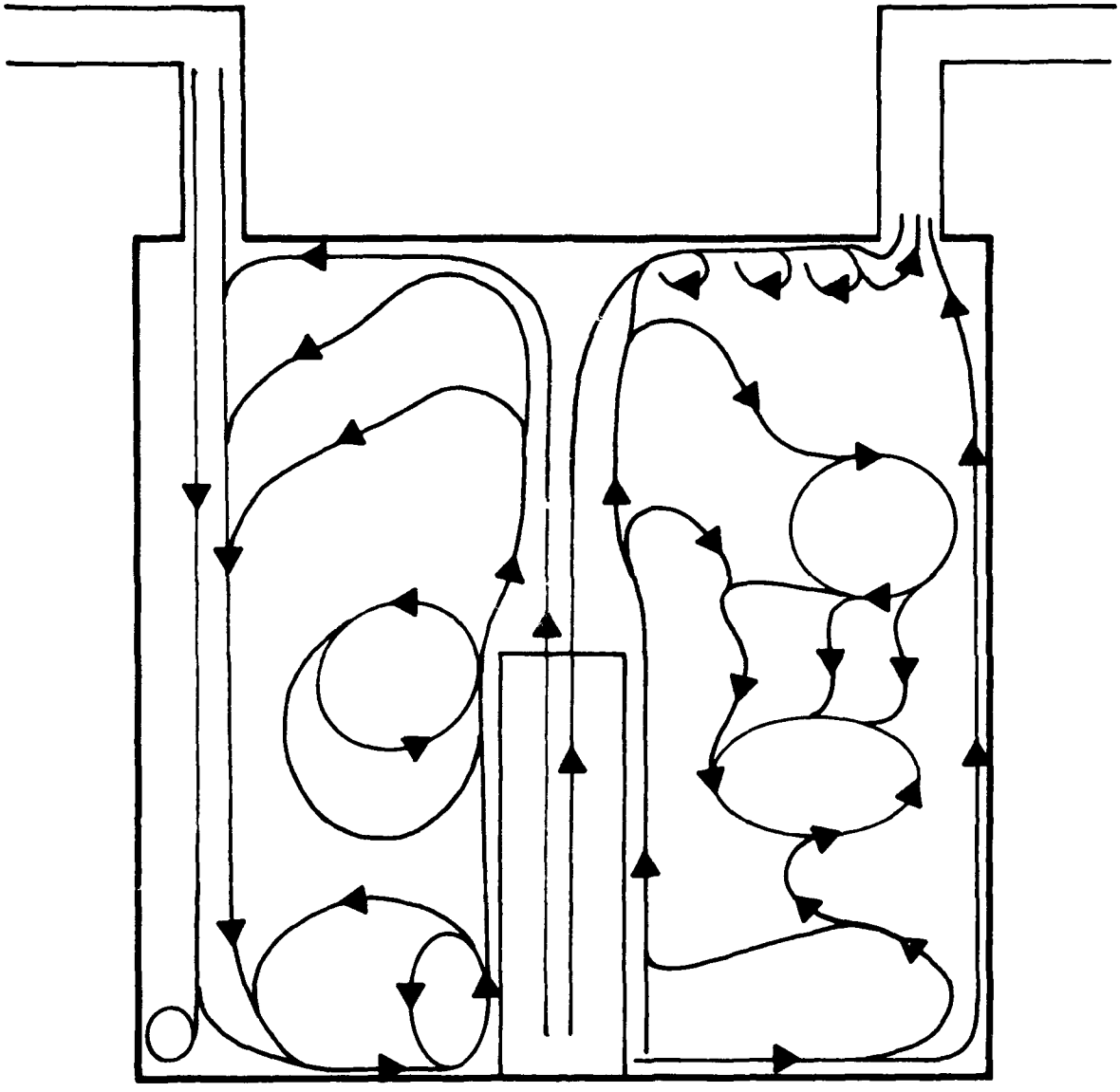

Figure 49 Schematic of flow distribution for Condition IV (refer to figure 48)

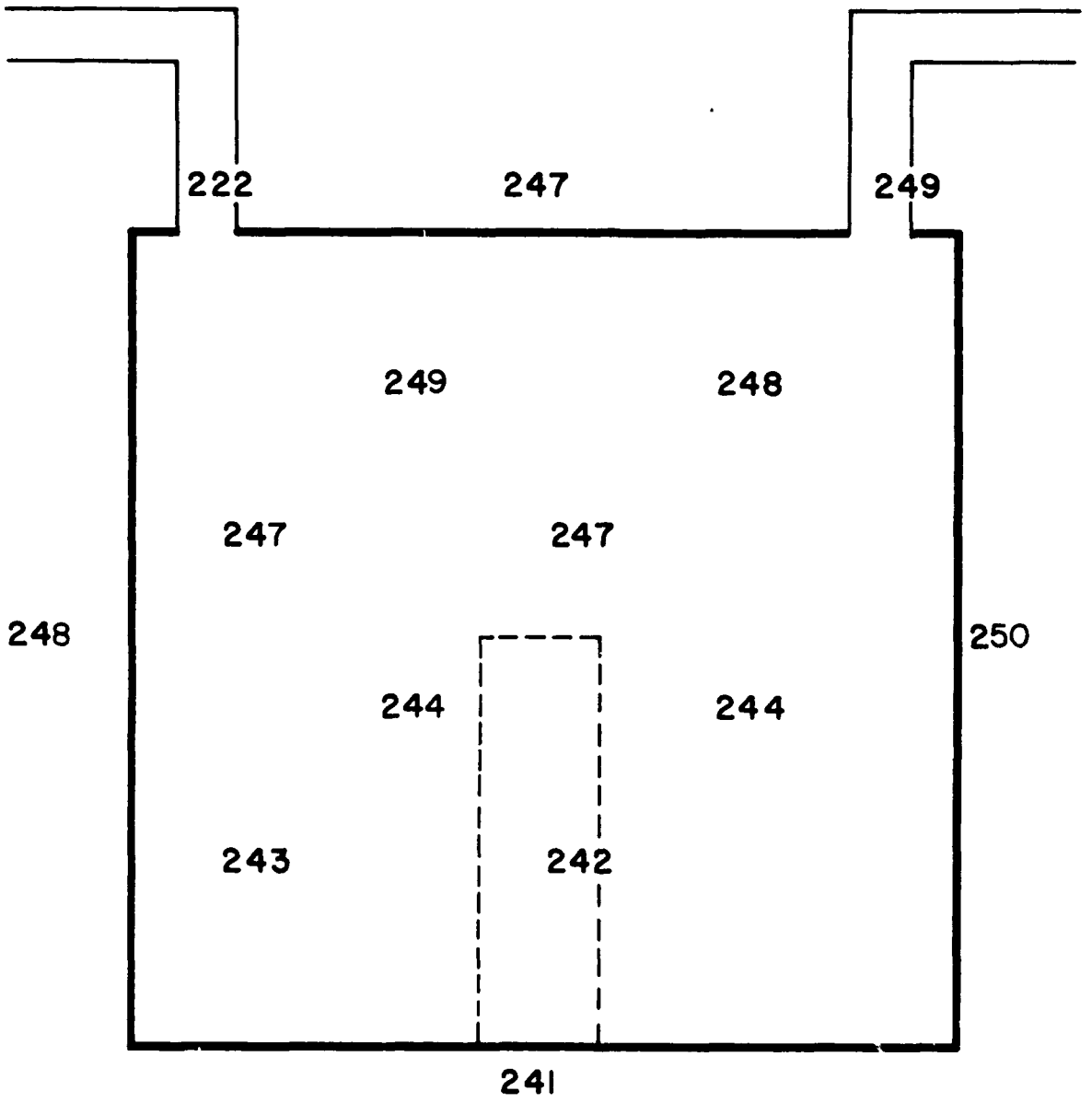

Figure 50 Temperature distribution for Condition IV (refer to figure 48)

The flow in this case, as in the previous one-occupant case, was divided down the middle by the rising currents leaving the occupant. Upon reaching the ceiling the flow from the left side of the occupant moved toward the left. The flow moved downward and to the left until it united with the columnated downward flowing water leaving the supply duct. Two counter-clockwise turning vortexes were located just to the top left and bottom left of the occupant. The flow leaving the right side of the occupant rose to the ceiling. After arriving at the ceiling the stream moved to the right toward the exhaust duct. Considerable turbulence occurred at the ceiling. A clock-wise-rotating vortex was formed approximately one and a half inches below the exhaust duct. This vortex was primarily fed by a stream leaving the vertical water column above the occupant. A second vortex, turning counter-clockwise, was formed about one inch beneath the first vortex. Downward-flowing streams connected the two vortexes. A stream leaving the boundary layer near the bottom right corner bent back and fed both the bottom vortex and the upward-flowing boundary layer on the right side of the occupant.

The second test for this condition involved two occupants. The water temperature was 250 °F, the ΔT between the wall surfaces was 3 °F, and the ΔT between the two ducts was 12 °F. The flow pattern for this test can be seen in figure 52.

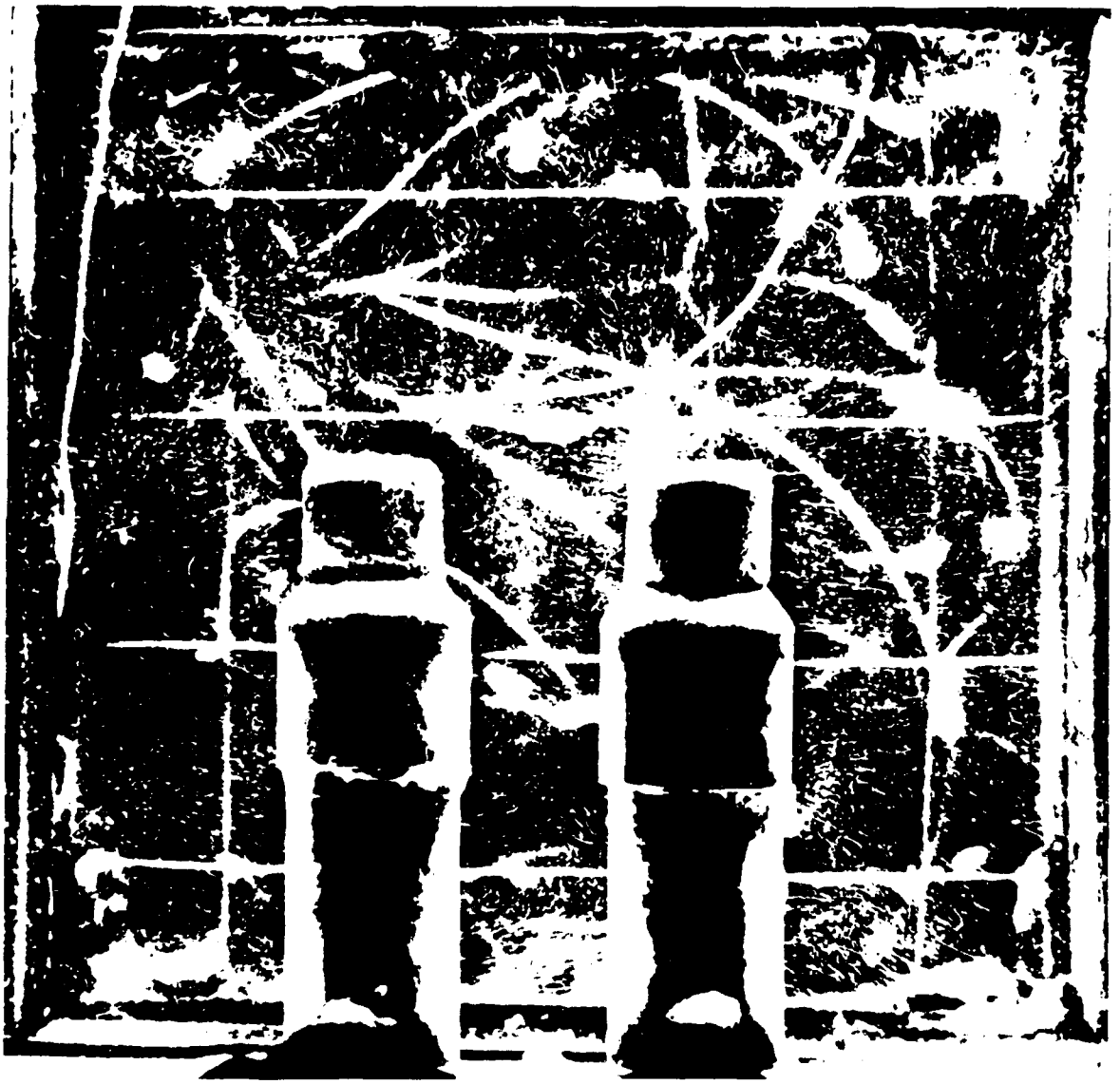

Figure 51 Photo of convection in chamber with 254 °F water, a 3.6 °F ΔT between walls and a 4 °F ΔT between supply and exhaust ducts (two simulated occupants, Condition IV)

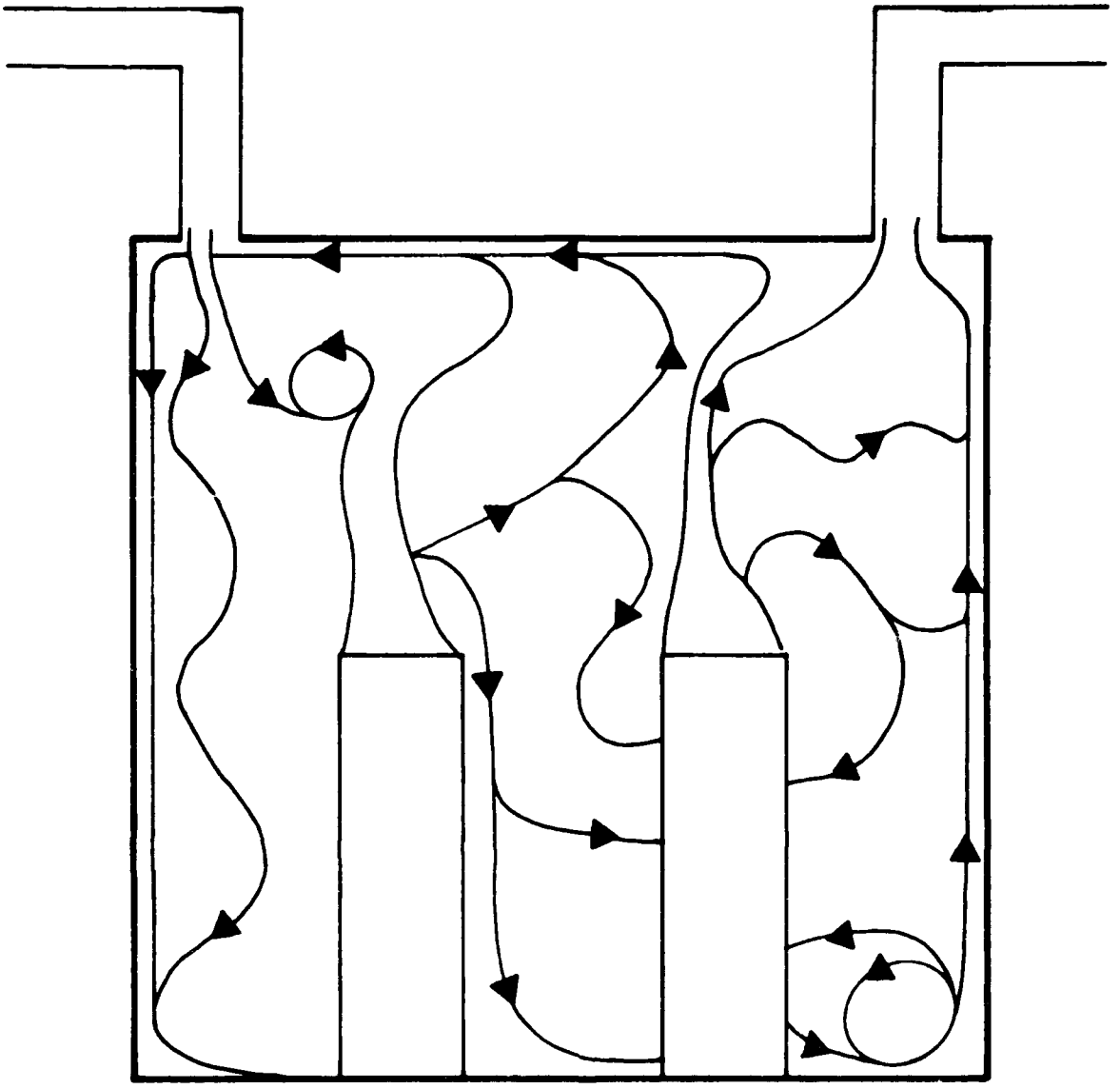

Figure 52 Schematic of flow distribution for Condition IV (refer to figure 51)

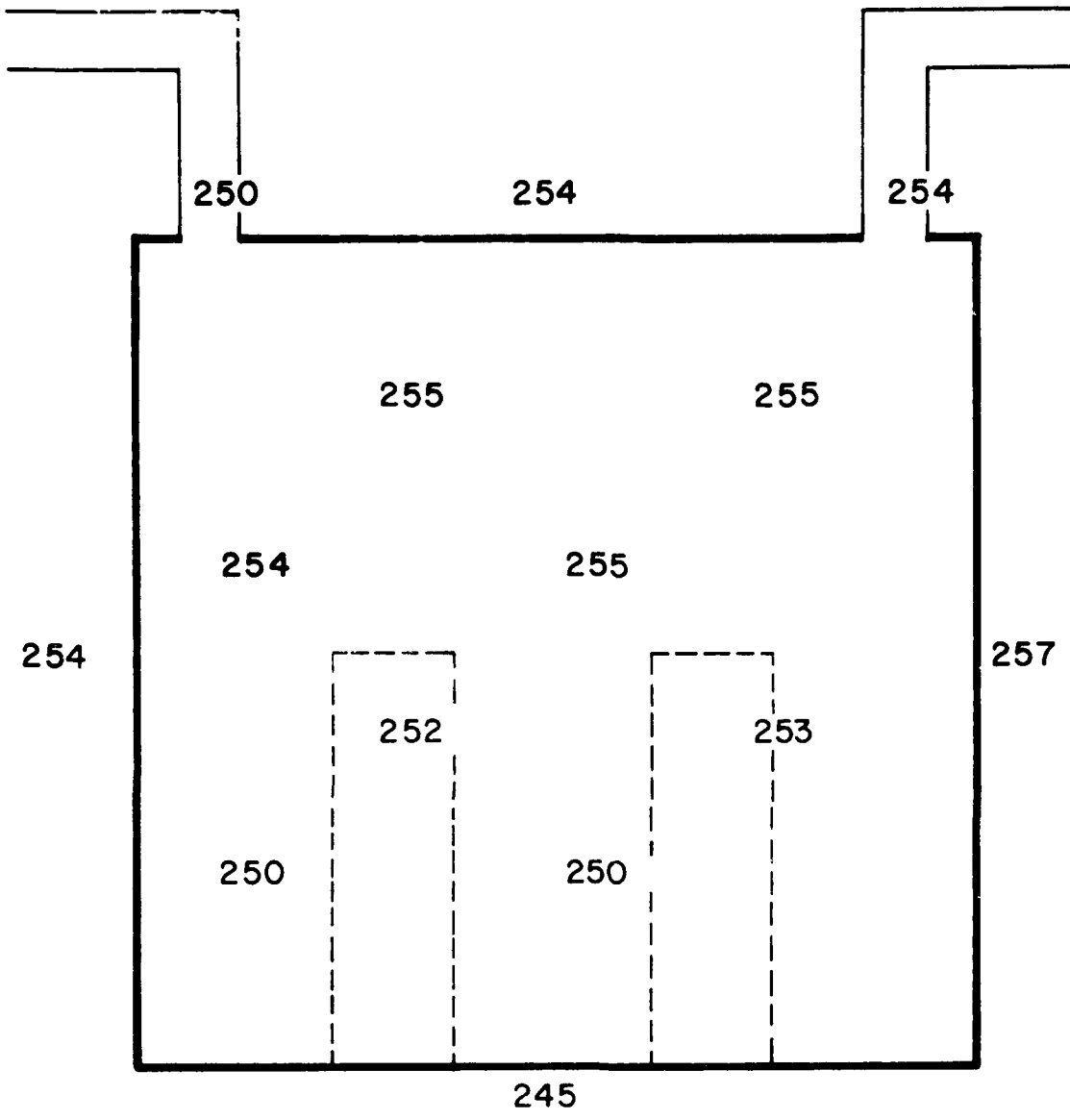

Figure 55 Temperature distribution for condition 1 (refer to figure 51)

In this test, as in the previous two-occupant test, three-dimensional effects were observed. The velocity of the water entering and leaving the ducts was considerably slower than in any of the previous tests. This low velocity was due to the relatively small ΔT maintained between the two ducts.

The rising currents from the right occupant fed both the ceiling boundary layer and the exhaust duct. The ceiling boundary layer moved from right to left. Two streams, originating from the rising currents of the right occupant, flowed horizontally to the right wall boundary layer. The lower of these two streams divided into two branches and one of these branches terminated in the boundary layer. The second of these branches flowed behind the occupant. A vortex, turning counter-clockwise, was established in the bottom right corner. All the flow between the occupants appeared to originate from a source behind the rising currents of the left occupant. One stream from this source flowed upward and ended in the ceiling boundary layer. Another flowed downward and terminated in the floor boundary layer. Both of these streams bifurcated. The two resulting secondary streams flowed behind the right occupant. The water leaving the supply duct flowed in an "S" path to the floor boundary layer. One stream from the supply duct and another from the rising currents of the left occupant combined to produce a vortex which rotated counter-clockwise. This vortex was approximately two inches above the left occupant.

6. Discussion of Method and Results

The tracer particles used in this study were very small flakes of aluminum. Since the density of aluminum is greater than that of water, these flakes eventually settled at the bottom of the chamber. At first it was expected that some discrepancy would exist between the motion indicated by the traces on the photographs and the true fluid motion. The settling velocity, however, was found to be quite small. For example, when the tracer was put in room temperature water (72 °F), most of it remained suspended in the water overnight. When put in warm water (120 °F) most of the trace remained suspended for four hours or more, and when put in 500 °F water about 50% of the original amount settled in about one half hour.

Due to the shape of the aluminum particle there was room for error in the velocity measurements. The particle is flat in one plane and a multi-sided polygon when viewed in a plane perpendicular to the first. When the flake moved in the fluid it tended to align with the direction of shear of the fluid. If the flow were laminar, a flake could move a considerable distance exposing only one side to the viewer. If the fluid motion were turbulent, the particle tended to tumble. A particle could present an edge view to the film and leave no trace at all. When the traces made by the flakes were used to determine the velocity of the fluid it was often difficult to tell whether the length of the streak indicated the actual distance moved or just the distance moved when the trace was reflecting light to the film. Spherical particles would probably be the most desirable shape for velocity measurement because

they would constantly reflect the same amount of light regardless of orientation. But of those tried none were of sufficient density to remain suspended in the high-temperature water. To reduce the chance of error due to the particle shape, a fairly large number of streaks were measured for each velocity determined.

The model was essentially designed for a study of two-dimensional convection. The apparatus was constructed with sufficient depth to minimize end effects at the midsection of the model enclosure. While the end effects were reduced, there were still three-dimensional effects due to a longitudinal temperature gradient. When the glass plate viewing port was insulated on its outside surface, it was usually two or three degrees cooler than the rear wall and the three-dimensional effects were small. But when the insulation was removed for fifteen or twenty minutes during photographic sessions, the temperature difference between front and rear became greater and these three-dimensional effects increased. The error due to this factor was minimized by taking the photographs immediately after the insulation was removed from the glass viewing port.

The Prandtl number of room temperature air is 0.72. Water at 500 °F has approximately the same Prandtl number as room air (0.87). Further, a Grashof number equivalent to that found in a full-sized room can be obtained by using high temperature water in a small-scale model. Another attractive feature of high temperature water is that above 350 °F the Prandtl number is relatively constant with respect to temperature change. This characteristic minimizes inaccuracies due to property value changes across the thermal boundary layers next to the heat transfer surfaces.

Because of physical limitations of the modeling apparatus used here, water at 250 °F was used for the simulations. The saturation pressure of water at 250 °F is about 30 psia, while at 500 °F it is about 680 psia, thus a considerably stronger container is required for higher temperature simulations. Also rusting occurred in this particular apparatus at temperatures above 250 °F. As the temperature increased rusting occurred to such an extent that the trace particles in the water were obscured.

By using 250 °F for this series of simulations, the same Grashof number, and aspect ratio, and nearly the same Prandtl number ($Gr \sim 10^{10}$, $L = 1.$, $Pr = 1.41$) were reproduced in the small-scale model (6" x 6", width x height) as are normally found ($Gr \sim 10^{10}$, $L = 1.$, $Pr = 0.72$) in a full sized room (8' x 8', width x height).

One test was run at an average water temperature of 124 °F to show the difference between convection at this temperature and the other tests of 250 °F. Figures 18, 19, and 20 show the results of that test. In the low temperature test the flow is slower, more viscous, and there is much less turbulence. The Grashof number is an order of magnitude less for the low temperature test.

The differences between the two tests are due almost entirely to the viscosity of the water. The viscosity of the 124° water is nearly twice that of the 250° water. The lower the viscosity the higher the Grashof number and the faster the flow due to a given temperature difference.

Figures 33, 34, and 35 show the results of a simulation at an average water temperature of 292 °F, approximately 40 degrees above normal simulation temperatures. At this higher temperature the Prandtl number of water (about 1.1) more closely approximates the Prandtl number of air (0.72). Thus operation at this level is more desirable for an accurate simulation. However, as noted, there were considerable experimental difficulties involved with operating at this high temperature. The fact that results were obtained at all was largely due to good fortune.

The effect of the increased temperature on predicted fluid motion is apparent. Since the effect of the higher temperature is to lower the viscosity of the water, the same temperature differentials across the model operated at a higher temperature level would have high velocities. The higher velocities would increase the ventilation rate and turbulence level. Further, when the ventilation rate is high the temperature difference between the floor and ceiling is smaller as was observed here.

A comparison of the results obtained from small-scale modeling of test Conditions I - IV with the results of similar tests in a full-sized model would certainly be desirable. Unfortunately there has been little previous work in full-scale models that can be compared quantitatively with the results of these simulations. A comparison cannot be made because the boundary conditions of other full scale tests were not the same as those in this model, or because the boundary conditions were not available in the reports of the other tests.

However, a qualitative comparison with Daws' results [15] may be made with some interesting agreements. Daws observed that for any flow of air moving along a wall a point downstream is reached where the velocities of that flow are comparable with those of the room. At that point, which is dependent upon the strength of the flow, all entrainment ceases and the stream spreads out in all directions, breaking away from the wall and joining movement induced by entrainment elsewhere. This phenomena also was observed in this small-scale modeling study. When the temperature differential between the ventilation supply and

The effect of the increased temperature on predicted fluid motion is apparent. Since the effect of the higher temperature is to lower the viscosity of the water, the same temperature differentials across the model operated at a higher temperature level would have high velocities. The higher velocities would increase the ventilation rate and turbulence level. Further, when the ventilation rate is high the temperature difference between the floor and ceiling is smaller as was observed here.

A comparison of the results obtained from small-scale modeling of test Conditions I - IV with the results of similar tests in a full-sized model would certainly be desirable. Unfortunately there has been little previous work in full-scale models that can be compared quantitatively with the results of these simulations. A comparison cannot be made because the boundary conditions of other full scale tests were not the same as those in this model, or because the boundary conditions were not available in the reports of the other tests.

However, a qualitative comparison with Daws' results [15] may be made with some interesting agreements. Daws observed that for any flow of air moving along a wall a point downstream is reached where the velocities of that flow are comparable with those of the room. At that point, which is dependent upon the strength of the flow, all entrainment ceases and the stream spreads out in all directions, breaking away from the wall and joining movement induced by entrainment elsewhere. This phenomena also was observed in this small-scale modeling study. When the temperature differential between the ventilation supply and

exhaust air was small the supply air was observed to move down the left wall for a short distance, then to mix with the room as described above.

Daws noted that air streams close to a room surface are drawn to the surface by what appears to be a slight sucking action at the wall surface (known as the Coanda effect). This phenomena was also observed in the small-scale model when the ventilation streams entered the model. As the ventilation supply air moved toward the floor it was drawn to the wall. The distance from the ceiling to the point where the fresh air stream came into contact with the wall was dependent upon the strength of the stream. The stronger the flow the more it resisted the sucking effect of the wall.

Daws noted that the action of the air leaving the room was confined to the immediate vicinity of the outlet. This was also observed in the small-scale model simulations.

The photographs in Daws' paper show the horizontal motion of room air due to entrainment with vertically moving streams. This occurrance can also be seen in the photographs of small-scale model simulations.

7. Summary

The problem of obtaining a quantitative velocity distribution map of a natural convection field has become a classic of engineering research. Numerous approaches to the problem have been made using both theoretical and experimental techniques. While the experimental method presented here is not the complete answer, it is a step toward solution of the problem. Limitations within the method as well as with this particular experimental apparatus prevent it from becoming the complete answer.

The experimental apparatus used here is suitable for two-dimensional flow studies only. An apparatus can be designed and constructed to extend the method to three-dimensional studies.

The experiment discussed in this report is not conclusive proof that the method is qualitatively accurate, even for a two-dimensional simulation. A comparison with the results of a dynamically similar full scale test is required. For example, it is necessary to know the difference between these experimental results and full scale results as a function of the Prandtl number. It may be that the overall air flow pattern, which is the dominating influence on the occupants' comfort, is not as dependent on the Prandtl number as the boundary layer velocity profile Another factor leading to inaccuracies between the results observed in this model and those in a prototype room is the dissimilarity of boundary conditions. The temperature distribution over the walls of this model do not closely represent those over the surface of an actual room wall. Greater control of wall temperature

distribution must be built into a future model. The magnitude of these effects are not known and it can only be determined by tests in a full sized room.

In spite of these shortcomings in rigorous duplication of actual room conditions, it is strongly felt that an ultimate solution to natural convection velocity patterns may be attained through modeling techniques. The construction advantages of a model over a full scale apparatus are more than enough to merit further development of this technique.

8. References

[1] Ducar, G. J., Engholm, G., "Natural Ventilation of Underground Fallout Shelters", ASHRAE Transactions, 1965, Volume 71, Part 1, pp. 88-100.

[2] Baschiere, R. J., Lokmanhekim, M., Moy, H. C., Engholm, G., "Natural Ventilation of Underground Fallout Shelters", ASHRAE Transactions, 1965, Volume 71, Part 1, pp. 101-114.

[3] Svaeri, O. W., Dembo, M. M., "Simulated Occupancy Tests and Air Distribution in a 480-Person Community Fallout Shelter", 1965, done under Office of Civil Defense, Work Order No. OCP-PS-65-17, Subtask No. 1217A.

[4] Fromm, J. E., "A Numerical Method for Computing the Non-Linear, Time Dependent Buoyant Circulation of Air in Rooms", Proceedings of First Symposium on the Use of Computers for Environmental Engineering Related to Buildings, National Bureau of Standards Building Science Series, November, 1970 (in print).

[5] Sparrow, E. M., Cess, R. D., "Radiation Heat Transfer", Brooks/Cole Publishing Company, 1966, pp. 262-298.

[6] Kreith, F., "Principles of Heat Transfer", 1959, International Textbook Company.

[7] Eckert, E. R. G. and Drake, R. M., "Heat and Mass Transfer", McGraw-Hill, 1959.

[8] Wilkes, J. O., "The Finite Difference Computation of Natural Convection in an Enclosed Rectangular Cavity", PhD Thesis, The University of Michigan, 1963, pub. University Microfilms, Inc.

[9] Torrance, K. E., Orloff, L., and Rockett, J. A., "Numerical Study of Natural Convection in an Enclosure with Localized Heating From Below--Creeping Flow to the Onset of Laminar Instability", J. Fluid Mechanics, (1969), Vol. 36, Part I, pp. 33-54.

[10] Torrance, K. E., Orloff, L., and Rockett, J. A., "Experiments on Natural Convection in Enclosures with Localized Heating From Below", J. Fluid Mechanics, (1969), Vol. 36, Part I, pp. 21-31.

[11] Eckert, E. R. G. and Jackson, T. W., "Analysis of Turbulent Free-Convection Boundary Layer on Flat Plate", NACA TN2207, October, 1950.

[12] Griffiths, E. D. and Davis, A. E., "The Transmission of Heat by Radiation and Convection", Special Report No. 9, Food Investigation Board, British Department of Science and Ind. Research, 1922.

[13] Kusuda, T., Barber, E. M., "Theoretical Considerations for Scale Modeling of Natural Convection in Air", (in process).

[14] Barber, E. M., Kusuda, T., "A Photographic Technique and the Use of Metaldehyde for Studying Natural Convection in Rectangular Enclosures", (in process).

[15] Daws, L. F., "Movement of Air Streams Indoors", Symposia of the Society for General Microbiology, Number XVIII, Airborne Microbes, 1969.

Appendix

Simulated Air Distribution in a Single Room Shelter

The results presented in the main body of this report have been transformed into a simulated case of air in a full sized shelter and are presented in this appendix. Quantified data, such as temperatures and velocities, have been scaled through the appropriate similarity parameters. Flow patterns shown here are identical to those presented in Chapter 5. The order of presentation and the types of conditions considered also follow those in Chapter 5.

Condition I: Simulation of Air Distribution in a Shelter Without Ventilation or Simulated Occupant

This condition represents the simplest set of boundary conditions considered. Figures A1 and A2 show the air current patterns and temperature and velocity profiles predicted by the small-scale model for the full-scale shelter. The size of the full-scale shelter is 8 feet wide by 8 feet high, the length is not considered.

Several features are apparent from observing the predicted air temperatures. The first is the thermal stratification of the air at the inner core of the room. The inner core being defined as that volume of air extending from the center of the room to within about one foot of all the surfaces. This stratification may be observed throughout the simulations for all four conditions studied.

The cause for the flow shown in figure A1, is the preset temperature difference between the left and right walls. Since the right wall is warmer than the left a thin boundary layer will flow up the right wall, cross the ceiling and then fall down the cooler left wall to the floor. On reaching the floor the flow will continue to hug the boundary while crossing to the right wall. This produces a general counter-clockwise rotation at the interface of the air and the room surfaces. It also produces a secondary motion in the inner core air. The secondary motion is due to the inner air becoming entrained with the rapid moving boundary layers along the walls.

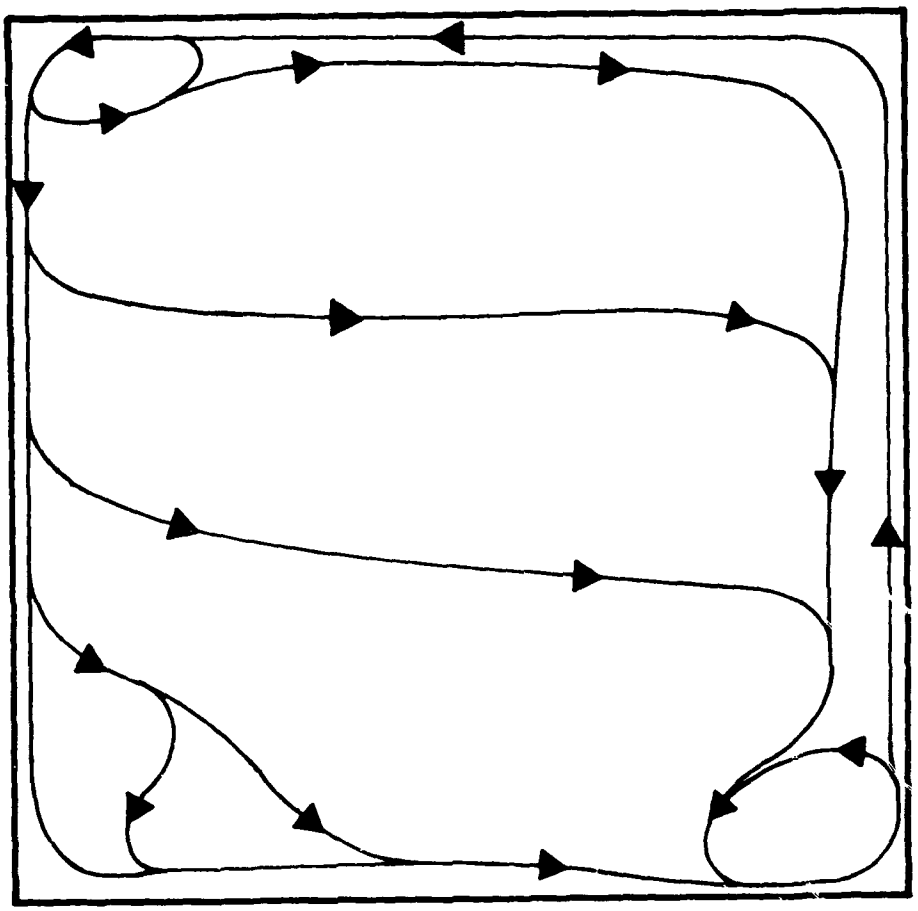

Figure A1 Air distribution predicted for an 8' x 8' shelter without natural ventilation or simulated occupant (Condition I)

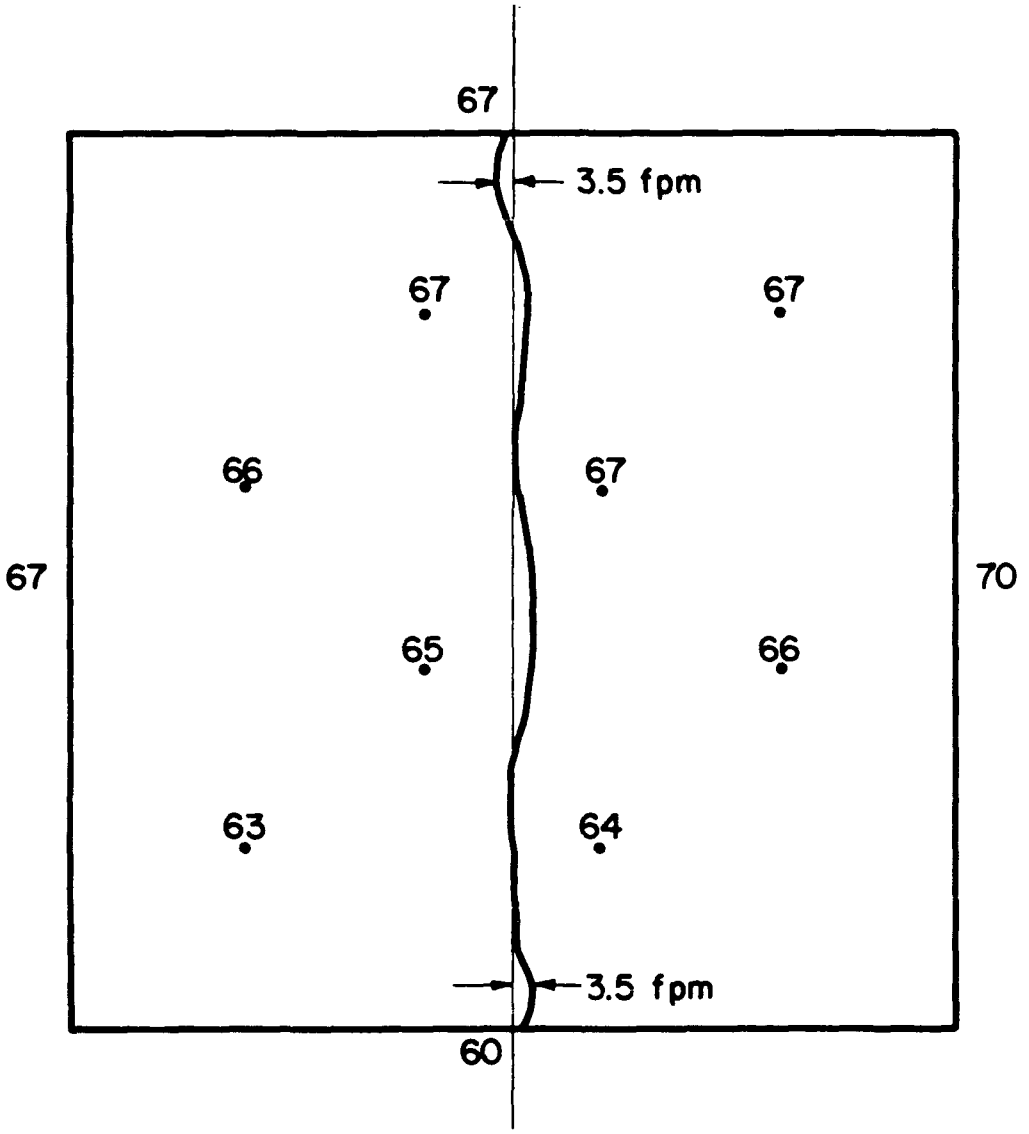

Figure A2 Air temperatures and velocities predicted for an 8' x 8' shelter, without natural ventilation or simulated occupant (Condition I)

A quantitative estimate of the boundary layer and its velocity in the model is not noted due to experimental limitations. It is suggested though, to be several times thinner and faster than the flows across the ceiling and floors. From the measurements made, the predicted air flow across the ceiling is approximately 3.5 feet-per-minute, and the boundary layer would be on the order of 9 in. to 12 in. thick. The predicted air flow across the floor, while in the opposite direction is about the same velocity and thickness. The predicted velocity of the air in the inner core is considerably lower and mainly in a horizontal direction. The maximum core air velocity would be near the center of the room and slightly over one foot per minute.

Condition II: Simulation of Air Distribution in a Shelter With Ventilation, But Without a Simulated Occupant

Simulations were made for a number of variations on this condition. The boundary conditions varied were the temperature difference between the left and right walls, the temperature difference between the ventilation supply and exhaust air, the temperature level of the modeling fluid and the positions of the ventilation duct openings.

Figures A3 and A4 show the air distribution patterns and temperature and velocity profiles predicted for a full sized (8' x 8') naturally ventilated shelter. The ventilation ducts are flush with the ceiling and in a full sized shelter would be located approximately 18 in. from either side wall. The inside diameters of the ventilation ducts are equivalent in size to 3.75 in. round ducts.

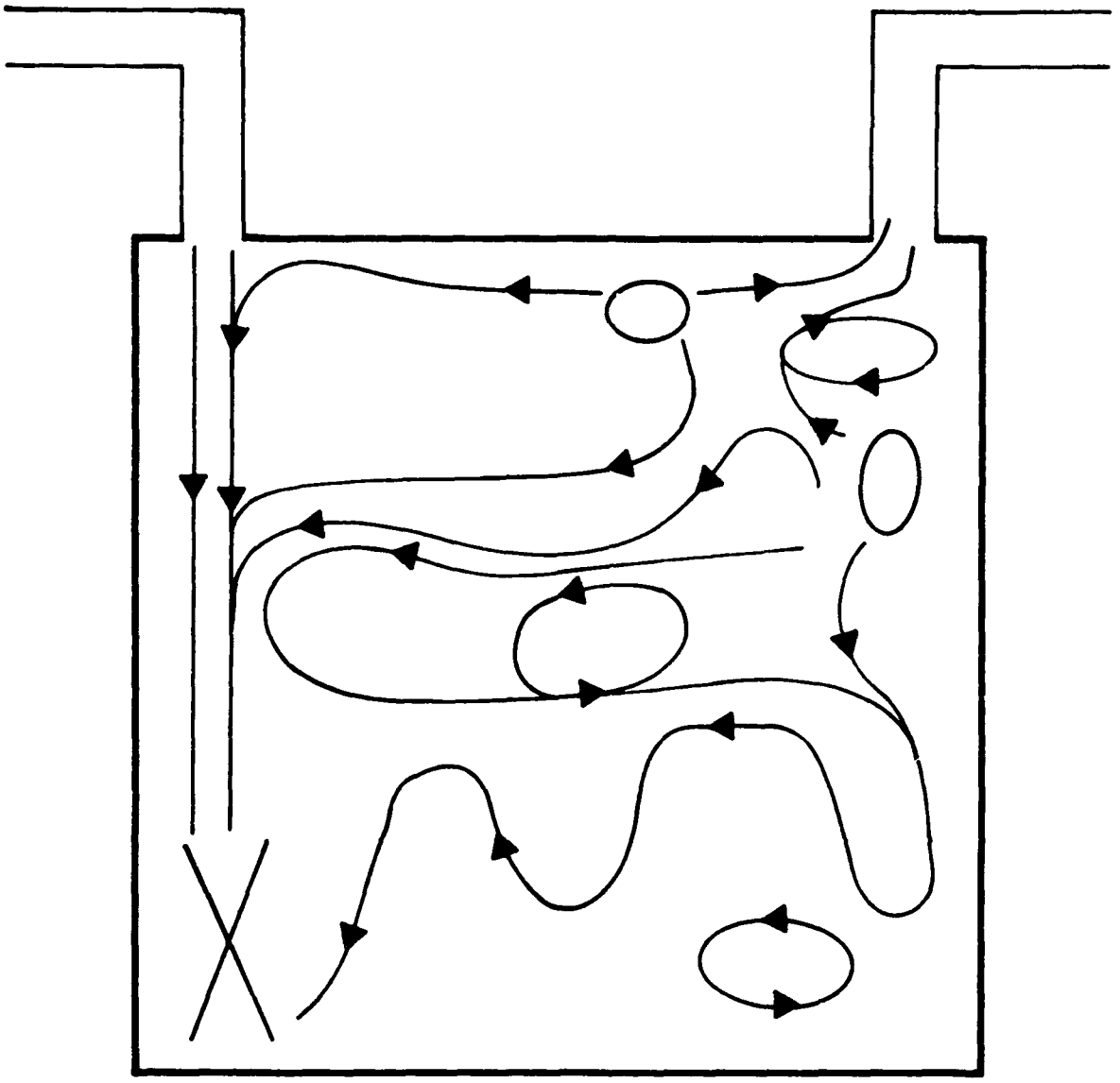

Figure A3 Air distribution predicted for an 8' x 8' shelter with natural ventilation but without a simulated occupant (Condition II)

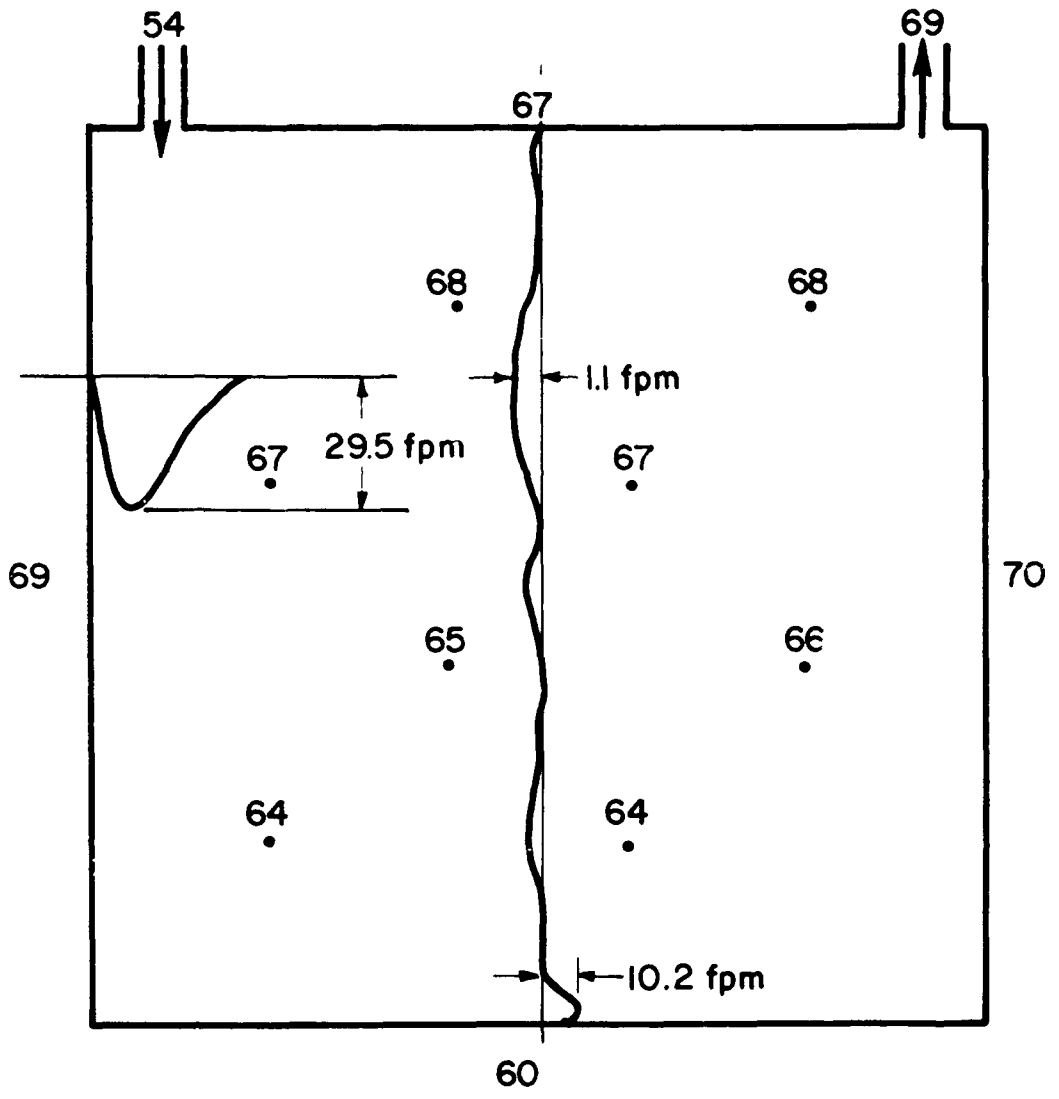

Figure A4 Air temperatures and velocities predicted for an 8' x 8' shelter with natural ventilation but without a simulated occupant (Condition II)

The same thermal stratification of the inner core observed in Condition I can be seen here. Assume a one degree temperature difference exists between the left and right walls, while a comparatively large difference (15 °F) exists between the ventilation supply and exhaust air. This indicates that most of the motion is due to the ventilation. The predicted temperature of the air leaving through the ventilation exhaust is slightly above the predicted temperature of the air near the ceiling. This is due to some of the warmer air from the right wall boundary layer mixing with the warm air near the ceiling as both were exhausted.

The predicted velocities of the different air flows in the full-sized shelter are shown in figure A4. The cold incoming air falls directly to the bottom of the shelter. On its way to the floor it is drawn towards the left wall, due to the Coanda effect. The entering air entrains the room air as it falls, and causes a horizontal motion of the room air toward the incoming stream. The horizontal velocity of the room air is highest adjacent to the opening to the ventilation supply duct, since the entrainment of room air with the entering air is highest at this location.

As the ventilation air moves down the wall its velocity diminishes and the fresh air becomes increasingly mixed with the room air. Upon reaching the floor the ventilation air spreads out across the floor. Although a little of the fresh air may become entrained in the slight boundary layer rising along the right wall, most of it remains in the lower portion of the room.

The velocity of the incoming ventilation air has been determined approximately three feet below the supply duct opening. The maximum predicted velocity of the air stream for this case is 29.5 feet-per-minute. The horizontal velocity near the center of the room would be 1.1 feet-per-minute and the maximum velocity of the flow across the floor would be 10.2 feet-per-minute. The boundary layer at the floor would be about 9 in. thick.

Several variations on the above simulation have been made for different temperature differences between the ventilation supply and exhaust ducts. Results of these simulations will be discussed, but the figures will not be shown since the shelter configurations are the same as those already discussed.

If the temperature differential between the ducts is increased to 29 degrees, considerably more turbulence will occur in the shelter. The room air will mix with the fresh air much more rapidly, the horizontal velocities due to entrainment with the supply air will be higher than before, and the temperature differential between the floor and ceiling will decrease. The velocity of the entering air, measured at the same location as before, will have a maximum value of 41 feet-per-minute. The temperature difference between the floor and ceiling will be reduced to 4 °F.

If the temperature difference between the supply and exhaust is reduced to six degrees, a significant reduction in the air motion will occur throughout the room. As the air enters it will be deflected toward the left wall close to the inlet. The fresh air will move down the wall a short distance and then turn horizontal about halfway down the wall.

The velocity of the supply air, at the same location as before, will be a maximum of 17.8 feet-per-minute. The temperature differential between the floor and ceiling will be 9° higher than for the original case shown in figure A4.

The next set of figures depicts results for some other tests conducted under Condition II. The significant difference between these tests and those already discussed for Condition II is the position of the ventilation ducts.

Figures A5 and A6 show the combined effect on the room air, of a 23 degree F temperature difference between the supply and exhaust air and a 5 degree difference between the left and right wall temperatures. Here the ventilation ducts are protruding down about three feet from the ceiling. The considerable horizontal motion of the room air is due to its entrainment with the faster, vertically moving streams. Since the supply air enters the room closer to the floor it undergoes less mixing with the room air before reaching the floor. After spreading out across the floor there is little further mixing with the room air, except for the small amount that is entrained in the boundary layer rising along the right wall. Due to the low position of the opening to the exhaust duct, air is removed from that elevation. This causes a layer of warm stale air to build up near the ceiling.

Figures A7 and A8 show the results of a simulation closely resembling the one just discussed. The significant difference here is the small, two degree, temperature difference between the left and right walls. The ventilation rate is almost exactly the same as before. Thus, the reduced air motion throughout the room is due to the small circulation effect of

the boundary layer. The net effect of the smaller temperature difference between the walls is to cause a larger temperature difference between the floor and ceiling.

In figures A9 and A10 can be seen the effects of placing the ventilation supply duct close to the floor. In a full-sized room this would be equivalent to the duct opening about 18 in above the floor. Mixing is poor because the air enters close to the floor, then spreads out in all directions at the floor level. Some circulation occurs due to the 5° differential between the left and right walls, but this circulation does not cause significant mixing of the air in the shelter. The relatively large, 10 degree, temperature difference between the floor and ceiling is further evidence of the poor mixing.

Although the mixing is poor, this simulation indicates a definite advantage to be gained from locating the ventilation supply close to the floor of a shelter, rather than close to the ceiling. When the temperature differential between the supply and exhaust air becomes small, as it may during the summer months, the ventilation rate will be small. As has already been shown, when the ventilation rate is small and the supply duct opening is close to the ceiling, the entering air may never reach the shelter occupants. On the other hand, if the ventilation supply duct opening is located near the floor then the occupants will benefit from even a small amount of fresh air.

In figures A11 and A12 can be seen the results of a simulation when the direction of the openings to the ventilation ducts is changed from vertical to horizontal. One of the first things to notice is the apparent good mixing of the room air with the ventilation air, in spite of the

small, 14 degree, difference between supply and exhaust temperatures. This mixing is further evidenced by the relatively small, 5 degree, temperature difference between the floor and ceiling.

Actually the mixing throughout the shelter is not quite as good as it appears when one considers a three-dimensional shelter. The supply duct is highly directional thus the ventilation air is discharged directly toward the right wall. Once the flow reaches the right wall it does not spread out uniformly across the floor but tends to divide and go toward the rear and front of the shelter. The temperature difference between the walls was relatively small; thus, it did not contribute in any great part to the circulation in the shelter.

The advantage of having the ventilation duct discharge horizontally is that the flow of air can be directed toward a specific location in the shelter. This would be a disadvantage however, in a crowded shelter, because many of the shelter occupants would be missed by this highly directional stream.

The changed direction of the exhaust duct opening had no apparent effect upon the air distribution in the shelter.

Condition III: Simulation of Air Distribution in a Shelter Without Natural Ventilation But With a Simulated Occupant

Condition III resembles the situation that would occur when the outside air temperature exceeded the shelter temperature or when the shelter must be operated under sealed conditions.

Figures A13 and A14 show predicted air current patterns and velocities and temperatures in a full-sized, 8 feet wide by 8 feet high, naturally ventilated shelter.

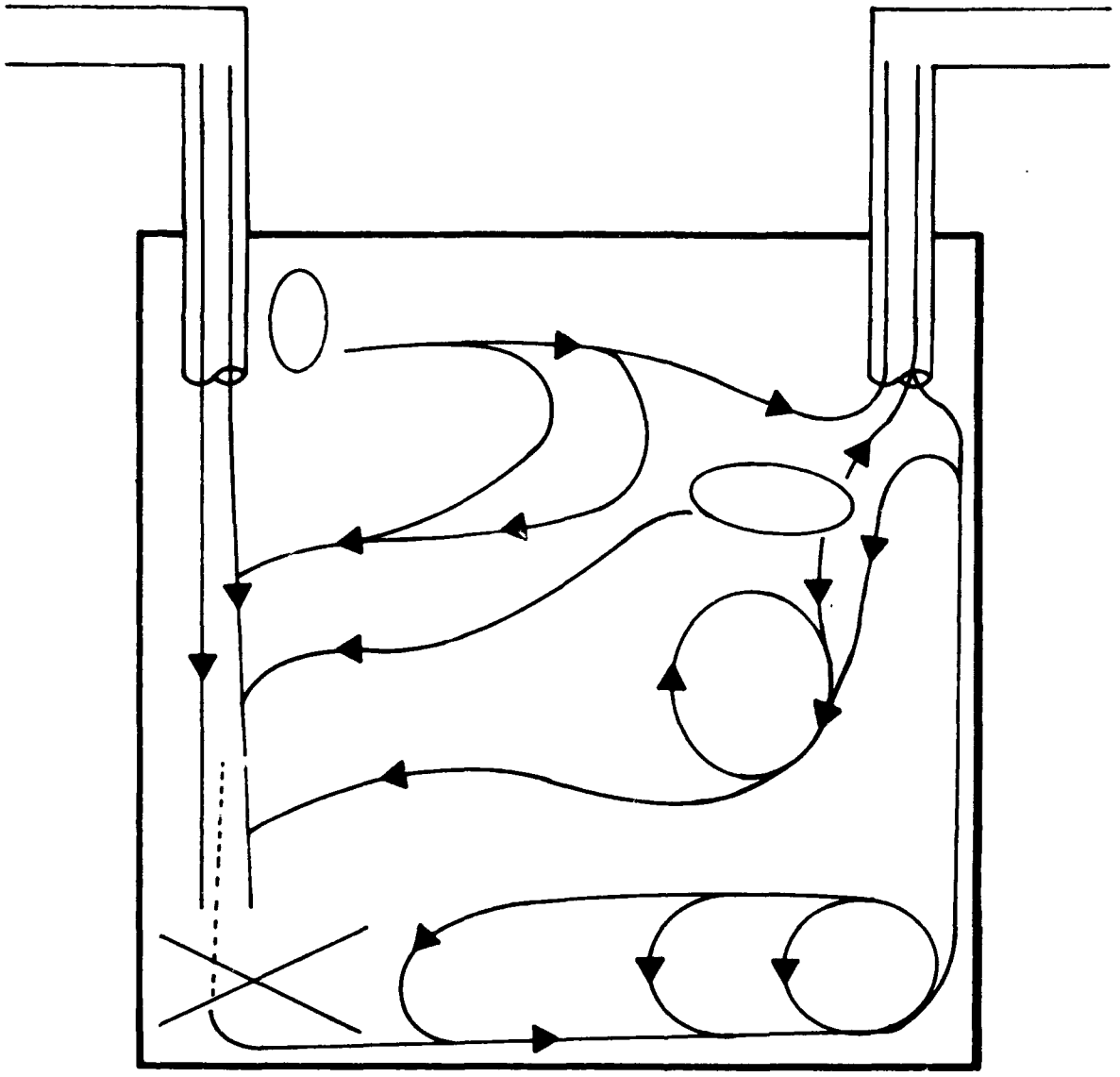

Figure A5 Air distribution predicted for an 8' x 8' shelter with natural ventilation but without a simulated occupant (Condition II)

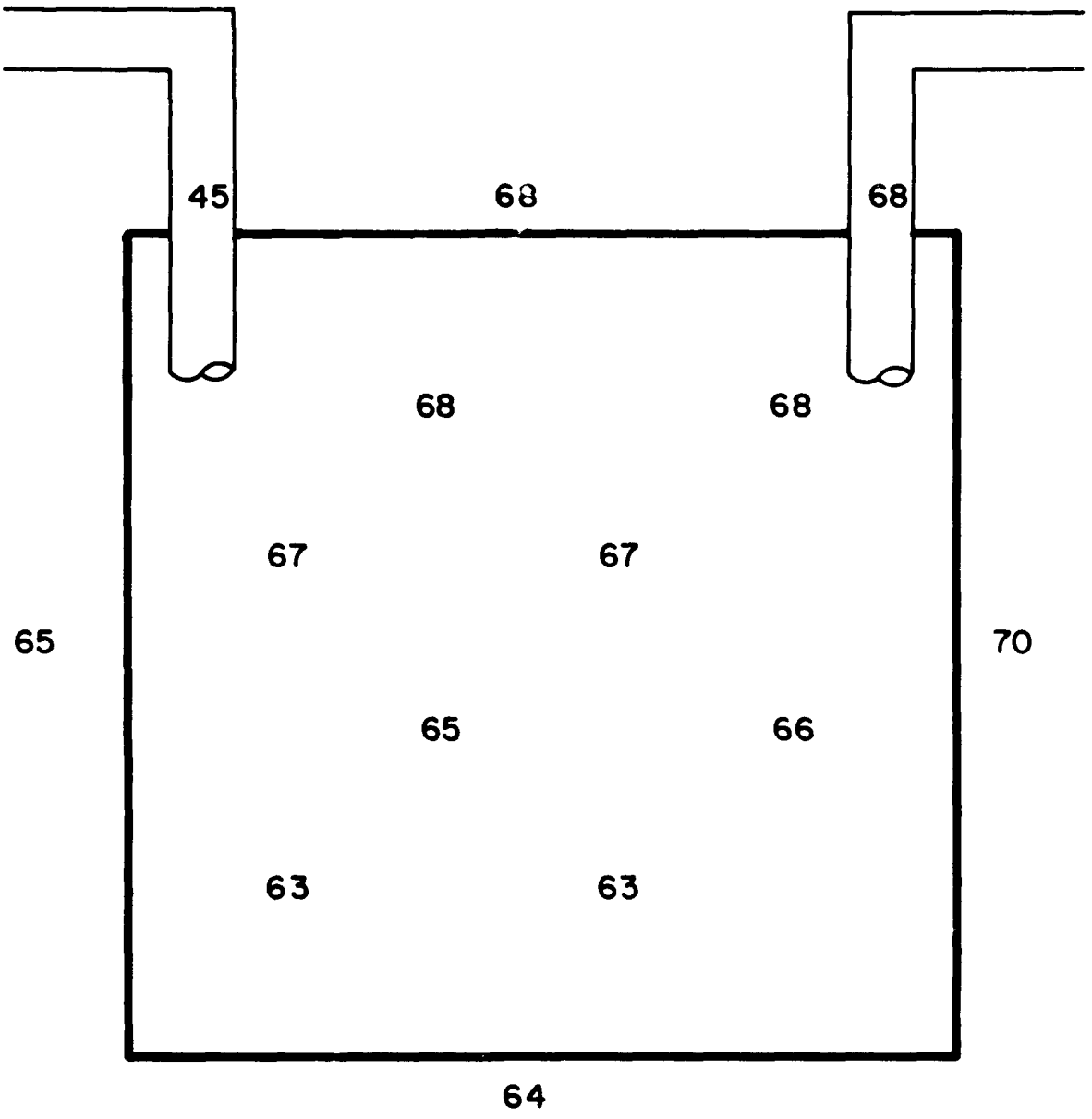

Figure A6 Air temperatures predicted for an 8' x 8' shelter with natural ventilation but without a simulated occupant (Condition II)

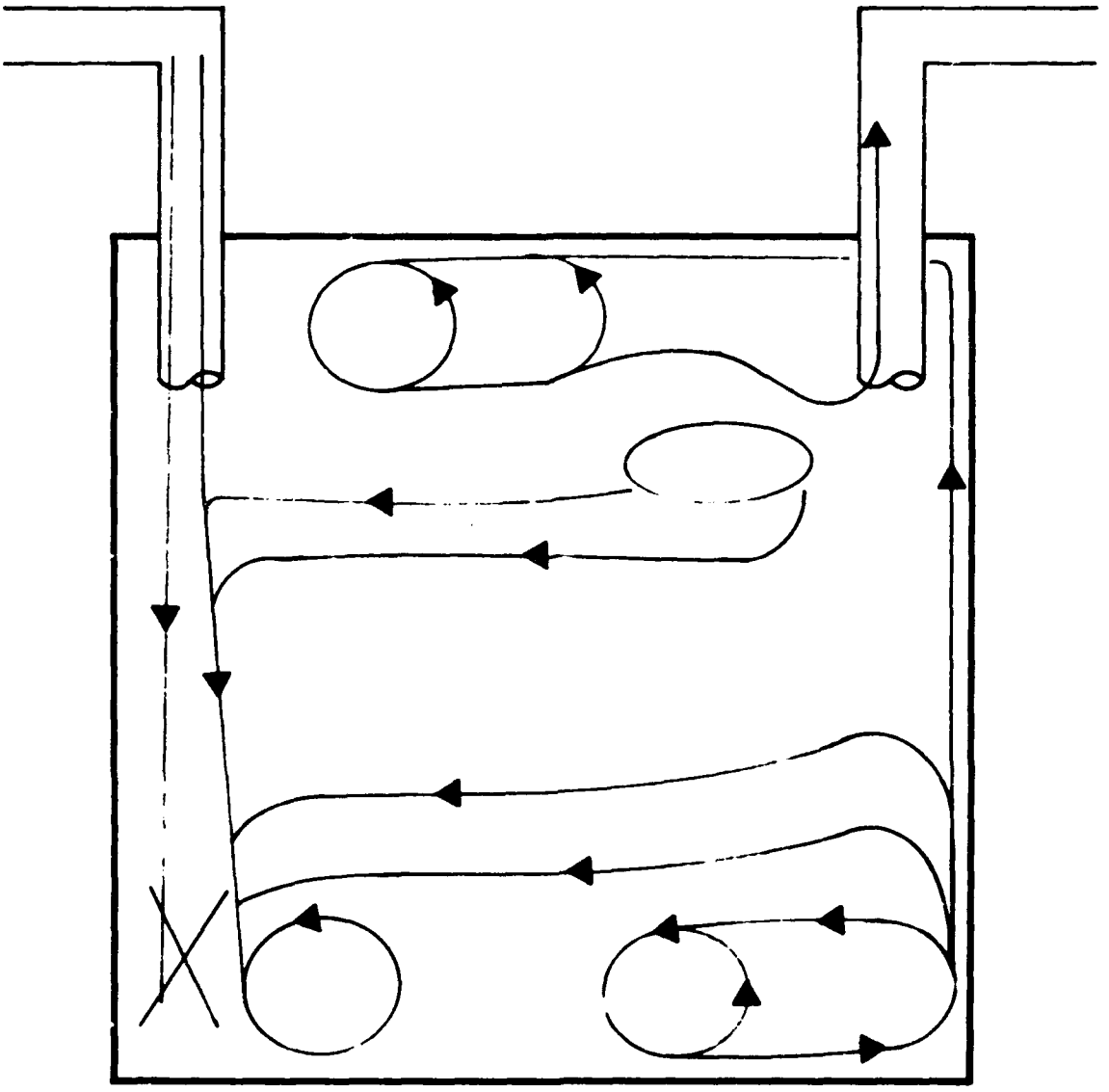

Figure A7 Air distribution predicted for an 8' x 8' shelter with natural ventilation but without a simulated occupant (Condition II)

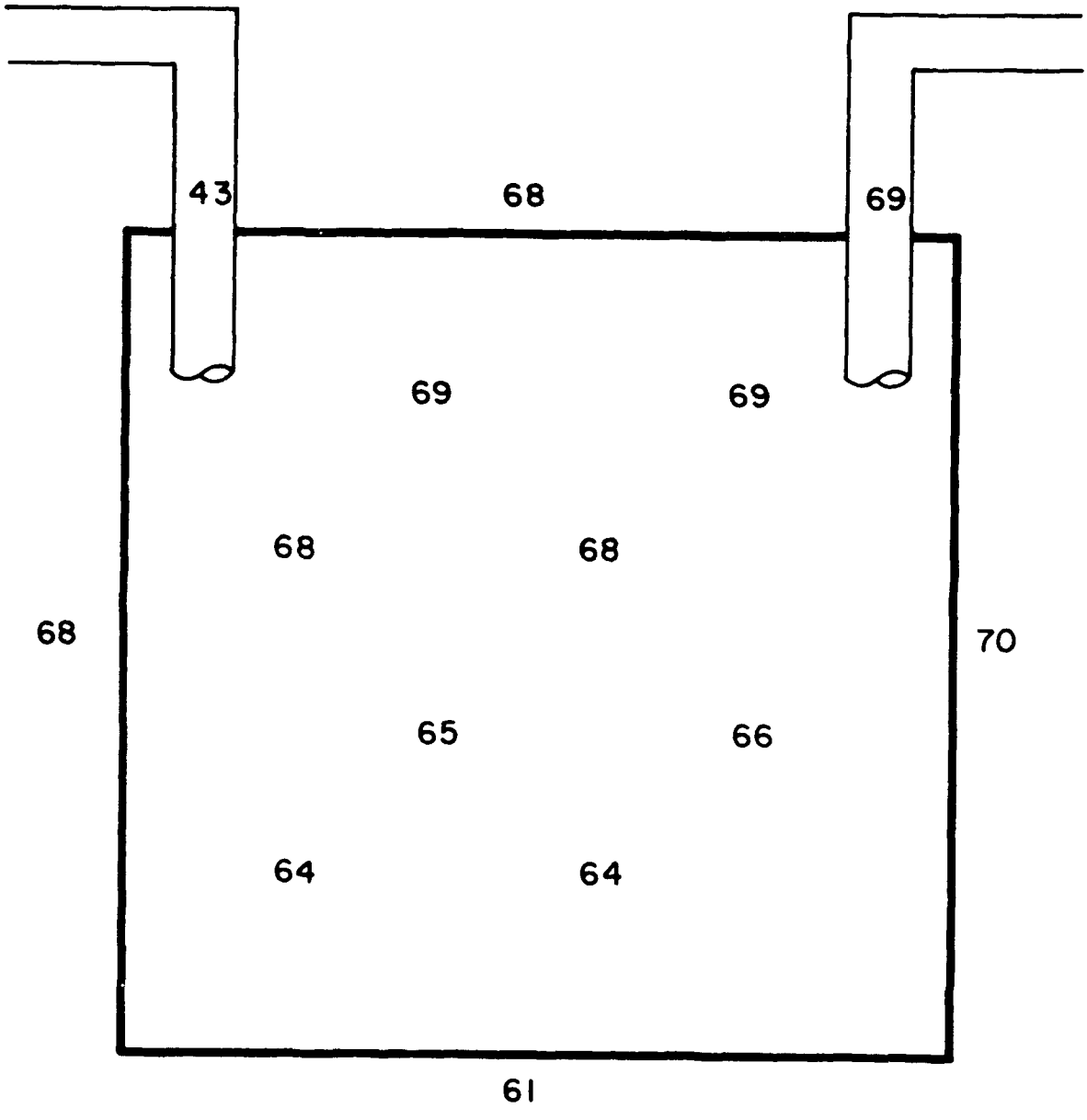

Figure A8 Air temperatures predicted for an 8' x 8' shelter with natural ventilation but without a simulated occupant (Condition II)

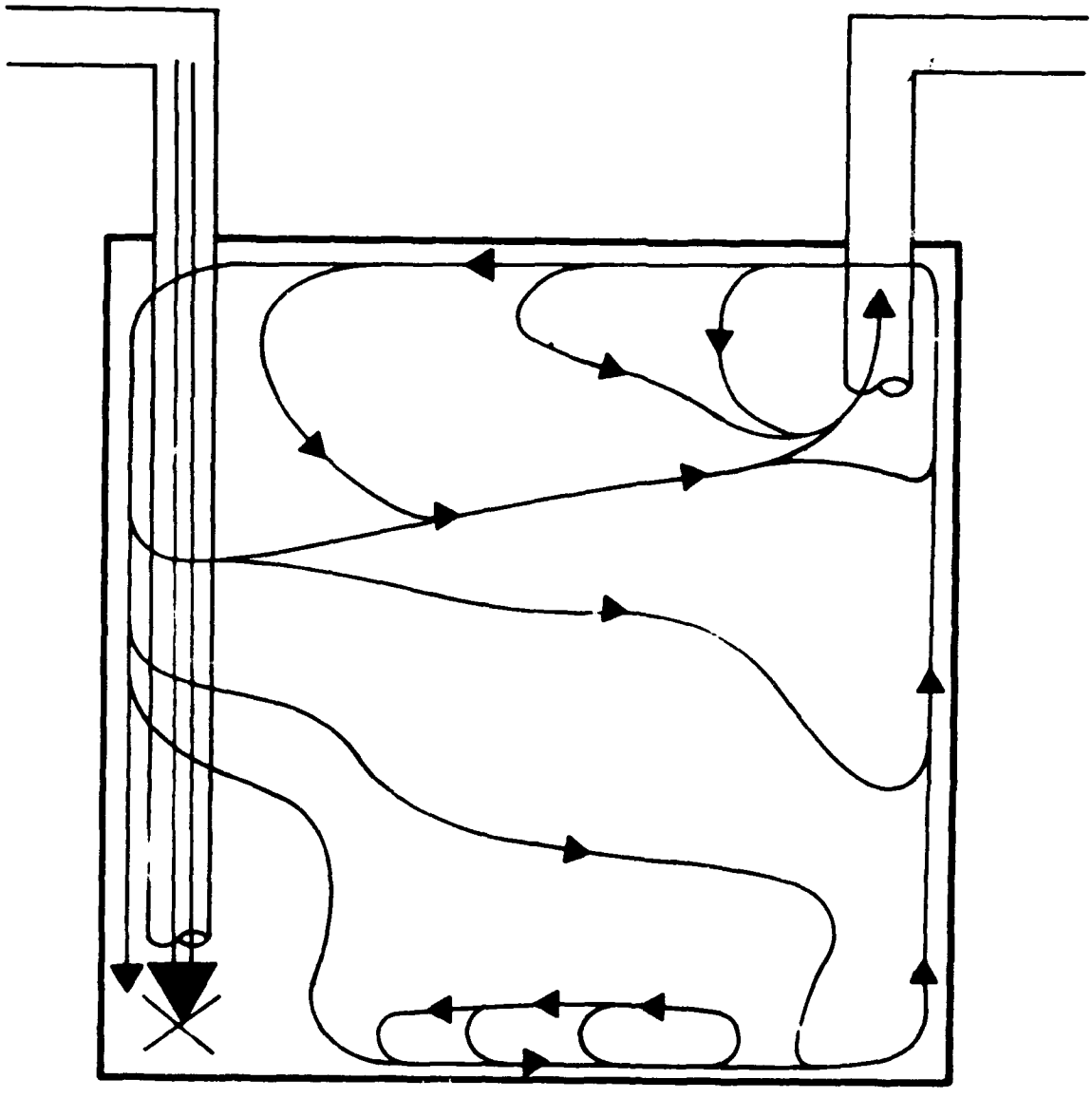

Figure A9 Air distribution predicted for an 8 x 8' shelter with natural ventilation but without a simulated occupant (Condition II)

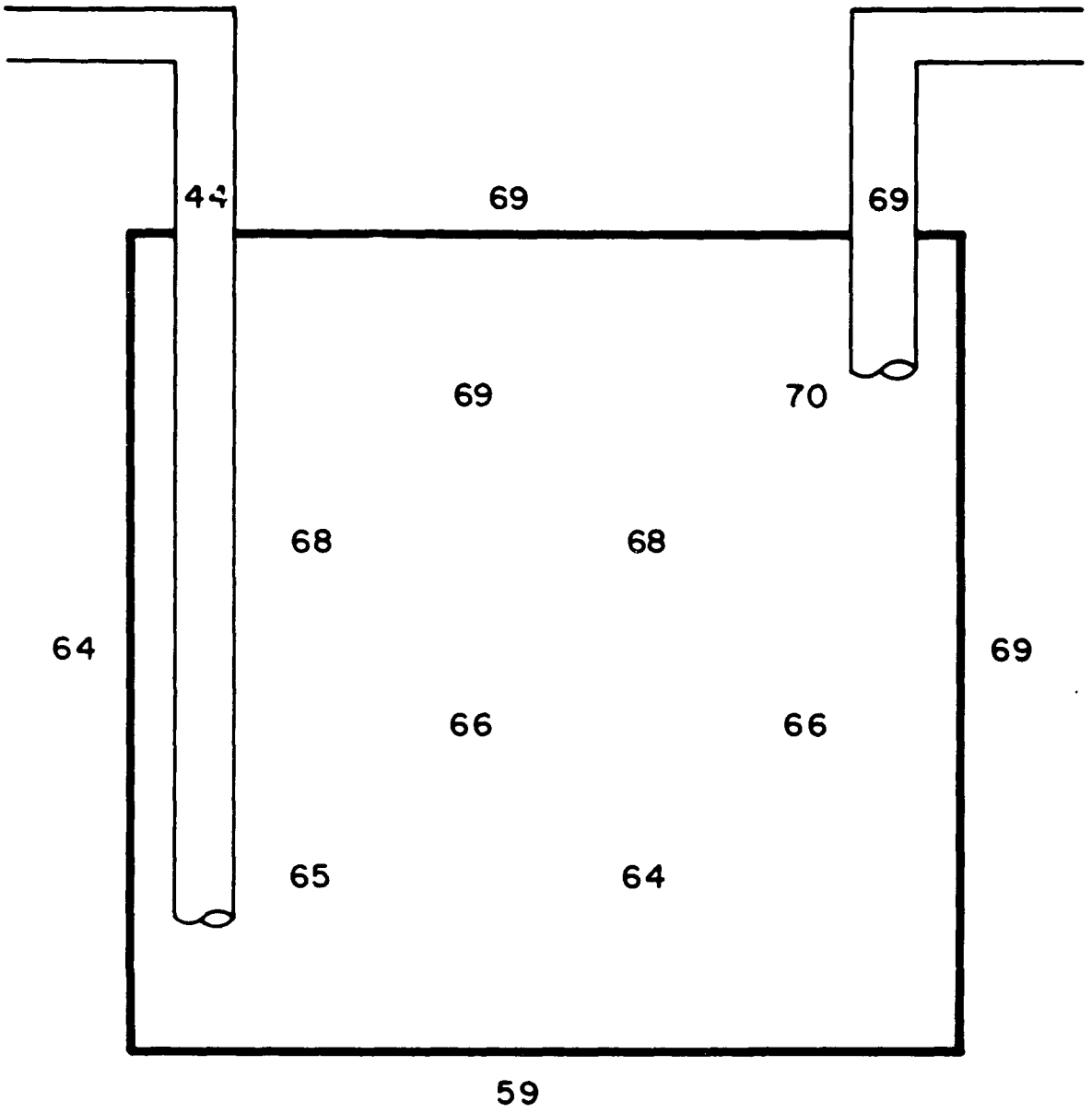

Figure A10 Air temperatures predicted for an 8' x 8' shelter, with natural ventilation but without a simulated occupant (Condition II)

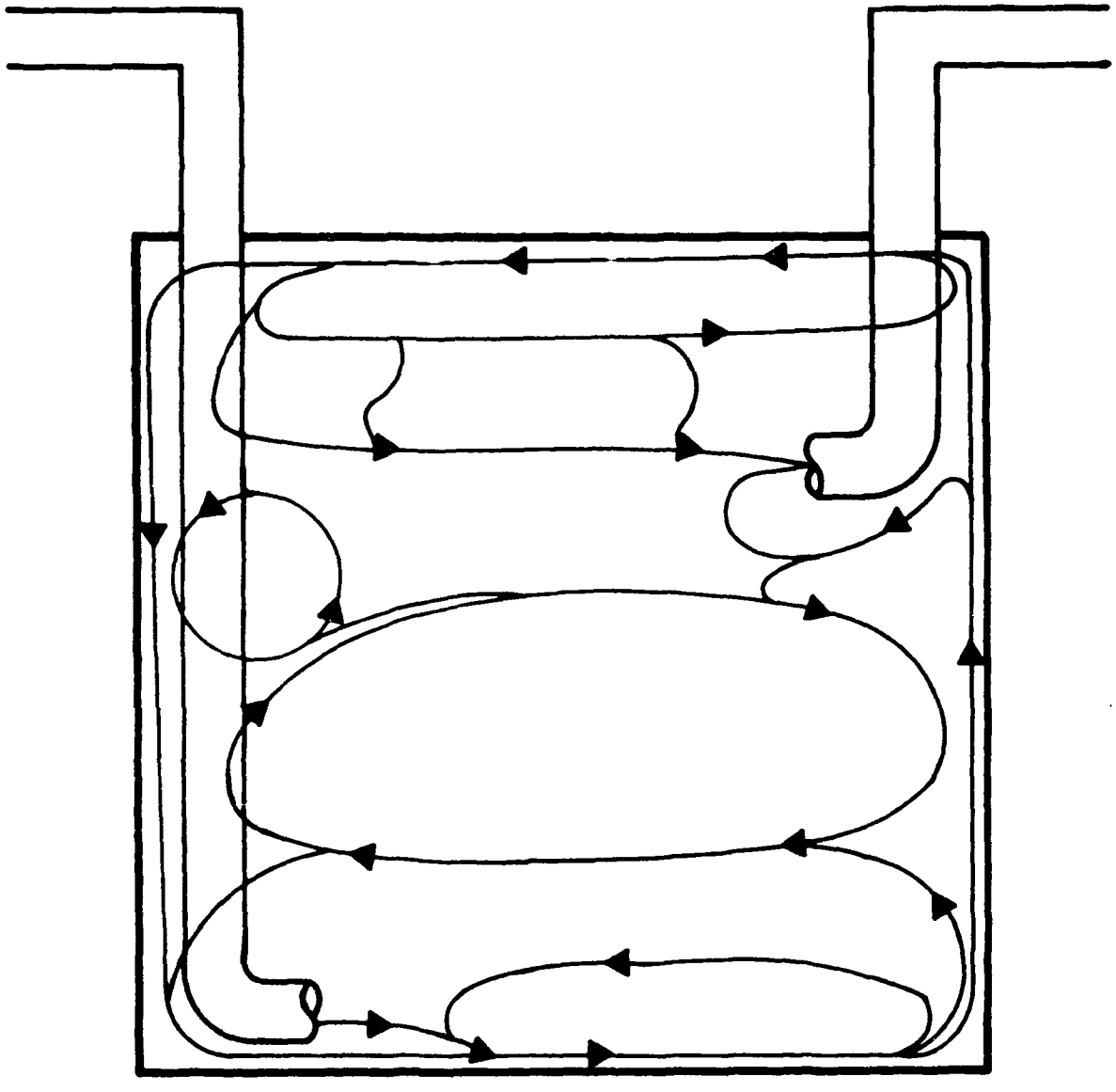

Figure A11 Air distribution predicted for an 8' x 8' shelter with natural ventilation but without a simulated occupant (Condition II)

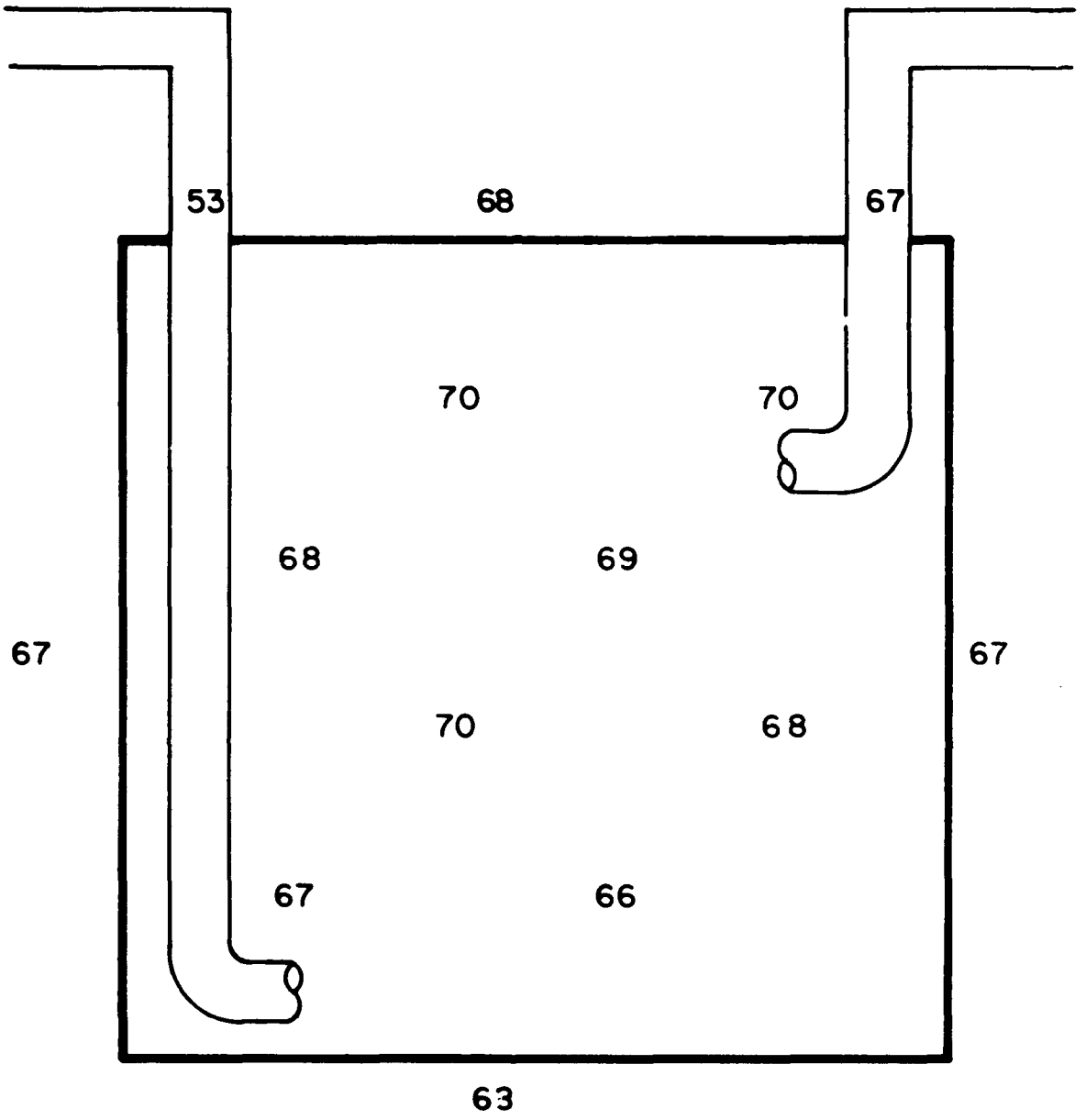

Figure A12 Air temperatures predicted for an 8' x 8' shelter with natural ventilation but without a simulated occupant (Condition II)

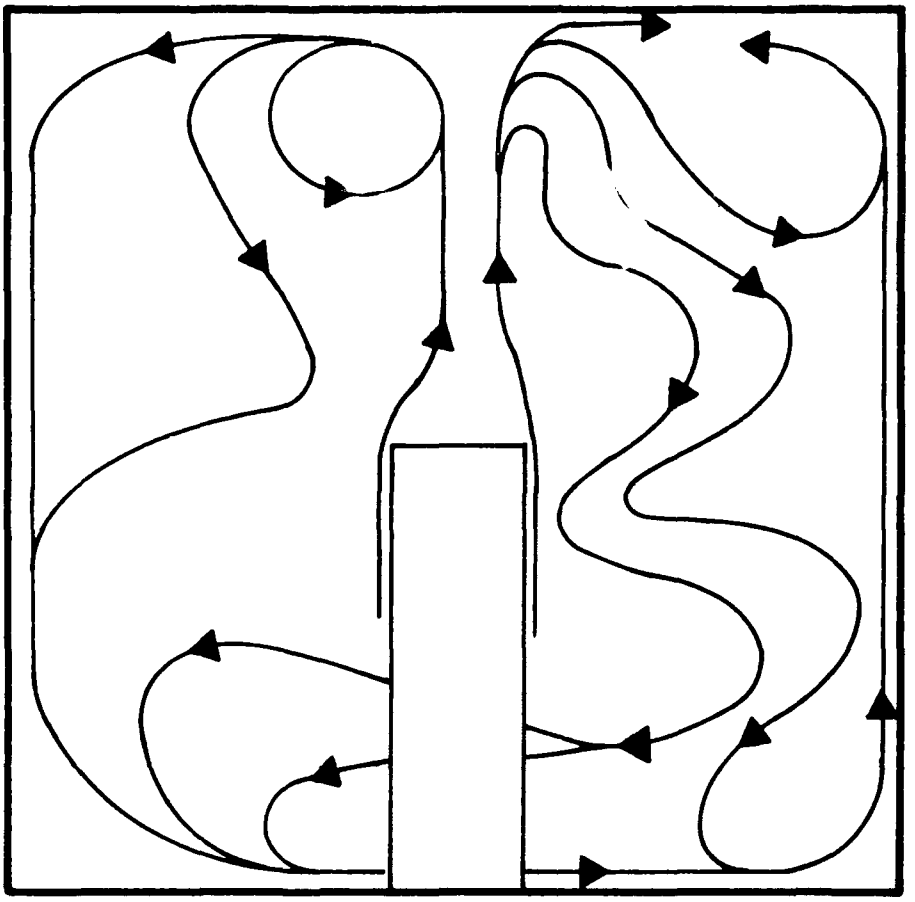

Figure A13 Air distribution predicted for an 8' x 8' shelter with a simulated occupant but without natural ventilation (Condition III)

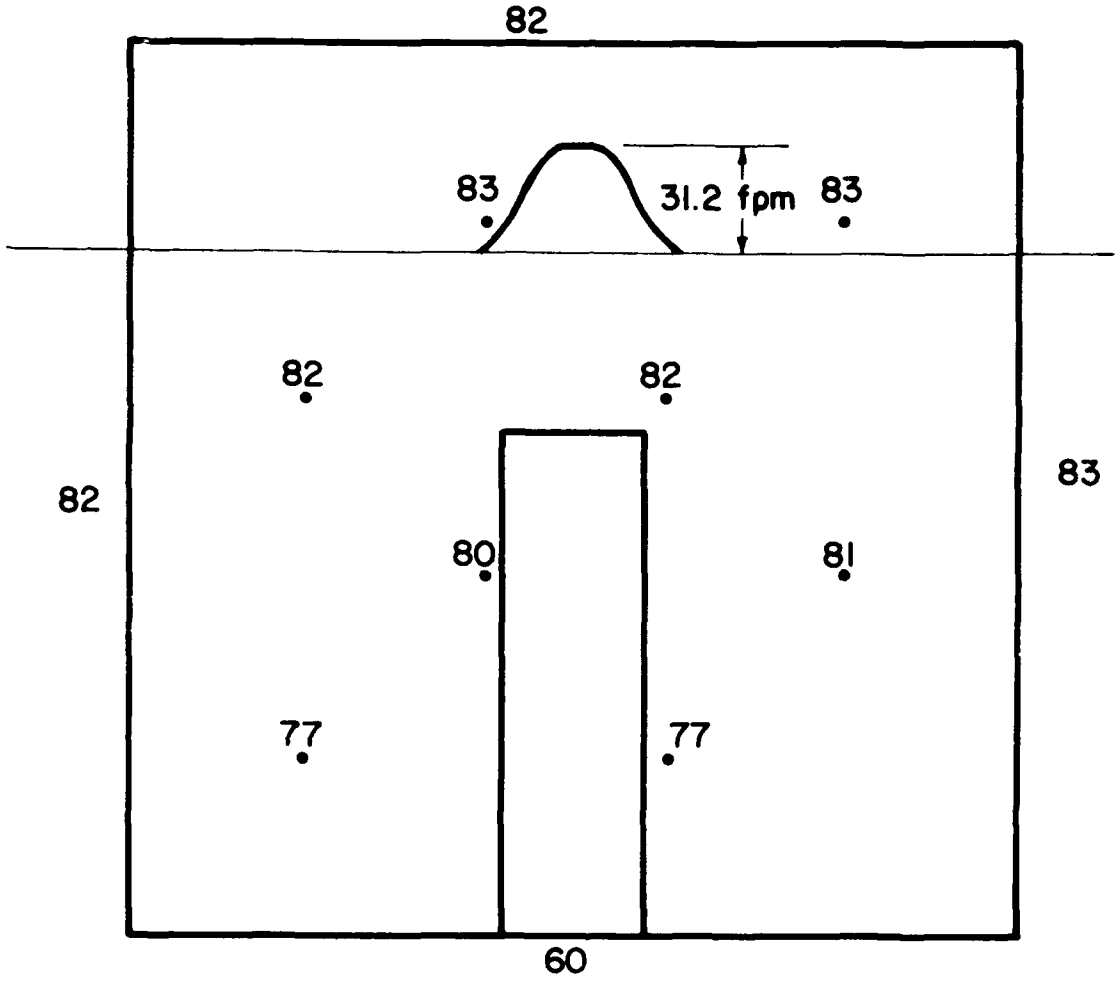

Figure A14 Air temperatures and velocities predicted for an 8' x 8' shelter with a simulated occupant (77 °F) but without natural ventilation (Condition III)

The temperature of the occupant's surface is about 17 °F above the floor temperature. The velocity of the air rising from the occupant would be 31.2 feet-per-minute.

One of the most apparent effects of Condition III is the large temperature differential, 22 degrees, between the floor and ceiling. In the absence of ventilation air to mix with and cool the room air, the heat from the simulated occupant is trapped at the ceiling. Further, a small, 1 degree, temperature difference between the left and right walls did not give a significant boost to circulation.

In terms of an actual shelter it seems surprising that there should be such a large temperature differential between the floor and ceiling. It seems especially surprising that there would be a 17 degree temperature difference between the floor and the room air two feet above the floor.

In general there is little motion in the shelter, except for that above the simulated occupant. The air rising from the occupant, despite its comparatively high velocity, does not produce a significant effect on the shelter air motion. The air warmed by the occupant moves vertically through the stagnant inner core until reaching the ceiling where it spreads out in all directions. As it passes through the inner core the rising column causes horizontal motion in the surrounding air. This happens because the surrounding air becomes entrained with the fast rising column of warm air.

Figures A15 and A16 show the same shelter but with two simulated occupants. Again notice even a larger temperature difference between floor and ceiling. This is due to the presence of an additional simulated occupant.

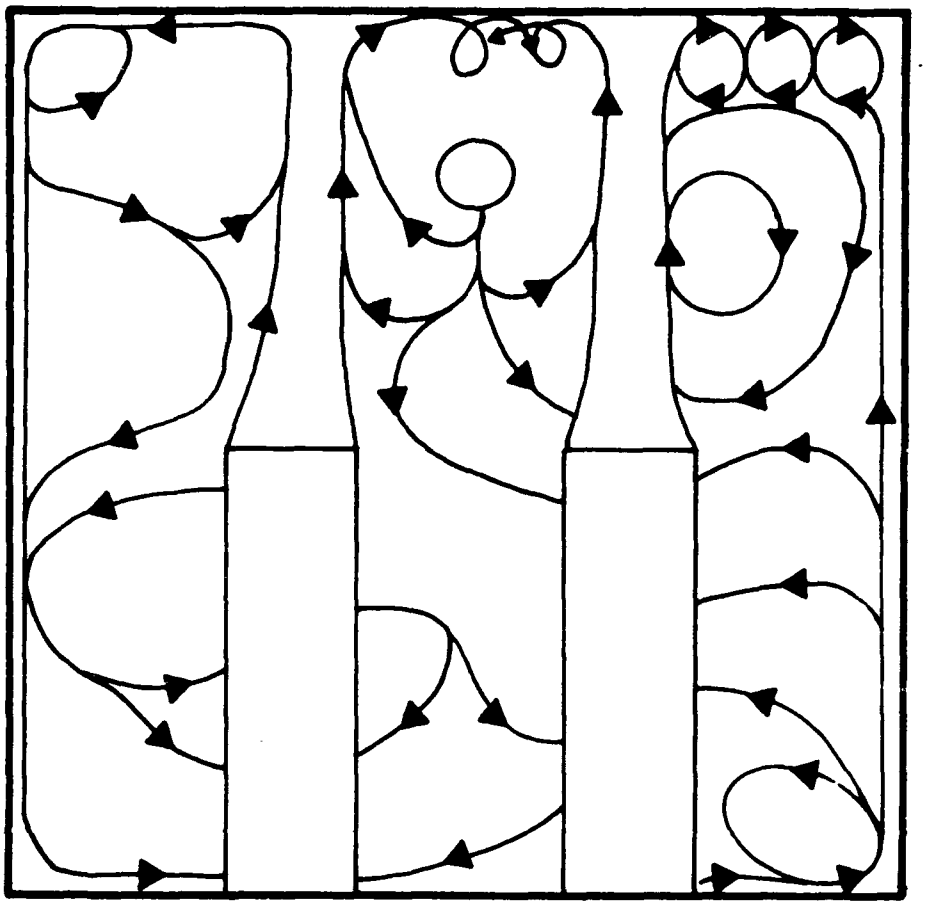

Figure A15 Air distribution predicted for an 8' x 8' shelter with simulated occupants but without natural ventilation (Condition III)

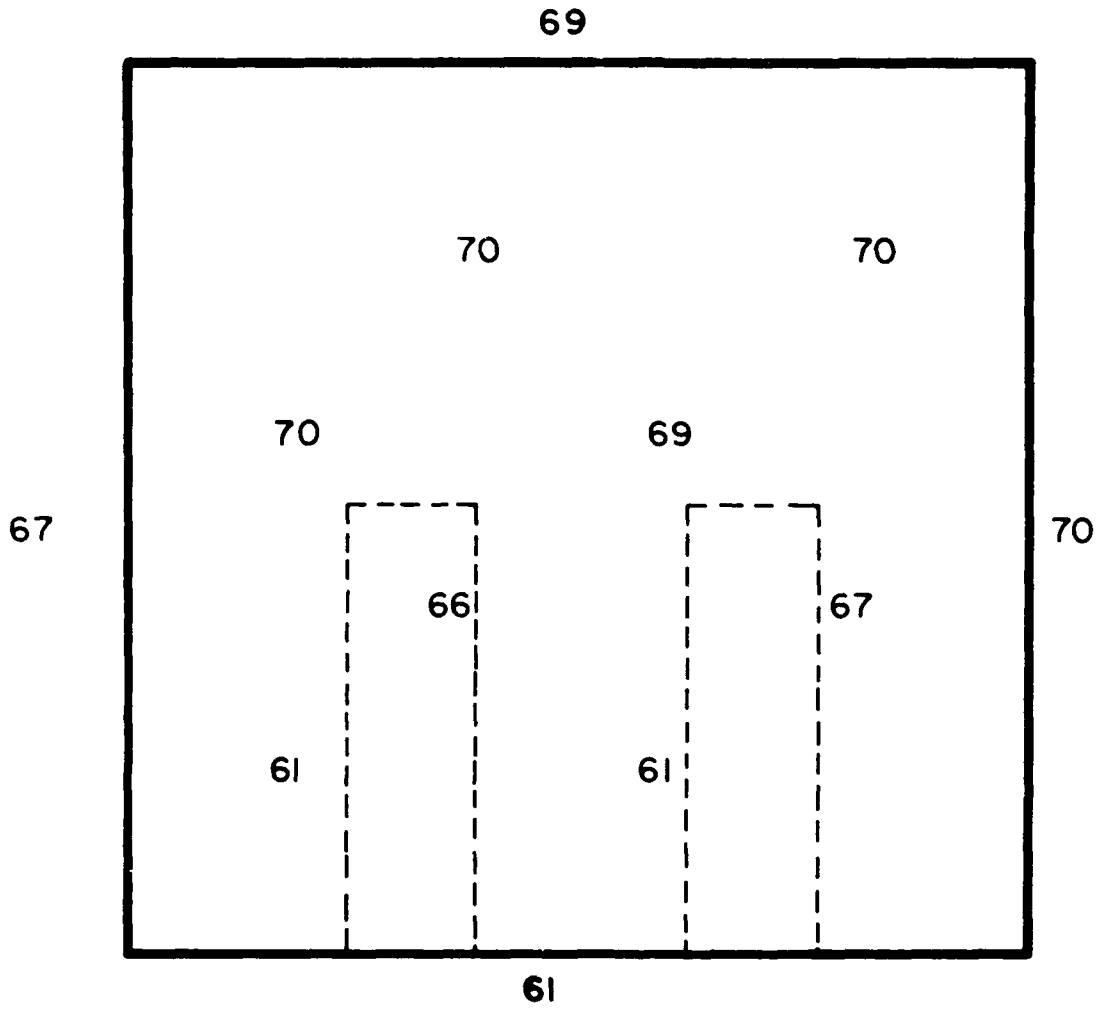

Figure A16 Air temperatures predicted for an 8' x 8' shelter with simulated occupants but without natural ventilation (Condition III)

The highest velocities in the shelter occur above the simulated occupants. The warm air rises to the ceiling then spreads out in all directions. The temperature difference between the right and left walls is 3 degrees which is enough to cause some circulation around the periphery of the room, but not enough to have a significant effect on the mixing of the room air.

Condition IV: Simulation of Air Distribution in a Shelter With Natural Ventilation and With a Simulated Occupant

This is the condition most likely to be encountered in a shelter, provided there is a favorable thermal driving force between the inside and the outside.

Figures A17 and A18 show predicted air current patterns and temperatures and velocity profiles for this condition.

The simulated occupant is at a temperature approximately 17 degrees above that of the floor. The velocity of the air rising from the occupant is slightly over 30 feet-per-minute.

Here there is roughly a 10 degree difference between the floor and ceiling whereas that difference is 22 degrees for Condition III. The ventilation effect would be primarily responsible for the smaller difference since it prevents the buildup near the ceiling of heat generated by the occupant. The temperature difference between the walls, 3 degrees, would cause a counter-clockwise circulation at the periphery of the air space, but it would not be the predominant influence on the air motion.

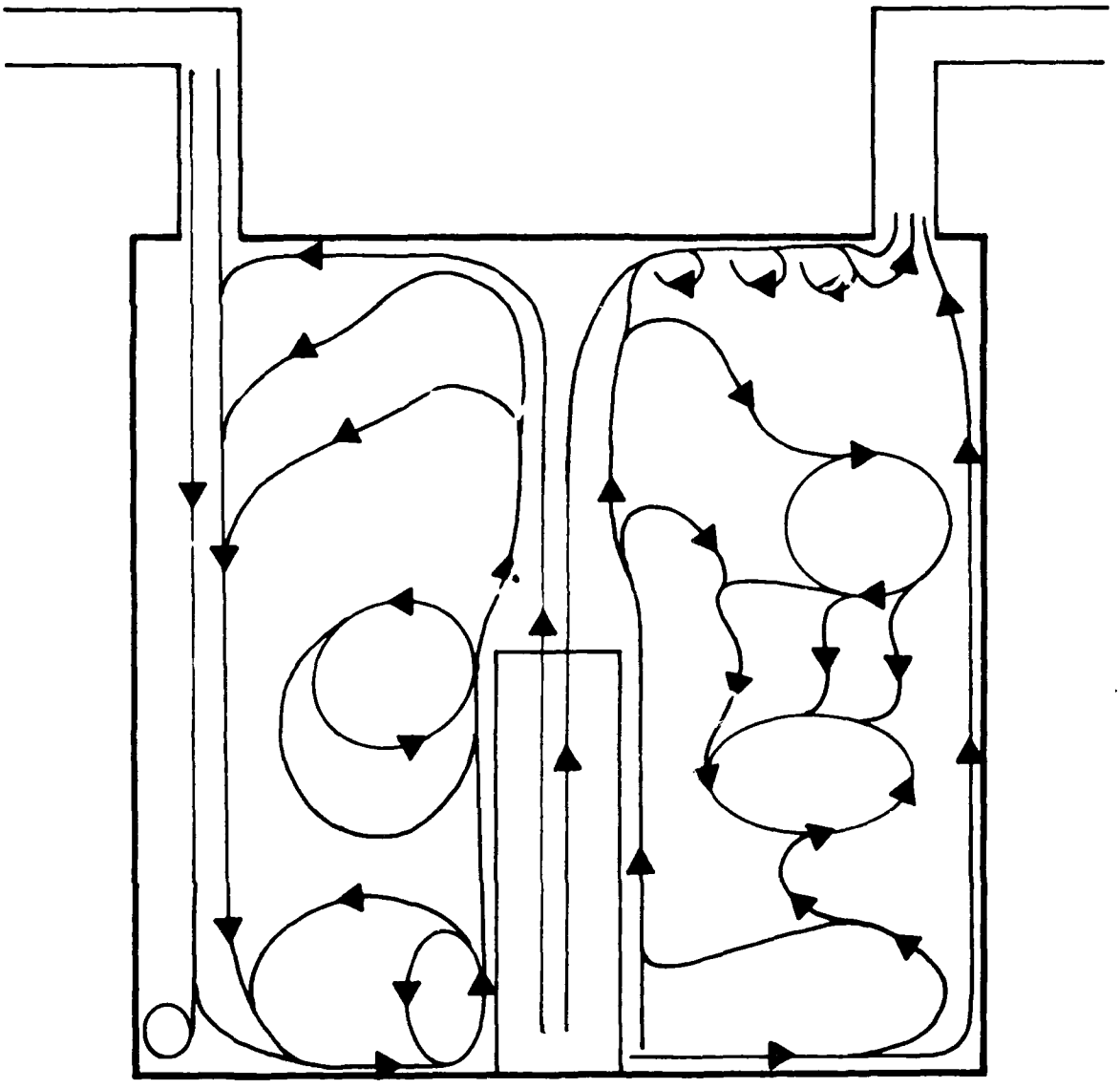

Figure A17 Air distribution predicted for an 8' x 8' shelter with a simulated occupant and natural ventilation (Condition IV)

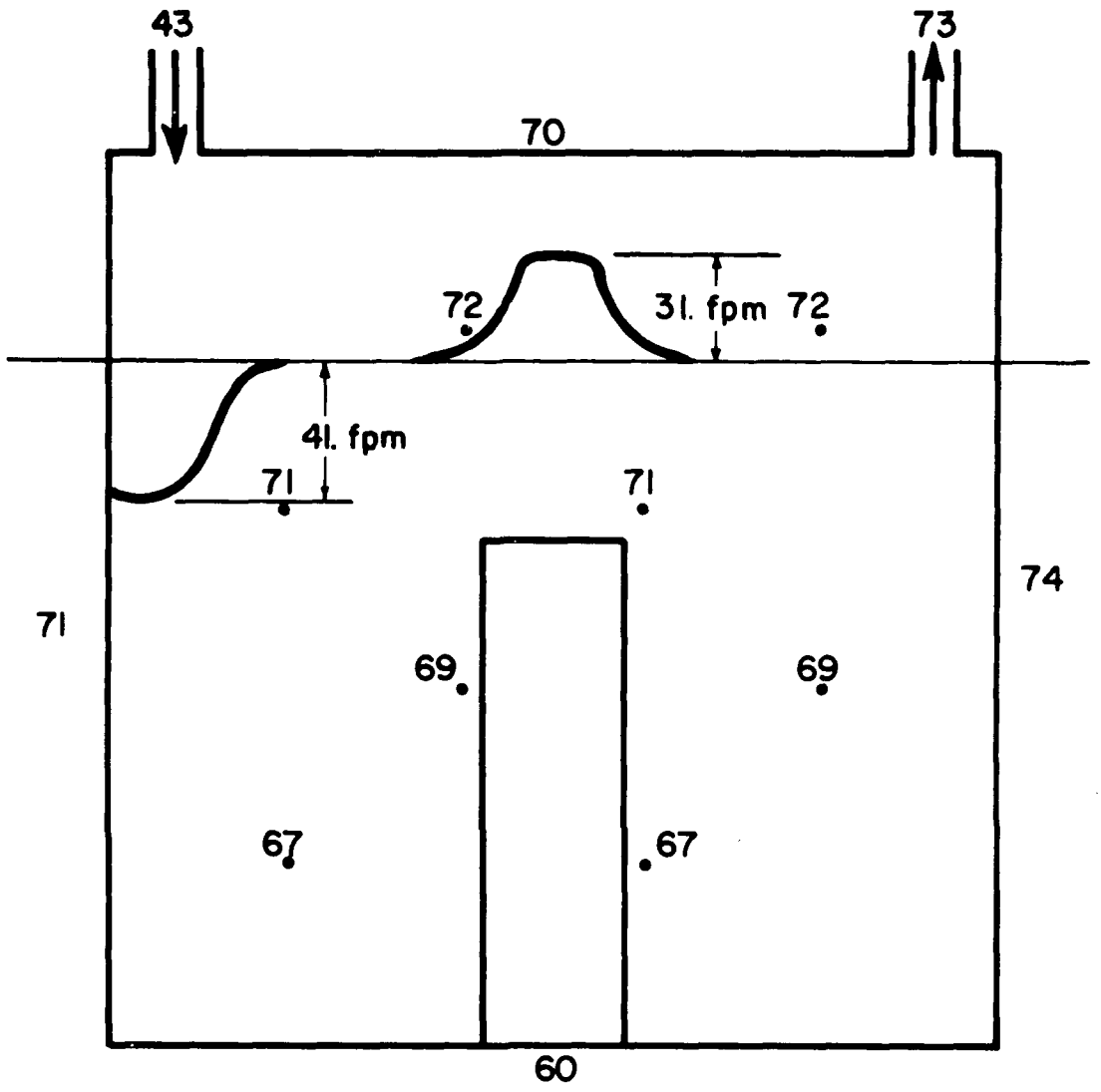

Figure A18 Air temperatures and velocities predicted for an 8' x 8' shelter with a simulated occupant and natural ventilation (Condition IV)

There would be considerable air motion due to the combined effect of the heat from the occupant, the ventilation, and the circulation due to the temperature difference between the walls.

Some thermal stratification noted in earlier cases would also be present here in spite of the rather vigorous air motion. This indicates that the inner core of air would be quite stable, and fairly resistant to the perterbing effect of streams passing through. Because of its large inertia in relation to that of the stream passing through, the core air would tend to absorb these streams or dissipate their effect, rather than to be excited by them.

Figures A19 and A20 show a ventilated shelter with two simulated occupants. Again the temperature of both occupants is assumed to be about 17 degrees above the floor temperature. The velocity of the air rising from the occupants would be approximately the same as before, slightly over 30 feet-per-minute.

The temperature difference between the floor and ceiling, about ten degrees, is somewhat higher than in the preceding simulation but this is due to the reduced ventilation rate. The heat rising from the occupants is trapped near the ceiling and drawn off gradually through the ventilation exhaust. Again some thermal stratification is apparent in this case.

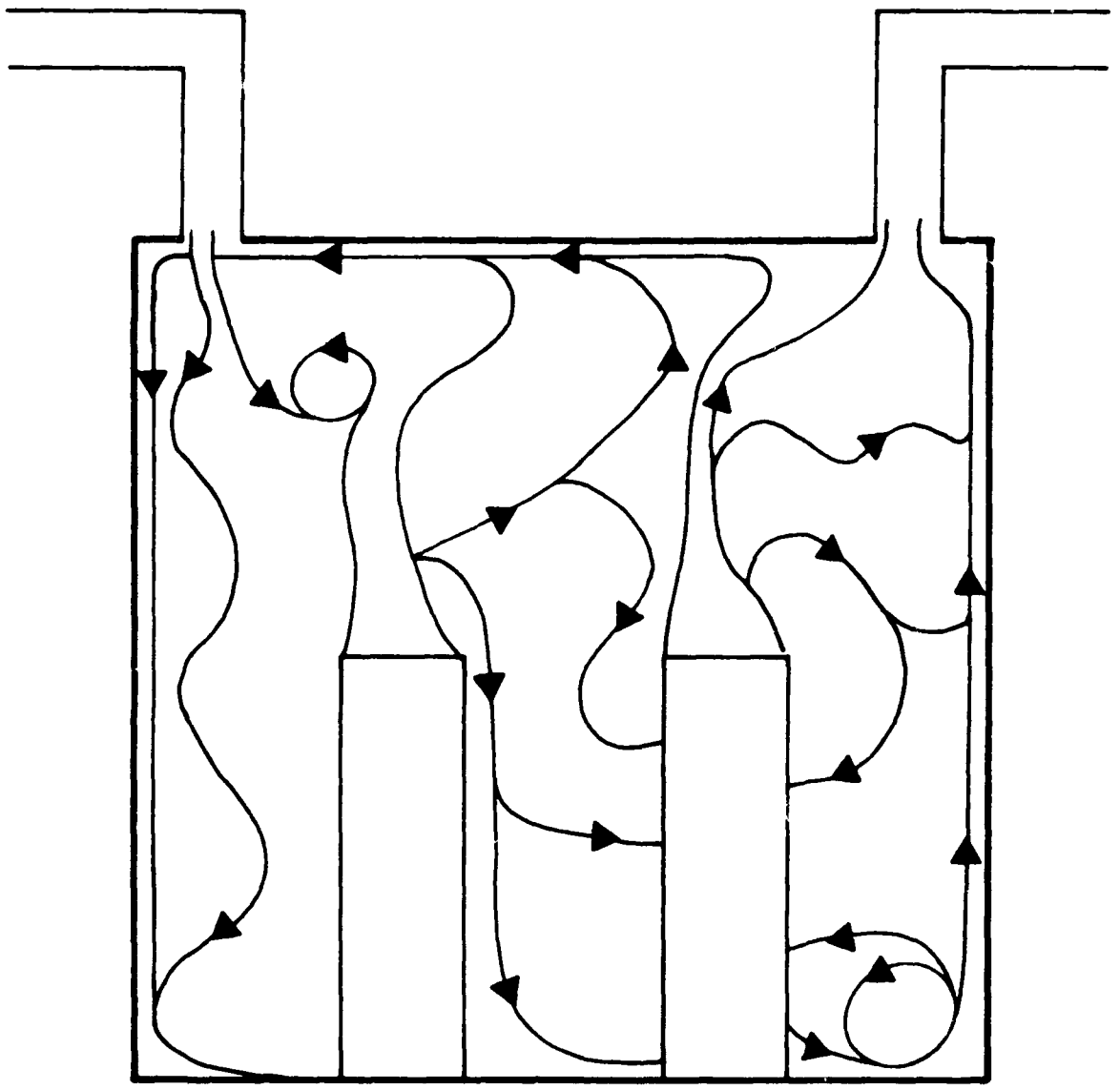

Figure A19 Air distribution predicted for an 8' x 8' shelter with simulated occupants and natural ventilation (Condition IV)

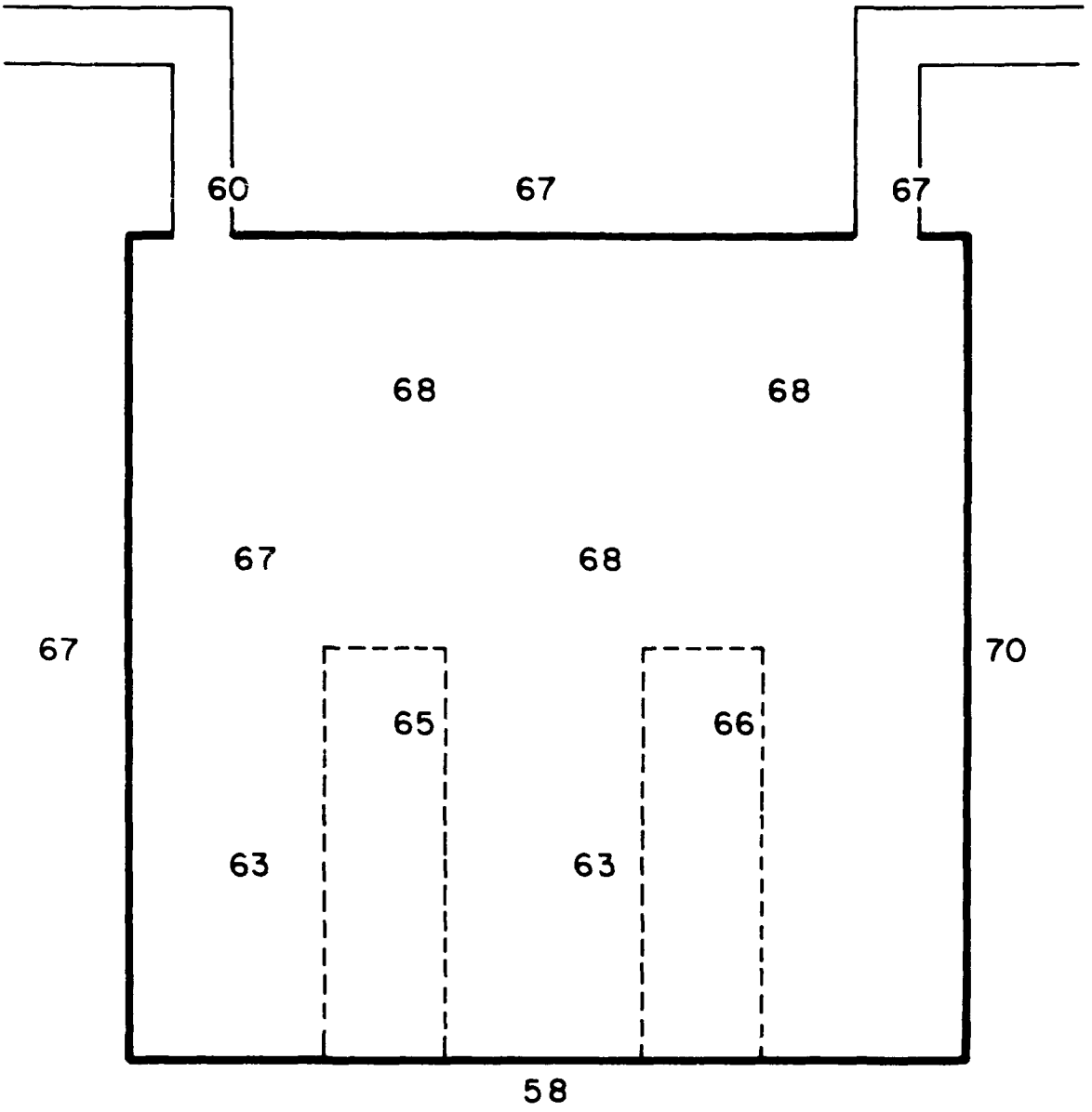

Figure A20 Air temperatures predicted for an 8' x 8' shelter with simulated occupants (77 °F) and natural ventilation (Condition IV)

The ventilation effect would be small because the difference between the supply and exhaust temperature is only 7 degrees. The air would enter the shelter and then be quickly drawn over toward the near wall. It would fall down the wall a short distance and then move horizontally toward the warm stream rising from the left occupant. The fresh air becomes entrained in the warm air rising from the left occupant and is returned to the ceiling. In this manner the fresh air would mix with the air near the upper part of the room and be eventually drawn off by the exhaust. This indicates, in effect, a "short circuiting" of ventilation air when the thermal driving force is small.

Based on the progression of simulations presented, the separate effects of the different convection producing mechanisms can be understood. Ventilation has by far been the greatest influence on the air distribution. The air rising from a single occupant while of surprisingly high velocity does not have as significant an effect on the distribution of air in the room as does the ventilation air, principally because the air warmed by the occupant is not generally as large a volume as the ventilation air. In the case where there are a number of occupants in the shelter their combined effect would be significant. The least effect on air distribution would be that of the circulation due to the temperature difference between the walls. If the temperature differences between the walls is of the order of twenty to thirty degrees, then the effect might be more significant. However, the condition of a large temperature difference between walls is not typical of a below ground shelter.

Conclusions

A number of conclusions regarding air distribution in a naturally ventilated shelter may be drawn from the results of these approximate simulations. Some of the more significant conclusions follow:

a. The temperature differential between the air inside and outside the shelter determines the rate of natural ventilation to the shelter.

b. A relatively large volume of the air in a naturally ventilated shelter is slow moving, has a surprising degree of thermal stratification, and is resistant to perturbing effects such as air currents produced by occupants or ventilation. This volume of air, referred to here as the inner core of air, extends outward from the center of the shelter to within about one foot of the walls, ceiling and floor.

c. The inner core acts as a sink for the energy of turbulent flows. That energy is dissipated by vortices produced at the interface between the inner core air and fast moving flows which pass through the inner core.

d. Vertical flows, within a foot or so of the wall, are drawn to the wall. This is due to the Coanda effect which gives the appearance of the wall drawing the flow toward it.

e. In those instances where a temperature difference exists between two opposite walls in a room or shelter, a flow of air is produced which circulates around the periphery of the room air space. The air rises along the warmer wall, crosses the ceiling to the cooler wall, drops along the cooler wall to the floor, and moves back across the floor to the warmer wall. The strength of the circulation is dependent upon the temperature differential between the two opposite walls.

f. At the warmer wall a boundary layer occurs which flows quickly up the wall. The thickness of the boundary layer predicted for air is between one and two inches. At the ceiling the speed of the boundary layer decreases and its thickness increases. The width of the predicted air boundary layer across the ceiling is predicted to be about nine inches. As the air falls along the cooler wall it returns to a layer about one to two inches thick. The flow across the floor although opposite in direction is much like that across the ceiling both in thickness and speed.

g. The temperature difference between the floor and ceiling of the shelter is dependent on the extent of air mixing within the shelter. If the mixing is good, as caused by a high rate of ventilation, then the temperature difference will be small. When the mixing is poor, as when the ventilation rate is low then the air in the shelter tends to stratify and produce a rather large temperature differential between floor and ceiling.

h. When the openings to the ventilation supply and return ducts are placed at the same elevation in a shelter and a low temperature differential is imposed between inside and outside air, then a short circuiting of the fresh air from the supply to the exhaust will occur.

i. The optimum location for a natural ventilation supply duct outlet is close to the floor. This location minimizes the possibility of short circuiting between supply and exhaust, and also puts the fresh air close to the occupants.

j. The optimum location for a natural ventilation exhaust duct outlet is at the ceiling level. The warmest stale air in the room is close to the ceiling and can be drawn off by an exhaust at that location.

k. The direction in which the opening to the exhaust duct faces had no influence on where the air is drawn from. Generally the air is drawn from a spherical area around the exhaust opening.

l. The direction in which the supply duct discharges has a significant effect on where the air goes.

m. When the temperature of the outside air equalled or exceeded that of the air inside the shelter then all natural ventilation stopped.

n. The maximum predicted velocity of air rising from an occupant was measured to be about 31 feet-per-minute and the maximum predicted velocity of the ventilation supply air, measured at a location three feet below the duct opening was about 41 feet-per-minute. Because the Prandtl number of the fluid was not closer to that of air, the velocities measured in the model are below those expected for air in a full-sized shelter.

Recommendations

As a result of these simulations a number of recommendations can be made for the design of naturally ventilated below ground survival shelters. These recommendations are as follows:

a. All shelters should have manually operated ventilating fans to change the air within the shelter. During hot days there is no assurance that the outside air temperature will not approach or even exceed the inside temperature. Once the temperature outside is higher than inside all natural ventilation ceases.

b. The opening to the supply duct should be close to the floor rather than close to the ceiling. This discharges air into the shelter close to where the occupants are located and prevents short circuiting of the air between the supply and exhaust ducts.

c. The supply air should discharge directly toward the floor rather than be directed out across the floor by a register. This causes the air to spread out across the floor more uniformly.

d. A diffuser or register should not be put over the opening of the ventilation supply duct since it adds resistance to the flow of air.

e. If the ventilation supply duct is inside the shelter, it should be insulated to minimize heating of the entering air.

f. The ventilation supply duct for new shelter designs could well be run through the earth outside the shelter. In this way the added cooling effect of the earth in the summer could be used to improve the thermal differential between the inside and outside of the shelter and hence to improve the rate of natural ventilation. In the winter the earth would be warmer than the ou side air and would tend to warm it to a more comfortable entering temperature.

g. A damper should be placed in the supply duct. This can be used to reduce the flow of air during cold days and to start the ventilation flowing in the correct direction. If the ventilation flows in the wrong direction in a system in which the supply duct is close to the floor and the exhaust is close to the ceiling, then the fresh air distribution will be quite poor. The ventilation can be started in the correct direction by closing the damper when the occupants enter, leaving it closed until their presence has warmed the shelter air sufficiently to insure that the shelter air is warmer than the outside temperature. Then the damper can be opened and the flow should go in the proper direction.

h. The opening to the exhaust duct should be at the ceiling level. The warmest air in the shelter is close to the ceiling and by locating the exhaust at the ceiling level the warm air can be drawn off. Further, since the ceiling is the warmest location in the shelter, exhausting the air from there will assist in providing a larger thermal differential between inside and outside, and thus improve the ventilation rate.

i. The more ventilation supply ducts used in a shelter, the better the fresh air distribution. The supply ducts should be evenly spaced throughout the shelter.